Advancing towards a controlled continuous dry granulation line

Inaugural-Dissertation

zur Erlangung des Doktorgrades der Mathematisch-Naturwissenschaftlichen Fakultät der Heinrich-Heine-Universität Düsseldorf

vorgelegt von

Annika Wilms

aus Essen

Düsseldorf, September 2020

Aus dem Institut für Pharmazeutische Technologie und Biopharmazie

der Heinrich-Heine-Universität Düsseldorf

Gedruckt mit der Genehmigung der
Mathematisch-Naturwissenschaftlichen Fakultät der

Heinrich-Heine-Universität Düsseldorf

Berichterstatter:

1. Prof. Dr. Dr. h.c. Peter Kleinebudde

2. Prof. Dr. Jörg Breitkreutz

Tag der mündlichen Prüfung: 09.12.2020

Für meine Familie

Table of contents

List of abbreviations

abbreviation	
A	area
A^*	cross sectional area of all active columns
A_0	cross section of a cylindrical die
A_f	area of the fracture plane
A_p	projected area
API	active pharmaceutical ingredient
c_0	control action at no error
CI	chemical imaging
CM	continuous manufacturing
CPP	critical process parameter
CQA	critical quality attribute
C_v	concentration of particle value in laser diffraction
d_a	mean value of the sieve class
DC	direct compression
dh/h	applied strain
DIA	dynamic image analysis
e(t)	error between actual and set-point value of controlled parameter at time t
EMA	European Medicines Agency
F	force
F_{calc}	granule failure load
FDA	United States Food and Drug Administration
F_f	failure force
GSD	granule size distribution
h_c	contact height
HM	Martens hardness
$k_{1\text{-}3}$	proportionality constants
K_c	gain factor
MCC	microcrystalline cellulose
MCS	manufacturing classification system
P	pressure
P'	compressive strength
PAT	process analytical technologies
PID	proportional – integral – derivative (controller)
QbD	Quality by Design
RCDG	roll compaction/dry granulation

RTD	residence time distribution
RTR	real-time release
RTRT	real-time release testing
SCF	specific compaction force
SOD	solid oral dosage form
T_d	derivative time constant
T_i	integral time
TSG	twin screw granulation
u(t)	control action at time t
u_{max}	maximal control action
u_{min}	minimal control action
y(t)	value of controlled parameter at time t
$y_{sp}(t)$	set-point value of controlled parameter at time t
α	pressure coefficient
$\in$	natural logarithmic of the applied strain
τ	shear failure stress
τ_0	sum of cohesive strength
τ_0'	cohesive granule strength

Publications

Published manuscripts:

1) Wiedey, Raphael, Rok Šibanc, Annika Wilms, and Peter Kleinebudde. *"How relevant is ribbon homogeneity in roll compaction/dry granulation and can it be influenced?"* European Journal of Pharmaceutics and Biopharmaceutics 133 (2018): 232-239.

- AW performed dry granulation, tableting, ribbon density, particle size and tablet characteristic measurements. She evaluated the data herself and provided it for the manuscript.

2) Wilms, Annika, Klaus Knop, and Peter Kleinebudde. *"Combination of a rotating tube sample divider and dynamic image analysis for continuous on-line determination of granule size distribution."* International Journal of Pharmaceutics: X 1 (2019): 100029.

- AW planned the experiments in agreement with KK and PK. AW conducted the experiments and evaluated the data. AW wrote the manuscript. KK and PK reviewed the manuscript.

3) Wilms, Annika, Robin Meier and Peter Kleinebudde. *„Development and Evaluation of an In-line and On-line Monitoring System for Granule Size Distributions in Continuous Roll Compaction/Dry Granulation Based on Laser Diffraction."* Journal of Pharmaceutical Innovation (2020):1-11.

- AW planned the experiments in agreement with RM and PK. AW conducted the experiments and evaluated the data. AW wrote the manuscript. RM and PK reviewed the manuscript.

4) Wilms, Annika and Peter Kleinebudde. *„Towards better understanding of the influence of process parameters in roll compaction/dry granulation on throughput, ribbon microhardness and granule failure load."* International Journal of Pharmaceutics: X 2 (2019): 100059.

- AW planned the experiments in agreement with PK. AW conducted the experiments and evaluated the data. AW wrote the manuscript. PK reviewed the manuscript.

5) Wilms, Annika and Peter Kleinebudde. *„Optimization of residence time distribution in RCDG and an assessment of its applicability in continuous manufacturing." Particuology (2020). Article in press*.

- AW planned the experiments in agreement with PK. AW conducted the experiments and evaluated the data. AW wrote the manuscript. PK reviewed the manuscript.

6) Wilms, Annika, Andreas Teske, Robin Meier, Raphael Wiedey and Peter Kleinebudde. *„ Implementing Feedback Granule Size Control in a Continuous Dry Granulation Line Using Controlled Impeller Speed of the Granulation Unit, Compaction Force and Gap Width."* Journal of Pharmaceutical Innovation (2020):1-11.

- AW planned the experiments in agreement with AT, RM and PK. AW conducted the experiments and evaluated the data together with AT. RW designed and wrote an analytical tool for data analysis. AW wrote the manuscript. AT, RM, RW and PK reviewed the manuscript.

Oral presentations:

- A. Wilms, K. Knop, P. Kleinebudde. **In-line determination of granule size distribution during continuous roll compaction / dry granulation**
  12th PSSRC Meeting, September 12-14, 2018, Leuven, Belgium

- A. Wilms, K. Knop, P. Kleinebudde. **Continuous determination of granule size distribution using Dynamic Image Analysis.**
  9th International Granulation Workshop, June 26-29, 2019, Lausanne, Switzerland

- A. Wilms, P. Kleinebudde. **In-line measurement of granule size distribution in a continuous manufacturing line**
  12th World Meeting on Pharmaceutics, Biopharmaceutics and Pharmaceutical Technology, *postponed.*

- A. Wilms, P. Kleinebudde. **Granule size control in a continuous dry granulation line.**
  EuPAT 9 ½, online conference, October 8, 2020.

Poster presentations:

- R. Wiedey, A. Wilms, P. Kleinebudde. **How relevant is ribbon homogeneity in roll compaction/dry granulation?**
  11th PBP World Meeting, March 18 – 22, 2018, Granada, Spain

- A. Wilms, P. Kleinebudde. **Particle size distribution in the product stream after roll compaction/dry granulation.**
  3rd European Conference on Pharmaceutics, March 25-26, 2019, Bologna, Italy

- A. Wilms, K. Knop, P. Kleinebudde. **In-line determination of granule size distribution during continuous roll compaction / dry granulation by laser diffraction.**
  PARTEC 2019, April 9-11, Nürnberg, 2019, Germany

- A. Wilms, P. Kleinebudde. **Representative sampling for roll compaction/dry granulation**
  Herbstkolloquium Prozessanalytik, November 25 - 27, Marl, 2019, Germany

- A. Wilms, P. Kleinebudde. **On-line measurement of granule size distribution by laser diffraction in a continuous manufacturing line**
  2nd APV Continuous Manufacturing Conference, February 18 - 19, 2020 Freiburg, Germany

- A. Wilms, P. Kleinebudde. **Dynamic image analysis to monitor the granule size distribution by dynamic image analysis in roll compaction/dry granulation**
  2nd APV Continuous Manufacturing Conference, February 18 - 19, 2020 Freiburg, Germany

1 Introduction

1.1 Continuous Manufacturing of solid oral dosage forms

1.1.1 Batch and continuous manufacturing of solid oral dosage forms

Concerning at-home therapy with drug products, solid oral dosage forms (SOD) (e.g. tablets, capsules, granules) are favored by patients as they typically offer easy and pain-free application and can be stored readily. The oral, next to the intravenous, application route is most common in preclinical safety testing [1]. Therefore, it is expected that routine medication in the form of SOD will remain relevant.

Historically, SOD's have been manufactured in batch mode. In batch mode a specified amount of material (e.g. 1000 kg) is transformed into the final product via several processes that are not linked. The easiest and thus preferred process is direct compression (DC), which typically comprises at least one blending and the tableting process [2]. Not all materials can be processed using DC and therefore granulation methods may be necessary. The number of processes that are needed to manufacture a tablet increases, if granulation is needed. An example of the manufacturing process of a coated tablet using roll compaction/dry granulation (RCDG) is shown in Figure 1 a). The products of each process are stored and tested for specified attributes. A batch record is compiled and evaluated. If the batch record passes the review, the batch is released by the qualified person. Depending on internal regulations, this can stretch the time-to-market relevantly. Furthermore, different manufacturing steps can be performed at different locations, which furthermore elongates the time-to-market [3, 4].

Contrary to batch manufacturing, and already established in non-pharma branches of business such as the food industry [5, 6], is the concept of continuous manufacturing (CM). It is characterized by linking each process and not storing the intermediates in between (see Figure 1 b)). Samples can be taken for off-line analytics, however, it is favorable not to disturb the process by sampling procedures and use validated in-line or on-line methods to measure critical quality attributes (CQA) or their surrogates.

If all CQAs can be monitored during manufacturing, it is possible to release the batch in real time (real-time release (RTR)). In this case, establishing real-time release testing (RTRT) is necessary. In 2016, Janssen-Cilag switched their Darunavir containing HIV-treatment (Prezista®) from batch to CM. This resulted in a decrease in the days needed for

release from above 21 to eight. In 2019, a surrogate dissolution model was implemented that further shortened the days needed for release to less than one [7]. Reducing the days needed for release means an earlier entry to the market with no relevant storage time, increasing the profitability of the manufacturing step.

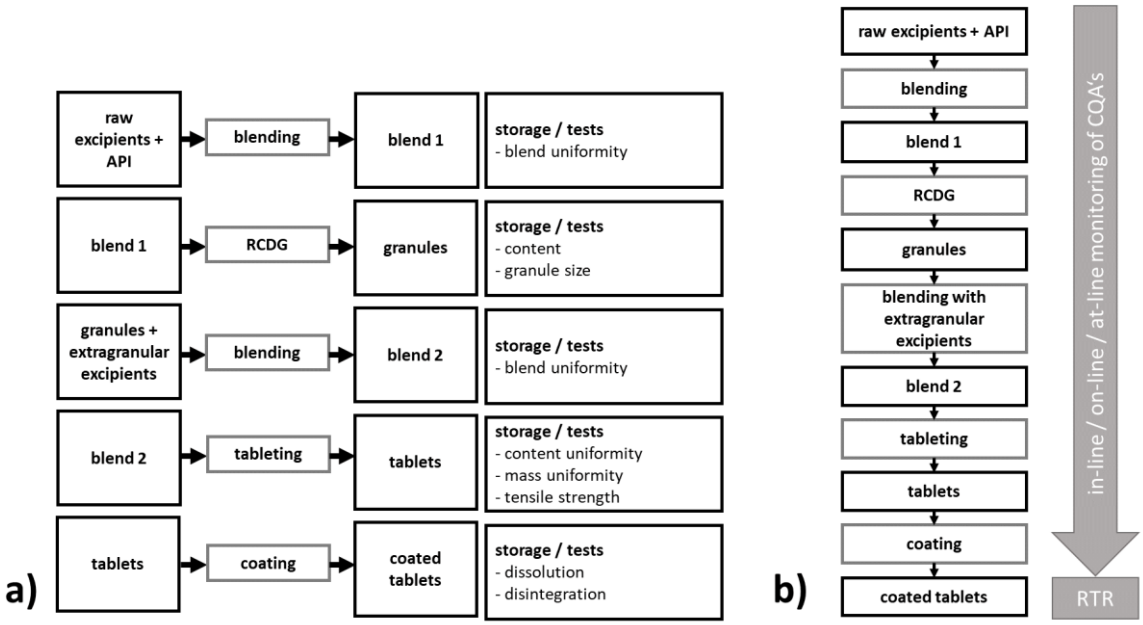

Figure 1: a) Batch manufacturing scheme b) Continuous manufacturing scheme

1.1.2 Possible benefits of implementing continuous manufacturing

In 1.1.1, the concepts of batch and CM were outlined. Most products obtained market authorization based on batch manufacturing. Therefore, for pharmaceutical manufacturers, there must be evident benefits in connection with CM to start investing in this manufacturing mode.

- **Quality improvement**

Quality, safety and efficacy are the essential attributes of a drug product to receive market authorization [8]. Quality needs to be guaranteed and tested for every batch that is manufactured. Therefore, quality is a major focus in development and manufacturing. Advanced quality considerations, such as Quality by Design (QbD) and process analytical technologies (PAT) are not limited to CM, as they can also be applied to batch processes [9]. However, to make full use of the CM advantages, they need to be implemented into the manufacturing line. Therefore, CM is a driving force for advancement of both concepts.

- **Cost reduction**

Cost reduction by the implementation of CM is a result of various factors. As previously mentioned, scale-up that can be avoided is a financial relief. Furthermore, CM equipment is not limited by batch size and hence, in-theory, large amounts of drug product can be manufactured dependent on manufacturing time. Manufacturing in a steady-state continuous process, avoiding multiple batch manufacturing processes (with all necessary documentation) and minimizing loss of material due to start-up and shutdown will reduce cost. Pharmaceutical industry has reported a yield of > 99 % when manufacturing 116 000 kg of tablets in a 4.5 day continuous process [10]. An additional aspect of avoiding scale-up is the decreased footprint of the manufacturing line. If PAT are implied and all CQA can be monitored/controlled in real-time, sampling, sample transfer and of-line analytics can be minimized. As off-line analytic requires laboratories including equipment and staff, this can be a source of long-term cost reduction.

- **Flexibility**

Various sources highlight that scale-up will not be necessary or will be simplified using CM [5, 11, 12]. This is certainly not generally true and must be evaluated for every process itself. However, in theory, scale-up can be avoided, if the market demand can be saturated by increasing the run time of the CM line. This facilitates flexible reaction to drug shortages and switching readily from clinical supply to market supply and thus reducing the time-to-market, which bears financial benefits and extended patent protection [5, 11, 13, 14].

- **Authorities view**

Regulatory agencies, especially the US Food and Drug Administration (FDA) and the European Medicines Agency (EMA), are supportive of CM and the concept of QbD. As regulators recognize advantages in quality and flexible reaction to drug shortages, the FDA's Emerging Technologies Team and the EMA's PAT Team are working together with the pharmaceutical industry on scientific challenges linked to incorporating CM approaches and obtaining market authorization [7, 13, 15-20].

- **Innovation**

The pharmaceutical industry is typically shy of risks that could lead to a danger to patients or unsuccessful attempts for market authorization. As authorities have demonstrated goodwill to bring innovation to the pharmaceutical industry, more companies aim at fostering innovation in their business and scientific environment. CM helps implementing innovative models and process control strategies. RTR as an innovative release option can be achieved and innovative testing strategies have to be developed to speed up the time from manufacturing to release. Therefore, implementation of CM helps to bring further innovative approaches to the pharmaceutical industry [21].

1.1.3 Challenges and limitations of implementing continuous manufacturing

The possible benefits of implementing CM refer to a CM line that is functional, validated, fully understood and has proven robustness over long periods. It is undisputed that establishing a CM line requires development efforts by specialists in their respective field and is a financial risk as chosen approaches that are incorporated in a CM line might not be suitable. Similarly to scale-up issues that are only recognizable in large scale, issues might only be recognized when long-term experiments or trial runs are executed. If such issues arise, solutions to overcome these might be necessary.

Current challenges include:

- **Probe fouling**

  Probes that are used in PAT tools often incorporate a measurement window or lenses. If these are constantly in a flow of powder or granulated material, probe fouling is an issue to be expected during development and preventive actions such as adding scavenging air should be evaluated from the beginning.

- **Interruption / OOS-material / recall decisions**

  To develop a CM process, procedures for interruption and OOS-material handling should be in-place and validated. Effectiveness of these procedures has to be evaluated. To avoid OOS-material, a robust control strategy should be in place for CQAs as well as monitoring tools for critical process parameters (CPP) that make it easy for the operator to see undesirable trends before an interruption takes place.

If, for any reason, after manufacturing material is under investigation, it is critical to have a full understanding of residence times in the line. Deviations in the granulation process can only be linked to batches of material, if residence times are known. This requires thorough process understanding and is crucial to prove to authorities that all possibly affected material can be traced and recalled [22].

- **Potential for microbial growth**

  Unexpected microbial growth in the manufacturing equipment could be especially relevant for wet granulation techniques and certain formulations (e.g. containing pharmaceutical starch or other sugars). In a CM line, run-times are supposed to be long (minimize start-up and shut down phases and manufacture large quantities of material during steady state). Hence, cleaning intervals will be chosen as far apart as possible. If they are only based on equipment or required amount of material (e.g. probe fouling or accumulation of material in dead zones) and they are minimized by engineering efforts, microbial growth could be a relevant factor that is almost impossible to detect without off-line laboratory tests. A retrospective infestation with microbes could lead to large quantities of material that have to be discarded [23, 24].

1.1.4 Market authorization status

While both, the US FDA and the European EMA, report various discussions with the pharmaceutical industry, drug products with market authorization are still scarce [16, 21]. The first authorized drug product that is produced using a CM line was Orkambi® by Vertex Pharmaceuticals Ltd. (Ireland). In 2018, Vertex Pharmaceuticals Ltd. also obtained authorization for Symkevi® (EU) which is manufactured using dry granulation [25]. Janssen Pharmaceutica (Belgium), Eli Lilly and Company (US) and Pfizer Inc. (US) also have drug products on the market that are produced using continuous direct compression. Table 1 summarizes the current market authorization status for different active pharmaceutical ingredients (API).

Table 1 current SOD with market authorization in the US or EU that were produced using CM

year	name	API	company	manufacturing mode	main ingredients
2015	Orkambi®	Lumacaftor/ Ivacaftor	Vertex Pharmaceuticals (Ireland) Limited	Wet granulation [26]	cellulose, microcrystalline; croscarmellose sodium; hypromellose acetate succinate; magnesium stearate; povidone; and sodium lauryl sulfate, carmine, FD&C Blue #1, FD&C Blue #2, polyethylene glycol, polyvinyl alcohol, talc, and titanium dioxide [27]
2016	Prezista®	Darunavir	Janssen Pharmaceutica N.V. / Johnson & Johnson GmbH [28]	Direct compression [29]	colloidal silicon dioxide, crospovidone, magnesium stearate, and microcrystalline cellulose. The 800 mg tablet also contains hypromellose, OPADRY® White, OPADRY® Orange, OPADRY® Dark Red. [30]
2017	Verzenio®	Abemaciclib	Eli Lilly and Company	Direct compression [31, 29]	croscarmellose sodium, lactose monohydrate, microcrystalline cellulose 101, microcrystalline cellulose 102, polyethylene glycol, polyvinyl alcohol, silicon dioxide, sodium stearyl fumarate, talc, titanium dioxide [32]
2018	Symdeko® / Symkevi®	Tezacaftor/ Ivacaftor	Vertex Pharmaceuticals (Ireland) Limited	Dry granulation [25]	Tablet core: croscarmellose sodium, hypromellose, hypromellose acetate succinate, magnesium stearate, microcrystalline cellulose, sodium lauryl sulfate Tablet film coat: HPMC/hypromellose 2910, hydroxypropyl cellulose, iron oxide yellow, talc, titanium dioxide [33]
2018	Daurismo®	Glasdegib	Pfizer Inc	Direct compression [34, 35]	Tablet: microcrystalline cellulose, DCPA, sodium starch glycolate, magnesium stearate Film coating: Opadry® beige, Opadry® yellow [36]
2018	Lorbrena®	Lorlatinib	Pfizer Inc	Direct compression [37, 38]	microcrystalline cellulose, dibasic calcium phosphate anhydrous, sodium starch glycolate, and magnesium stearate. The film-coating contains hydroxypropyl methylcellulose (HPMC) 2910/hypromellose, lactose monohydrate, macrogol/polyethylene glycol (PEG) 3350, triacetin, titanium dioxide, ferrosoferric oxide/black iron oxide, and iron oxide red. [39]

1.2 Process analytical technologies (PAT) and process control

1.2.1 Process analytical technologies (PAT)

PAT is most commonly defined as *"a complex system of multivariate (chemical, physical, microbiological, and mathematical) methods for material (e.g., materials, intermediates, products) and process (e.g., temperature, pressure, throughput, etc.) analysis, as well as process modelling and enhanced control strategies for improved product quality and process efficiency."[40, 41]*

The US FDA defines PAT as *"a system for designing, analyzing, and controlling manufacturing through timely measurements (i.e. during processing) of critical quality and performance attributes of raw and in-process materials and processes, with the goal of ensuring final product quality."[19]*

While both definitions are not contradictory, the US FDA emphasizes on critical quality and performance attributes. This underlines the necessary process understanding in order to know all CPPs of a process, all CQAs of an intermediate and the resulting product, and avoid massive data acquisition of non-critical quality attributes. Both definitions point out the importance of using the acquired data for control rather than only monitoring. Hence, PAT is more than simply adding a measurement tool to a process. In the following sections, the most important factors to implement a PAT based control strategy will be discussed.

1.2.2 The analytical method / process analyzers

Basis for all PAT tools and control strategies is data that is obtained from the process. This information can be logged by the machine (e.g. torque, temperature), if the machine is equipped with appropriate sensors. More commonly, an analytical tool is implemented in the process (e.g. a NIR-probe). The analyzer should not impair the quality of the product. Concerning the set-up, there are four ways in which an analytical tool can be installed [19]:

- **In-line**
  Analysis is performed without diversion of material.
- **On-line / bypass**
  Analysis is performed on a diverted sample. Typically, the sample is afterwards reunited with the main product flow (bypass).

- **At-line**
  Analysis is performed after removal of material from process and in close proximity (time and space) to the process.

- **Off-line**
  Analysis is performed after removal of material from process. There is no proximity (either time or space or both) to the process.

Only in- and on-line methods can be incorporated in a fully instrumented control strategy and have been explored in this thesis. While at-line analysis can also be incorporated into a control strategy, its limited computerized automation can impede consistent quality control [42]. Figure 2 shows examples of an incorporated measurement cell into a product transfer. The cell is incorporated in-line (Figure 2 a)) or on-line using a bypass (Figure 2 b)). An overview of process analyzers studied for RCDG is given in Table 2 (section 1.3.3).

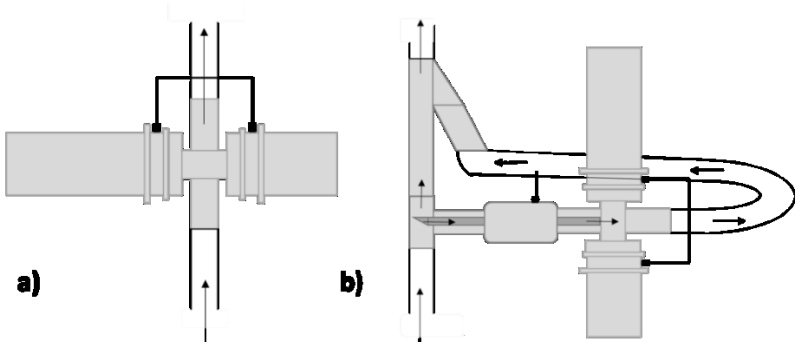

Figure 2: a) In-line and b) On-line implementation of a measurement cell into a product stream. Gray = measurement cell, white = product transfer tubes b) also in gray: bypass.

In order to proceed with an on-line monitoring or control tool, representative sampling must be ensured. Otherwise, the results are not applicable for the complete amount of material and its informative value is limited [43].

1.2.3 Process monitoring

Process monitoring in the context of CM is referred to as implementing a PAT tool to measure a certain characteristic of the material in real-time. The characteristic can be measured "as-is" or models can be used to translate a measured quantity into a product characteristic (e.g. NIR-spectra to API content). Ideally, the characteristic is a product CQA and the development of the value can be tracked in real-time on quality control charts [44]. These quality control charts can then be used for batch release, process reports etc.

With the advancement of PAT, a plethora of publications is available which aim at monitoring various CQA in pharmaceutical manufacturing processes [41].

1.2.4 Process control

Process control generally refers to comparing an actual process value to a pre-defined desired set-point and generating a response, if these deviate [42, 45].

In order to proceed with process control a robust monitoring method of a desired CQA must be established. Additionally, a parameter which impacts the CQA has to be identified (e.g. a CPP). Ideally, the control parameter can be readily varied and impacts only one CQA. The desired CQA typically has a range, in which the actual value should be located (e.g. 2 % variation allowed for tablet thickness [42]) and the center of this range is used as a set-point, or desired value, in process control. After defining the set-point ($y_{sp}(t)$), the difference (error $e(t)$) between actual ($y(t)$) and set-point for every time point realized by the monitoring strategy can be calculated according to Equation 1.

Equation 1: Error determination in process control

$$\boldsymbol{e(t) = y_{sp}(t) - y(t)} \quad (1)$$

As next step, a controller must be programmed to translate the error *e(t)* into a control action, commonly abbreviated as *u(t)*. There are various controller options [45]. Fundamentally, they can either be discrete or continuous. Discrete controllers can only modify the control valve to discrete, predefined values. The most prominent discrete controller is a so-called "on-off-controller". The control action will either be a minimum u_{min} or a maximum u_{max} depending on the error exceeding a threshold value or not. It is easy to program and understand but typically generates persistent oscillation of the actual value around the desired set-point [42, 45].

About 80 % of control loops in industrial applications are of continuous nature, defined by proportional (P), integral (I) and derivative (D) algorithms. The control action can be calculated according to Equation 2 [45].

Equation 2: PID control action

$$u(t) = c_0 + K_c\left(e(t) + \frac{1}{T_i}\int_0^t e(\tau)d\tau + T_d\frac{de(t)}{dt}\right) \quad (2)$$

c_0 is the control action value if there is no error ($e(t) = 0$ in Equation 2) to keep the control valve steady. K_c is called "gain factor" and the product of K_c and error $e(t)$ characterizes the proportional controller effect as it generates a direct, proportional control action $u(t)$. T_i is called "integral time" and $\frac{1}{T_i}\int_0^t e(\tau)d\tau$ characterizes the integral controller effect. The integral part considers the past behavior of the process as it accumulates the past errors over time. T_d is called "derivative time constant" and $T_d\frac{de(t)}{dt}$ characterizes the derivative controller effect. It equals the rate of the error changing and thereby elucidates future errors.

Depending on the process to be controlled, selective terms can be ignored. The controllers are then abbreviated by the terms that were taken into consideration (e.g. PI-controller, PID-controller) [45]. K_c, T_i and T_d are constants that can be varied according to the process, the determination of suitable control constants is referred to as "tuning". It can be based on rules of thumb, mathematic theories or automatic tuning by software [46].

For the process, a design space has to be defined. The design space characterizes a range of raw material attributes and CPPs ensuring that the resulting product will conform to the CQA requirements [47]. A control strategy can then be implemented in which the influencing process parameter can be controlled in range of the design space. The process then does not match the definition of a "steady-state". Myerson et al., named it a "quasi steady state" in which CPP may vary in the range of the design space in order to produce material that adheres to specifications, which can also be described as a "controlled-state" process [48]. Recently, advances of controlling CQA for pharmaceutical processes or end-to-end CM have been published [49-52].

1.2.5 Residence time in continuous processes

For batch manufacturing and its control, mass flow rates of the materials are of lower importance than in continuous processing, as each process in batch manufacturing is self-contained [42]. However, batch or continuous, if a process is to be controlled, residence time determinations are necessary between the control parameter action and the measurement tool in order to tune the process control constants. For continuous processes, the CQA monitoring tool can be used to divert material that is OOS. In this case, residence time determinations between the monitoring tool and the diversion valve are necessary. As each process is linked in CM, the residence time can be stretched immensely by back-

mixing tendencies in various, but especially blending units [53]. Therefore, determination of residence time is an important factor in CM [54].

The residence time of a reactor can be measured by pulse injection, step injection (step change), periodic injection and random injection. All are based on a nonreactive species of similar properties to the main material (tracer) being added into the process. The tracer is measured at the process outlet. Due to disadvantages, the periodic and random injection methods are uncommon and will not be discussed further [55]. Resulting from the experimental measurements are characteristic residence time distributions functions. The most important ones will be briefly summarized here.

A pulse injection is defined as an injection of a specified amount of tracer into the reactor (at time t = 0). Resulting plots are shown in Figure 3. Tracer concentrations at the reactor outlet are measured over time and generate the c(t) – function (see Figure 3 a)). At constant volumetric flow, the c(t)-function can be normalized by division by the total amount of tracer (area under the curve of the c(t)-function). The resulting function is the residence time distribution (RTD) function E(t) (Equation 3, Figure 3 c)) [55].

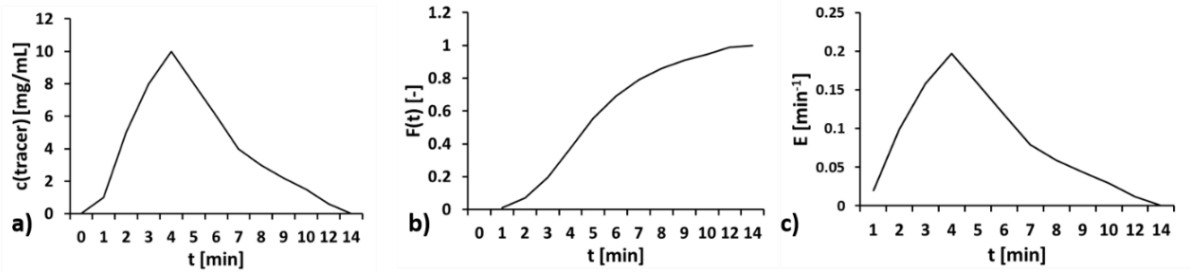

Figure 3: Examples of experimental data obtained from a pulse injection experiment. a) c(t)-function b) F(t) c) E(t)

Equation 3: RTD function E(t)

$$E(t) = \frac{c(t)}{\int_0^\infty c(t)dt} \tag{3}$$

The cumulative distribution function F(t) can be derived by integrating E(t) (Equation 4, Figure 3 b)). It characterizes 0 – 100 % of tracer that has left the process at time t.

Equation 4: Cumulative residence time distribution function F(t)

$$F(t) = \int_0^t E(t)dt \tag{4}$$

A step change is characterized by changing the complete material input to tracer-containing material whilst keeping the process constant (e.g. changing from 0 mg/100 mL tracer concentration to 350 mg/100 mL tracer concentration). Resulting plots are shown in Figure 4. The tracer concentration (c(t)-curve) will increase (or decrease) from concentration c_0 (e.g. 0 mg/100 mL) to concentration c_{step} (e.g. 350 mg/100 mL, see Figure 4 a). Afterwards, it will stay constant as all previous material is washed out of the reactor.

The cumulative residence time distribution curve can be directly obtained from a step change experiment by normalization of the outlet mass fraction by the inlet mass fraction (see Equation 5) It characterizes 0 – 100 % of the initial material that has left the reactor at point t (Figure 4 b)).

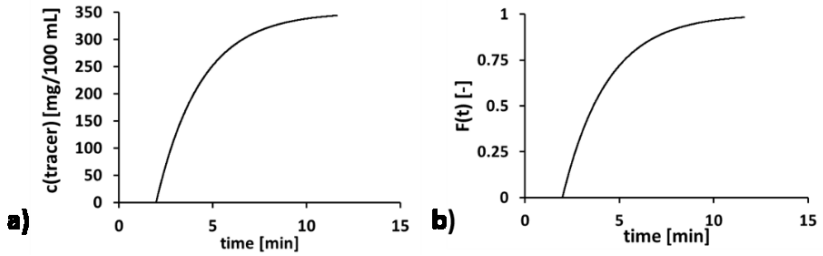

Figure 4: Examples of experimental data obtained from a step change experiment. Inlet concentration tracer here 0 mg/100 mL. Step change concentration = 350 mg/100 mL. Dead-time = 2 minutes. a) c(t) b) F(t)

Equation 5: Cumulative residence time distribution function F(t) for step change experiments

$$F(t) = \frac{c(t)}{c_0} \tag{5}$$

In all cases, there will be a lag time between the start of the measurement and the first tracer detected (see Figure 3 and 4). It is also referred to as dead-time.

A variety of key parameters can be calculated from experimental RTD data. Idealized reactor models (e.g. plug-flow reactor, continuous stirred tank reactor) can be used in conjunction to model the behavior of real reactors [55-57].

1.3 Roll compaction/dry granulation

RCDG is a well-established technique in pharmaceutical granulation. A scheme of a roll compactor can be seen in Figure 5. Typically, a powder blend is fed into the powder inlet, which sits above the feeding auger. A rotating impeller prevents core flow and possible de-mixing tendencies (Figure 5, 1). The feeding auger (Figure 5, 2) transports the material on to a tamping auger (Figure 5, 3). The tamping auger transports the powder in between two counter rotating rolls (Figure 5, 4). The smallest distance between the two rolls is called the compaction gap. Afterwards, a compacted string of material is produced (ribbon). Material that does not detach from the rolls is removed by scrapers (Figure 5, 5). The ribbons are then milled down to granules in a dry granulation unit (Figure 5, 6) [58].

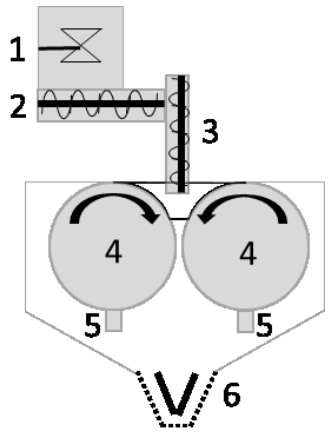

Figure 5: General set-up of a roll compactor 1) powder inlet including bridge breaker 2) feeding auger 3) tamping auger 4) rolls 5) scrapers 6) milling unit

RCDG is the first choice, if a water-susceptible API should be granulated. There is no need to dry the material. As the drying step is cost- and energy-intensive, RCDG is a cost-efficient and comparably environmental friendly process. During scale-up the roll width can be increased, which will linearly increase the throughput. This makes scale-up easy and cost-efficient. Hence, RCDG is a cost-efficient, fast and readily scalable granulation process, which has retained its relevance despite numerous modern techniques emerging. Based on these advantages, a proposed Manufacturing Classification System (MCS) classifies RCDG as the granulation method of choice [58, 2].

There are drawbacks of this technique as well. Milling of the compacted ribbons leads to granules of mostly bimodal granule size distribution. A large quantity of fines is typical for granules produced by RCDG. This fraction of fines is the main reason why RCDG delivers granules with only slightly improved or unchanged flowability. Furthermore, reduced tabletability is observed for granules produced by RCDG. This effect was widely studied in literature. To this day, two effects are described that explain the reduced tabletability. “Granule hardening” (a more precise description of the phenomenon previously referred to as “work hardening”), which is an increased resistance of the granules for further compression, and the particle size enlargement through the granulation process [58-63].

Additionally, the large throughput and broad size distribution make representative in-line sampling challenging. There are reports of relevant differences in measured particle size depending on probe position in a RCDG product stream [64]. To this day, no representative sampling method is established for continuous RCDG, albeit this is necessary to develop on-line PAT-tools.

1.3.1 Critical process parameters of RCDG

There are various parameters that can be varied in a RCDG process. Depending on the equipment and the control system, certain parameters can be set while others result.

- **Specific compaction force (SCF)**

  The SCF is the force that is transmitted to the material by the rolls normalized to roll width to obtain comparable values for different equipment types. It is the dominant process parameter in RCDG. Applying a greater force to the material in the compaction gap will lead to a denser ribbon, a harder ribbon and larger granules after milling [65-67]. At increasing SCF, the reduced tabletability is more pronounced as well [59].

  The force is measured in the equipment using strain gauges. It is a resultant of the compaction gap width and the amount of material that is fed into the compaction gap. Due to its importance, most roll compactors provide a SCF PID-control tool. Thereby, the SCF can be set while the control loop will vary e.g. the gap width until the desired SCF is met. Typically, the SCF unit is kN/cm.

- **Gap width**

  The gap width is the smallest distance between the two compaction rolls. It determines the initial thickness of the ribbons (the thickness of the ribbon can change after leaving the compaction gap due to relaxation phenomena). If the same SCF is applied at different gap widths, the properties of the resulting ribbon and granules will vary. In general, increasing the gap width at otherwise constant settings will lead to smaller granules [68, 69]. The gap width is frequently used to control the SCF, as a change in gap width has a fast impact on the resulting SCF. However, it might also be desired to compact at constant SCF and constant gap width settings. Therefore, a controller can be implemented to adjust the feed rate of

material into the compaction gap accordingly. This poses a challenge as the gap width is used as variable parameter to control the SCF, while its deviations generate controller responses to the material feed rate. The first priority, obtaining a constant SCF, generates a fast control response while the second priority, a constant gap width, is linked to a slower control response. The gap width is given in the unit mm.

- **Roll speed**

  The roll speed of the compaction rolls is the CPP exerting the main influence on throughput. The throughput will increase linearly with roll speed as long as the flowability of the material into the compaction gap is sufficient and all material that is compacted to ribbons can be milled down in the milling unit. Typically, the roll speed can be set and is displayed in rpm.

- **Rotational speeds of the feeding and tamping auger**

  Material is transported into the roll compactor by a volumetric feeder which is equipped with a feeding auger (see Figure 5,2). The feed rate is determined by its rotational speed. Control tools in the roll compactor often vary the feeding auger speed in order to reach a desired gap width. The speed is then a resultant of constant SCF, gap width and roll speed. Often, the rotation speed of the tamping auger is higher than the feeding auger by a fixed ratio to prevent pre-compaction at the feeding auger - tamping auger transition. Auger speeds are displayed rpm.

- **Impeller speed (powder inlet unit)**

  The powder inlet unit of a roll compactor is often built up similarly to continuous, volumetric feeders, in which an impeller (also known as bridge-breaker or agitator) rotates in the hopper and a screw at the bottom is used to transport material in direction of the compaction gap. The agitator is supposed to counteract bridge-building and core flow which could lead to dead zones [70, 71]. The rotational speed unit is rpm.

- **Impeller speed (milling unit)**

  The impeller speed of the milling unit (also called sieve speed) is a process parameter of the milling step. It characterizes movement of the mill. It influences the granule properties as a faster rotation of the impeller in the granulation unit will

lead to smaller granule sizes [72]. Depending on the type of mill, it is displayed in various units (e.g. rpm).

1.3.2 CQAs of intermediates and granules and state-of-the art process analyzers in RCDG

As previously mentioned (section 1.2), it is of interest to monitor and control CQAs. It is therefore necessary to determine CQAs and their target ranges. For pharmaceutical applications there are three main process steps, which can follow granulation: sachet/stick-pack filling, capsule filling and tableting. CQAs of the intermediate granules and ribbons are those characteristics that determine, whether the following process will be feasible and the product will adhere to specifications. Intermediate CQAs of ribbons and granules are shown in Figure 6.

Intermediate CQAs of granules for further processing are residual moisture, granule size and shape distributions, blend uniformity, the solid state of the API and all excipients, granule porosity, granule strength, compactability and compressibility (Figure 6) [41].

In all cases, a filling step is part of a following process, either into a sachet/stickpack, a capsule, or a tablet die. The filling step must be accurate in order to achieve the desired mass and API uniformity. Accuracy of the filling step strongly depends on the flow properties of the material that is to be filled, and thus flow properties are a main CQA of granules [2, 73, 74]. Flowability itself can be measured, but these determinations are not suitable for continuous measurements [75]. Moisture content, granule shape and granule size distribution (GSD) impact granule flow properties [2, 76]. Hence, each of them is a surrogate CQA for granule flow properties. Granule shape is predominantly determined by the production process [77]. Moisture content is of low importance for dry granulation as no water is added during the process. The GSD impacts the flowability, is strongly dependent on CPPs and can vary in large ranges. It is therefore of great importance and worth monitoring/controlling [12]. As a rule of thumb, if granules are supposed to be tableted in a following process step, a D50 of 50 – 500 µm is desirable [2].

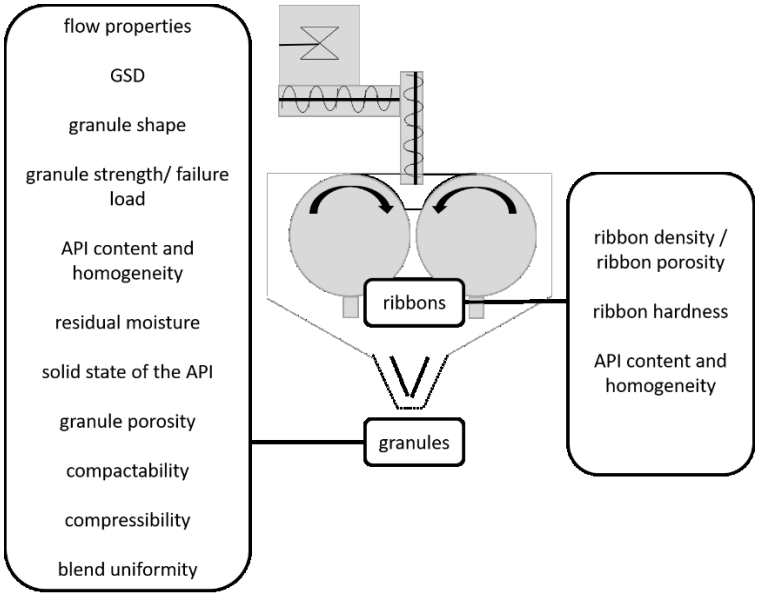

Figure 6: CQAs of ribbons and granules in RCDG

Granule hardness, expressed as granule strength / failure load is important in the cases, in which the packaged granules are supposed to be reconstituted by the patient and the granular characteristic is supposed to be retained (e.g. granules to be dispersed in water or sprinkled on food for pediatric patients). It is also critical for tablet production as the hardness of the granules will impact the tensile strengths of the resulting tablets [77]. Granule density affects compactability and disintegration / dissolution and should also be monitored [78, 79]. The API content range in the final dosage form should be monitored and controlled throughout the production process [80].

As the granule characteristics strongly correlate with ribbon characteristics, CQA analysis can also be performed on the intermediate ribbon [81]. This was utilized by various researchers as measurements were conducted on the ribbon and correlated to granule CQAs. Examples are given in laser-based thermo-conductometry to determine ribbon solid fraction [65, 82, 83] and NIR measurements to determine ribbon density and API content [80, 84-87]. Intermediate ribbon CQA's are also highlighted in Figure 6.

1.3.3 Real-time process analyzers in RCDG

Since RCDG is a relevant process in pharmaceutical manufacturing, multiple research groups have published their work on continuous determination of CQAs (Table 2).

Table 2 Process analyzers in pharmaceutical granulation processes

evaluated CQA	process analyzer	source
-	acoustic emission	[88-90]
ribbon hardness	torque of the granulation unit	[91]
	vibration and acoustic pressure	[92]
ribbon envelope density	IR-thermography	[65, 82, 83]
	NIR/ NIR-CI	[80, 84-87, 93, 94]
	microwave resonance	[95]
GSD	NIR/ NIR-CI	[84, 86, 87]
	spatial filer velocimetry	[96]
API content	NIR	[80, 56, 84-87, 97]

- **Hardness**

In 1993, Hakanen and Laine published their experiments detecting acoustic emission signals during roll compaction [88, 89]. This work can be seen as a predecessor to later work using vibration and acoustic pressure to correlate to ribbon hardness [92]. Ribbon hardness was also correlated to the torque of the granulation unit 2012 by Müller [91]. Müller found a correlation of SCF, torque of the granulation unit and the drilling force needed to drill a hole in the ribbon using a tablet drill. Increasing the SCF increased the hardness of the ribbon and the torque of the granulation unit. Furthermore, the torque depends on roll speed in contrast to the ribbon hardness. No solution to evaluate the effect of hardness independent from the effect of the throughput on the torque was elaborated. No hardness parameters of the resulting granules were accessed and thus a correlation between ribbon and granule hardness was assumed, but not proven. Further varying factors (e.g.

type of sieve, distance between sieve and granulator, age and wear of the sieve, speed of the granulation unit oscillation) were varied of which most were found to have an impact on the torque of the granulation unit. The approach of utilizing the torque of the granulation unit to determine hardness of material was not followed up by the group, as they focused on vibration and acoustic pressure analysis [92].

- **Ribbon envelope density**

Frequently determined is ribbon envelope density, ribbon solid fraction (the ratio between ribbon envelope density and the true density of the ribbon material) or ribbon porosity. They are not CQA's itself, but it was shown that the values are indicators of ribbon hardness [98] and GSD of the resulting granules [81]. It was therefore of interest for numerous scientists to develop methods to determine ribbon envelope density in-line (see Table 2). Ribbon solid fraction and porosity can be generated based on these methods. However, experimental data published by Gupta et al. underlines that the use of ribbon envelope density as a surrogate for hardness must be evaluated carefully as microcrystalline cellulose (MCC) ribbons of similar density could vary in hardness, especially under the influence of ambient moisture [85].

- **Granule size distribution**

Determining the GSD of the resulting granules is impeded by the broad granule size distribution and large throughput. Therefore, methods to determine the GSD in continuous RCDG are scarce. Mangal published results of using spatial filter velocimetry to determine GSD in RCDG. Especially the high dependency of the results on probe position limited this approach and no satisfactory results were obtained [64, 96].

NIR spectroscopy, a versatile, non-invasive PAT tool was applied to RCDG. Off-line spectra were correlated to ribbon strength, ribbon density as well as GSD data [80, 84-87]. Gupta et al. [84] were the first to report a shift in NIR spectral baseline at an increased roll speed. The increased roll speed was coupled with constant feeding auger settings, which equals a decrease in SCF (see section 1.3.1). The slopes of the spectral baseline were correlated with ribbon characteristics (force at break, thickness and width). The work also included a set of experiments, in which the SCF was varied and a shift in spectral baselines was observed. Slopes were plotted against the d50 and d90 GSD parameters and showed good agreement. As described by the author, this was a promising approach to GSD

determination using NIR-spectroscopy. However, it lacked determination of specificity, sensitivity, reproducibility and applicability [84]. While the group went on to publish further work on NIR spectroscopy in RCDG, the approach to determine GSD based on NIR measurements was either not followed up on or not reported [80, 85].

Khorasani et al. applied off-line NIR – chemical imaging (NIR-CI) to determine ribbon porosity, API concentration, granule sizes and tablet characteristics [86]. The API content was determined using NIR-CI and partial least squares regression. NIR-CI and principal components analysis was applied to obtain score value distributions for each analyzed ribbon. Using these distributions, the d10, d50 and d90 fractions score distribution was calculated and compared to d10, d50 and d90 values obtained using laser diffraction. As expected, an increase in ribbon density lead to an increase in granule size. While linear correlations with R^2-values of 0.88 and 0.96 described the correlation between principal component score and d90 and d50 GSD parameter the d10 parameter was not described by linear correlation.

The group expanded their research by implementing an in-line NIR probe to RCDG. Spectra of the granules were recorded at the outlet of the milling unit. An algorithm determined the slope of the spectral baseline in-line. An increase in slope of the spectral baseline and of off-line determined GSD parameters was reported at increasing compaction pressure (confirming previous results by Gupta et al. [84]). The group did not derive a quantitative model to predict granule size parameters, although the feasibility of such an approach was highlighted [87]. To this day, no direct measurement and no model is available to determine the GSD of dry granulated material in-line.

- **API content**

Martinetz et al. utilized NIR-spectroscopy to determine API content in continuous RCDG. The study underlines the ability of NIR spectroscopy to monitor the API content in a RCDG CM line [57]. However, the API content can be quantified at various stages during a manufacturing run. There is no specific need to monitor during RCDG. In theory, an API content control of the final dosage form is sufficient for RTRT.

Granule size distribution and hardness should be monitored in-line during RCDG because either bears information that is necessary to guarantee successful tableting and/or filling.

There are no valid methods to determine GSD and granule hardness in-line to this day and the use of surrogate parameters must be treated carefully.

1.3.4 Residence time distribution in RCDG

As mentioned in section 1.2.5, knowledge of residence time is required to run a CM line. The most important publications on RTD in RCDG will be briefly summarized.

Mangal and Kleinebudde analyzed the RTD in the milling unit of the RCDG in detail. They reported mean residence times between 5.4 and 46.4 seconds depending on material, applied SCF and sieve type [99]. Kruisz et al. reported residence times from the tamping auger to the outlet of the milling unit [56]. The work focuses on RTD-modelling. Experimental data aligns well with the data published by Mangal and Kleinebudde, as based on the experimental set-up similar RTD values were to be expected. Martinetz et al. published a comprehensive analysis of residence time distributions in different unit operations of a CM line equipped with a roll compactor [57]. Residence time between a bucket conveyor transporting material to the roll compactor and the outlet of a roll compactor was accessed at different throughputs. The group found more narrow residence time distribution curves at higher throughputs. A large part of the research was focused on modelling and combining the individual unit operations [57].

A process parameter for which the impact on residence time is not yet characterized, is the impeller speed of the powder inlet unit (see section 1.3.1).

1.4 Real-time particle size determination

As explained, there is limited experimental data on determining the GSD during continuous RCDG. However, particle size information is valuable for many industries and applications. Therefore, numerous methods exist to determine particle size in-line. Table 3 summarizes published efforts to determine granule or particle size distributions continuously in the pharmaceutical environment.

Table 3: Process analyzers for in- or on-line particle or granule size distribution

analytical method	process	source
dynamic image analysis	TSG fluidized bed coating	[100, 101] [102, 103]
laser diffraction	spray drying crystallization, jet mill grinding	[104] [105, 106]
spatial filter velocimetry	RCDG fluidized bed process	[96] [51, 107-110]
focused beam reflectance	fluidized bed granulation	[111]
NIR (correlation)	fluidized bed granulation fluidized bed drying bin blending TSG RCDG	[112-114] [115] [116] [117] [87]
NIR-CI	RCDG	[86]

- **Dynamic Image Analysis (DIA)**

Particle size determination via image analysis refers to methods that utilize 2D-images of a particle for size determination. The term “dynamic” indicates that particles are measured in movement. So called static image analysis are microscopy methods that can be highly precise (e.g. scanning electron microscopes) but time consuming. To measure particles in movement, they must flow individually through the field of a camera. In contrast to static image analysis the particles in movement show random orientation and therefore a bias due to particle shape is minimized [43, 118].

The determination of particle shape is a major advantage of image analysis compared to spectral size determinations [118]. A sufficient amount of particles ($x*10^6$) is necessary to obtain reliable results. A size distribution based on the number of particles is obtained. It can be transformed to a volume based distribution using models. However, the information of particle shape is lost after applying these transformations [43]. DIA is limited to a maximal particle size by the size of the visual field of the camera and to a minimal particle size by the cameras resolution. It is the best method to determine particle/granule sizes of multiple millimeters. The method lacks suitability to determine particle sizes below 15 – 30 µm [43]. Real-time dynamic image analysis in pharmaceutical manufacturing processes is described for TSG [100, 101] and fluidized bed coating [102, 103]. So far, DIA was not applied to RCDG.

- **Laser diffraction spectroscopy**

In laser diffraction spectroscopy, the diffraction behavior of laser light that comes in contact with a particle surface is used to determine the size of the particles. Based on particle size distribution, distinct diffraction patterns can be observed in radial intensity profiles. If circular detector plates are mounted, the diffraction pattern is measured and an algorithm transforms the signal to determine the size of a sphere that would generate this diffraction pattern [119, 120]. Analysis was extended to extract shape information from the diffraction pattern by sensing the azimuthally scattered light intensity. However, no link to a tangible shape parameter (e.g. aspect ratio) was reported yet and relevance of this shape determination remains unproven [118, 121, 122].

Mie scattering and Fraunhofer scattering are two theories which are implemented in the calculation algorithms. Mie scattering is a solution to Maxwell’s equations for scattering

spheres found by Gustav Mie. A detailed explanation would exceed the scope of this thesis. It is important to note that the Mie scattering describes scattering patterns without size limitations. It takes into account refraction phenomena and the refractive index of the material must be known [119, 120].

Fraunhofer scattering / approximation is a simplified expression of Mie scattering. It requires particles to be opaque and at least 10 – 40 times the laser light wavelength in size (depending on source) because only then diffraction at the edges is the only phenomenon that is detected on the detector plates and Mie scattering can therefore be simplified significantly [123]. A common wavelength in laser diffraction is 670 nm [124]. This results in 6.7 to 26.8 µm to be the lowest particle size detectable. Modern equipment also utilizes a second laser light source in the same equipment (e.g. 470 nm) to lower the particle size that can be detected to 4.7 – 18.8 µm using Fraunhofer approximation [119, 120, 124].

Using laser diffraction is fast and comparably easy to conduct. However, the algorithm needed to transform the signal from the detector plates to a particle size is not known to the user. Different algorithms can lead to different results and the user should be well aware of the assumptions and limitations when utilizing Fraunhofer approximation [119].

Ma et al. implemented particle size and shape determination on-line during crystallization and in-line within the jet milling process. The group showed particle growth during crystallization. They also showed breakage caused by implementing a stirrer. In-line measurements in jet milling allowed to monitor changing particle sizes at varying nozzle pressures. This opened the option to control the jet mill process using in-line laser diffraction [105, 106]. On-line laser diffraction was performed by Medendorp et al. for a spray drying process. The work did not focus on implementing laser diffraction for a control strategy and did not investigate the impact of process parameters on the particle size. Main focus of the article is comparing in- and off-line laser diffraction. They observed a difference in results and concluded that comparisons of laser diffraction data from different instruments must always be evaluated with caution [104].

Despite its wide distribution, there are no publications describing in- and on-line laser diffraction in pharmaceutical dry granulation.

- **Spatial filter velocimetry**

Spatial filter velocimetry is a method to determine velocity of moving objects. Its principles were first published by Ator in 1963 [125]. It was linked with fiber-optical spot scanning to determine particle size [126, 127]. Manufacturers of a commercially available spatial filter velocimetry probe define the probes measurement range to 50 – 6000 µm chord length at a velocity of 0.01 – 50 m/s [128].

The principle was applied to fluidized bed processes and research was also conducted in RCDG. Pitfalls of this technique in RCDG was probe positioning in the product stream. As the stream is inhomogeneous and results are highly sensitive to probe position [64, 96]. This is not the case for traditional fluidized bed processes. The particles fluidized during the process repeatedly pass by the probe and if measurements are averaged it is possible to obtain a representative size distribution [51, 64, 96, 107-110].

- **Focused beam reflectance**

Focused beam reflectance measurement measures a particles chord length by utilizing laser light to scan across particles that pass by a probe window. Particles are immersed in a fluid. Upon being hit by the laser beam, the light is reflected. The duration of this reflection is subsequently linked to particle size. As particles need to be dispersed for this measurement, only at-line analysis for a pharmaceutical granulation process is described in literature so far [111]. For processes, in which particles are processed in liquid, the method can be used for in-line determination of particle sizes [129].

- **NIR / NIR-CI**

The published efforts of various groups to correlate in/ and off-line spectral information from NIR spectroscopy were discussed in detail in section 1.3.3.

1.5 Hardness determination

1.5.1 Ribbon microhardness

By definition, the hardness of a material is a characteristic surface property which quantifies the resistance of a material to a permanent shape modification [130, 131]. Mathematically, Martens hardness (HM) is described as the force loaded (F) divided by the projected contact area (A_p) it is loaded on (Equation 6).

Equation 6: Martens Hardness (HM)

$$HM = \frac{F}{A_p} \; / \; N * mm^{-2} \tag{6}$$

Instrumented (micro-) hardness determination is commonly used in the metal industry [130-132]. Aulton was the first to publish on determining the HM using instrumented microhardness determination of tablets [133]. In 1993, Duncan-Hewitt used a Vickers-pyramid to determine tablet hardness [134]. Reports on determination of ribbon hardness are rare [66, 91, 135, 136]. This is possibly due to the popularity of ribbon porosity / solid fraction determination. However, as mentioned before, MCC ribbons of similar density can show a difference in their microhardness [85].

The measurement principle is illustrated in Figure 7. The curve starts at a point of 0 µm indentation height and 0 N loaded force. The loaded force increases as the indenter penetrates into the ribbon. At the maximum force of 2000 mN, the loaded force is kept constant for a specified time (here 5 seconds). The indenter is then retrieved from the sample. During the initial loading, the material is deformed but no information whether this is plastic or elastic deformation can be derived. During the constant phase of maximum force, plastic flow can lead to an increase in indentation height at constant force. In the exemplary curve of Figure 7, the indentation height decreases during retraction of the indenter. This is due to elastic recovery. If the

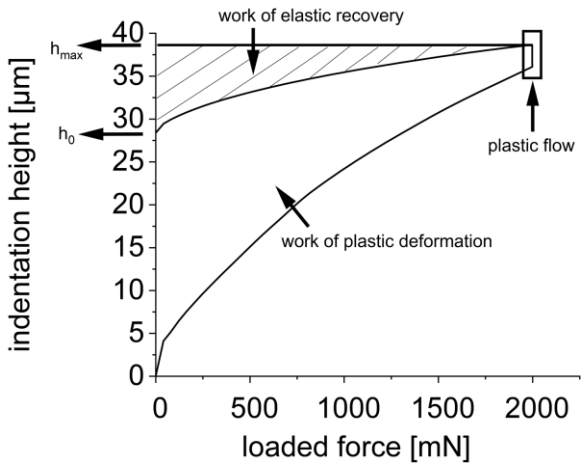

Figure 7: Microindentation measurement plot

tested material shows only plastic properties, the indentation height would be constant at h_{max} during indenter retrievement ($h_{max} = h_0$). A material of only elastic properties is characterized by overlapping curves of loading and un-loading. The area in between the loading and un-loading curve characterizes the work of plastic deformation while the area between the unloading curve and h_{max} characterizes the work of elastic recovery. Therefore, the indentation curve can be used to characterize the plastic and elastic properties of materials with an even surface. The loaded force (F) is logged in the instruments software. Therefore, to determine HM, it is necessary to calculate the projected contact area based on the indenter geometry and the indentation height.

Equation 5 has to be modified according to the measurement method and the used indenter type. The maximum force is set in the analytical method. Determining the area includes a calculation depending on the used geometry of the indenter. The commonly used Vickers indenter is a four-sided pyramid with an angle between opposite faces of the vertex of the pyramid of 136° (Figure 8).

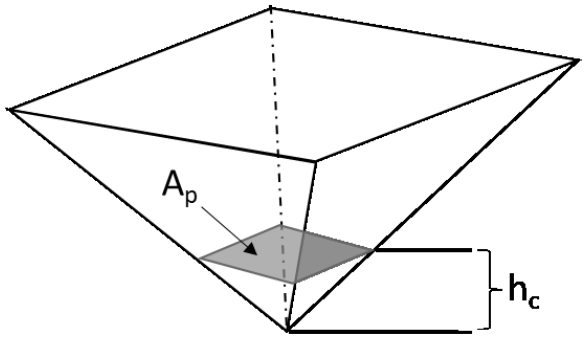

Figure 8: Vickers indenter geometry

The projected area (A_p) has to be determined based on the contact height (h_c). It is obtained by subtracting the elastic indentation height from the maximum indentation height (h_{max}) that is registered by the indenter. The elastic indentation height is the height of the sample that is not in direct contact with the indenter but has deformed as a result of the indentation process (Figure 9). To this date, it cannot be measured during indentation.

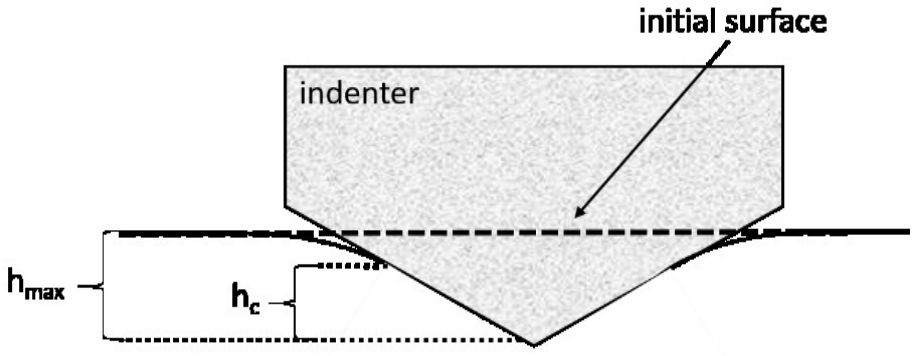

Figure 9: Microindentation. Modified from [137, 138]

The elastic indentation height was first modelled by Oliver & Pharr in 1992 [137]. Modern software uses this model and various adaptations to calculate the elastic indentation height and derive the contact height h_c. The projected area (A_p) can then be calculated, as a detailed formula for a pyramid indenter is shown in Equation 7 [139, 130]. With an angle of $\alpha = 136°$ for a Vickers indenter, the simplified Equation 8 is obtained. Afterwards, HM can be calculated (Equation 6).

Equation 7 A_p for pyramid shape indenter

$$A_p = \frac{4 \times \sin(\frac{\alpha}{2})}{cos^2(\frac{\alpha}{2})} \times {h_c}^2 \; / \; mm^2 \tag{7}$$

Equation 8 A_p for Vickers indenter

$$A_p = \; 26.43 \; \times {h_c}^2 \; / \; mm^2 \tag{8}$$

1.5.2 Granule hardness: granule strength and failure load

The determination of individual particles pressure resistance is possible and a routine examination e.g. in pellet characterization. It is a uniaxial pressure test in which failure of the individual particle occurs by tensile crack opening. Due to high variations a large sample size is required. In comparison to the narrowly size distributed pellets, determination of granules with a broad GSD is more intricate [140].

1993, Adams et al., published a method to determine the strength of an individual agglomerate by using an uniaxial confined compression analysis [141]. A bed of granules is filled into a cylindrical die and pressure is applied from one direction (see Figure 10). Based on work by Dunstan et al., Adams et al. modelled the powder bed as a series of parallel columns [142]. During compression, some columns are load bearing ("active") while others are not ("inactive"). Particles of the active columns then fracture as compression proceeds. Rearrangement takes place as the loaded paths diverge and more and more columns become active [141].

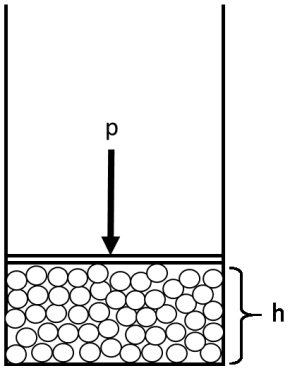

Figure 10 confined uniaxial compression

Opposing the method for single particles, the series of parallel columns introduces radial stress effects from neighboring columns. Based on work by Coulomb and Mohr the Mohr-Coulomb failure criterion was established as "linear equations in principal stress space describing the conditions for which an isotropic material will fail" [143, 144] (Equation 9). τ represents the shear failure stress, τ_0 the sum of cohesive strength, α is a pressure coefficient and P' the compressive strength. Multiplying the pressure coefficient and the compressive strength equals the fractional stress acting at failure planes [141].

Equation 9 Mohr-Coulomb failure criterion

$$\tau = \tau_0 + \alpha P' \tag{9}$$

Failure, as coalescence of micro-cracks will occur at a critical failure force (F_f) in uniaxial direction. The failure force of each column is proportional (proportionality constant k_1) to the failure stress multiplied with the cross section are of the fracture plane (A_f) (Equation 10).

Equation 10 Failure force F_f

$$F_f = k_1 \tau A_f \tag{10}$$

For the total failure force of the column model, individual failure forces of active columns are summed. If the cross section area of all active columns (A^*) equals the cross section area of the cylindrical die (A_0), all columns are failing. An increase in failure force (or pressure as $P = F_f/A_0$) will increase the amount of active columns. Adams introduced a dimensionless proportionality constant k_2. It connects the increment in nominal pressure to the shear failure stress and the applied strain (dh/h) (Equation 11) [141].

Equation 11 proportional behaviour of an increment of pressure at applied strain

$$dP = k_2 \tau \frac{dh}{h} \tag{11}$$

The applied pressure (Equation 9), is assumed to be proportional (proportionality constant k_3) to the nominal pressure P. Combining the assumption made by Adams et al. [141] and the Mohr-Coulomb failure criterion yields Equation 12. τ_0' equals $\frac{k_2}{k_3}\tau_0$, α' equals $k_2\alpha$ and $\in$ is the natural strain ($\ln(\frac{h_0}{h})$). It is a pressure-volume relationship.

Equation 12 Uniaxial confined compression analysis

$$lnP = \ln\left(\frac{\tau_0'}{\alpha'}\right) + \alpha' \times \epsilon + \ln\left(1 - e^{-\alpha' \times \epsilon}\right) \tag{12}$$

In a fully instrumented tablet press, force and displacement data can be tracked. The force recorded for the upper punch can be divided by the cross section area of the die to obtain compression pressure P. The natural strain as the natural logarithmic of the initial divided by the current difference between the punches can also be accessed. As applied by Arndt et al., this opens the uniaxial confined compression analysis to modern tablet press equipment [77]. Figure 11 shows experimental data as lnϵ is plotted against lnP. As Adams et al. state, at large values of ϵ, the plot is linear. With regards to Equation 12, the slope equals α' while τ_0' can be calculated from the intercept value.

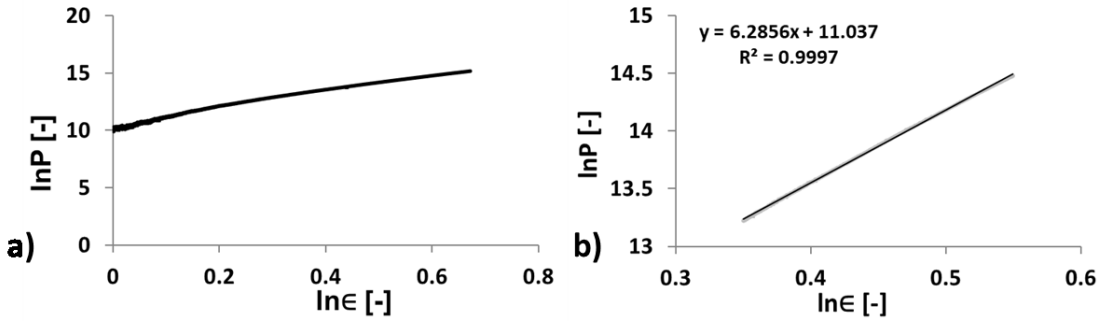

Figure 11 example experimental data of confined uniaxial compression analysis. a) all data points b) linear part separated and linear regression included

To determine the individual failure load (F_{calc}) of a particle, the cohesive granule strength (τ_0') is then multiplied with the particle cross sectional area (Equation 13) [141]. If sieve fractions are analyzed, the mean value of the sieve class is used as particle diameter d_a.

Equation 13 individual particle failure load F_{calc}

$$F_{calc} = \frac{\pi d_a^2}{4}\tau_0' \tag{13}$$

While the analysis is straightforward when an automated tablet press is used for compression analysis, it bears drawbacks as well. The basic model of Adams et al., was not updated with modern theories of cracking or fracture [145]. Furthermore, especially dry granulated material shows a broad particle size distribution and depending on the chosen sieve fractions, results can vary. If sieve classes are chosen too broadly, it might not be possible to assume that no interparticle sliding occurs without cracking of particles. This

questions one of the assumptions on which the theory bases. Choosing sieve classes with large differences in the upper and lower sieve size and broad distributions also lead to systematic errors in calculating the individual failure load based on a mean size value. On the other hand, choosing sieve classes tightly leads to time-consuming experimental procedures. Therefore, the method as stated by Adams et al. and refined by Arndt et al. is the current state-of-the-art in granule strength determination. The method was applied to granules produced using RCDG [77]. However, the granule failure load property was not yet linked to process parameters during the dry granulation process.

1.6 Aims of the Thesis / Outline of the thesis

Based on all considerations laid out in the introduction, there are multiple areas in which research must be conducted in order to obtain a RCDG process, in which CQA's are monitored and controlled in real-time. The following were studied in scope of this thesis:

The granule size and granule hardness can, to this day, not be accessed satisfactorily in RCDG due to lacking of reliable real-time determination methods. Part of this is attributed to difficulties of the material itself (e.g. broad size distribution and high throughput) but there are also no reliable methods to sample dry granulated material representatively during continuous RCDG. Representative in-line sampling would enable analytical methods that cannot process the large throughput in adequate time to be used as on-line measurement tools.

- A new representative in-line sampling approach is presented in section 2 (*Combination of a rotating tube sample divider and dynamic image analysis for continuous on-line determination of granule size distribution*).

To progress in-line and real-time GSD determination, an aim of this thesis was to evaluate and implement different methods of particle size determination in RCDG. The measurement should be robust, sensitive to changes in process parameters and timely. Real-time measurements had to be compared to off-line analytical methods. Dynamic image analysis and laser diffraction were chosen as GSD determination methods.

- On-line dynamic image analysis to monitor the GSD in continuous RCDG is presented in section 2 (*Combination of a rotating tube sample divider and dynamic image analysis for continuous on-line determination of granule size distribution*)

- In-line laser diffraction to monitor the GSD in continuous RCDG is presented in section 3 *(Development and Evaluation of an In-line and On-line Monitoring System for Granule Size Distributions in Continuous Roll Compaction/Dry Granulation Based on Laser Diffraction).*

Based on a suitable real-time GSD determination method, a control strategy was to be developed. Therefore, suitable control valves needed to be found and evaluated. A

controller had to be programmed and the principle of controlling the GSD in continuous RCDG had to be proven.

- A control strategy based on in-line laser diffraction is presented in section 4 *(Options for controlling a continuous dry granulation process using adjustable sieve speed, compaction force or gap width).*

An approach to monitor granule hardness in-line was developed to refine the work on ribbon hardness and the torque of the milling unit during RCDG. Sensitive methods to determine ribbon microhardness and granule failure load were implemented and evaluated. Real-time throughput determination was added and included in hardness determination.

- A monitoring tool for granule hardness is presented in section 5 (*Towards better understanding of the influence of process parameters in roll compaction/ dry granulation on throughput, ribbon microhardness and granule failure load*).

Finally, the knowledge on residence time in RCDG was deepened by adding a detailed analysis of the impact of roll speed and powder inlet impeller speed on residence time.

- Residence time determination is presented in section 6 *(Optimization of residence time distribution in RCDG and an assessment of its applicability in continuous manufacturing).*

1.7 References

1. Qiu Y, Chen Y, Zhang GG, Yu L, Mantri RV. Developing solid oral dosage forms: pharmaceutical theory and practice. 2nd ed. London, UK: Academic press; 2017.
2. Leane M, Pitt K, Reynolds G. A proposal for a drug product Manufacturing Classification System (MCS) for oral solid dosage forms. Pharm Dev Technol. 2015;20(1):12-21. doi:https://doi.org/10.3109/10837450.2014.954728.
3. U.S. Food and Drug Administration. Modernizing the way drugs are made: a transition to continuous manufacturing. 2017. https://www.fda.gov/drugs/news-events-human-drugs/modernizing-way-drugs-are-made-transition-continuous-manufacturing. Accessed 04.08.2020.
4. Kleinebudde P, Khinast J, Rantanen J. Continuous manufacturing of pharmaceuticals. 1st ed. Hoboken, NJ: John Wiley & Sons; 2017.
5. Plumb K. Continuous processing in the pharmaceutical industry - changing the mind set. Chem Eng Res Des. 2005;83(A6):730-8. doi:https://doi.org/10.1205/cherd.04359.
6. Rantanen J, Khinast J. The future of pharmaceutical manufacturing sciences. J Pharm Sci. 2015;104(11):3612-38. doi:https://doi.org/10.1002/jps.24594.
7. Boue K. Global regulatory experience - continuous manufacturing [conference presentation]. 2nd Continuous Manufacturing Conference, February 18, 2020; Freiburg im Breisgau, Germany.
8. International Council on Harmonization. ICH Guidelines. https://www.ich.org/page/ich-guidelines. Accessed 04.08.2020.
9. Yu LX, Amidon G, Khan MA, Hoag SW, Polli J, Raju GK et al. Understanding pharmaceutical Quality by Design. AAPS J. 2014;16(4):771-83. doi:https://doi.org/10.1208/s12248-014-9598-3.
10. Streil F. Real time release for continuous manufacturing of direct compression tablets [conference presentation]. 2nd Continuous Manufacturing Conference, February 18, 2020; Freiburg im Breisgau, Germany.
11. Ierapetritou M, Muzzio F, Reklaitis G. Perspectives on the continuous manufacturing of powder-based pharmaceutical processes. AIChE J. 2016;62(6):1846-62. doi:https://doi.org/10.1002/aic.15210.
12. Pishnamazi M, Casilagan S, Clancy C, Shirazian S, Iqbal J, Egan D et al. Microcrystalline cellulose, lactose and lignin blends: Process mapping of dry granulation via roll compaction. Powder Technol. 2019;341:38-50. doi:https://doi.org/10.1016/j.powtec.2018.07.003.
13. Lee SL, O'Connor TF, Yang XC, Cruz CN, Chatterjee S, Madurawe RD et al. Modernizing pharmaceutical manufacturing: from batch to continuous production. J Pharm Innov. 2015;10(3):191-9. doi:https://doi.org/10.1007/s12247-015-9215-8.
14. Schaber SD, Gerogiorgis DI, Ramachandran R, Evans JMB, Barton PI, Trout BL. Economic analysis of integrated continuous and batch pharmaceutical manufacturing: a case study. Ind Eng Chem Res. 2011;50(17):10083-92. doi:https://doi.org/10.1021/ie2006752.
15. Dahlgren G. Development of continuous manufacturing & real time release tests for tablets [conference presentation]. 2nd Continuous Manufacturing Conference, February 18, 2020; Freiburg im Breisgau, Germany.
16. Hernan D. Continuous manufacturing: Challenges and opportunities. EMA perspective [conference presentation]. 3rd FDA/PQRI Conference on Advancing Product Quality, 22-24 March, 2017 Rockville, MD, USA.
17. U.S. Food and Drug Administration. Advancement of emerging technology applications for pharmaceutical innovation and modernization: guidance for industry. 2017. https://www.fda.gov/files/drugs/published/Advancement-of-Emerging-Technology-Applications-for-Pharmaceutical-Innovation-and-Modernization-Guidance-for-Industry.pdf. Accessed 03.08.2020.

18. Lee SL. Current FDA perspective for continuous manufacturing [conference presentation]. MIT-CMAC 2nd International Symposium on Continuous Manufacturing of Pharmaceuticals, September 26-27, 2016; Cambridge, MA, USA2016.
19. U.S. Food and Drug Administration. Guidance for industry, PAT- a framework for innovative pharmaceutical development, manufacturing and quality assurance. 2004. https://www.fda.gov/media/71012/download. Accessed 03.08.2020.
20. U.S. Food and Drug Administration. Quality considerations for continuous manufacturing guidance for industry. 2019. https://www.fda.gov/media/121314/download. Accessed 03.08.2020.
21. O'Connor TF. FDA's continuous manufacturing journey [conference presentation]. 2nd APV Continuous Manufacturing Conference, February 18, 2020; Freiburg im Breisgau, Germany.
22. U.S. Food and Drug Administration. Guidance for industry - investigating out-of-specification (OOS) test results for pharmaceutical production. 2006. https://www.fda.gov/media/71001/download. Accessed 05.08.2020.
23. Rivera PLE. Cleaning validation in continuous manufacturing. Pharm Technol. 2016;40(11):34-42,55.
24. Jimenez L. Microbial contamination control in the pharmaceutical industry. 1st ed. Boca Raton: CRC Press; 2004.
25. European Medicines Agency. Assessment report Symkevi. 2018. https://www.ema.europa.eu/en/documents/assessment-report/symkevi-epar-public-assessment-report_en.pdf. Accessed 04.08.2020.
26. European Medicines Agency. Assessment report Orkambi. 2015. https://www.ema.europa.eu/en/documents/assessment-report/orkambi-epar-public-assessment-report_en.pdf. Accessed 04.08.2020.
27. Vertex Pharmaceuticals Incorporated. Product monograph Orkambi. 2019. https://pi.vrtx.com/files/Canadapm_orkambi_ci_en.pdf. Accessed 04.08.2020.
28. PharmTech.com. FDA approves tablet production on Janssen continuous manufacturing line. 2016. http://www.pharmtech.com/fda-approves-tablet-production-janssen-continuous-manufacturing-line. Accessed 04.08.2020.
29. ISPE. Continuous OSD manufacturing - a product & patient perspective. 2018. https://ispe.org/pharmaceutical-engineering/ispeak/continuous-osd-manufacturing-product-patient-perspective. Accessed 04.08.2020.
30. Janssen Pharmaceutical Companies. Highlights of prescribing information Prezista. 2018. http://www.janssenlabels.com/package-insert/product-monograph/prescribing-information/PREZISTA-pi.pdf. Accessed 04.08.2020.
31. Almaya A. Current perspectives on continuous manufacturing [conference presentation]. 2nd Continuous Manufacturing Conference, February 18, 2020; Freiburg im Breisgau, Germany.
32. Eli Lilly Canada. Patient medication information Verzenio. 2020. http://pi.lilly.com/ca/verzenio-ca-pmi.pdf. Accessed 04.08.2020.
33. Vertex Pharmaceuticals Incorporated. Product monograph Symdeko. 2020. https://pi.vrtx.com/files/Canadapm_symdeko_en.pdf. Accessed 04.08.2020.
34. Bechmann G. Pfizer continuous manufacturing container model - PCMM [conference presentation]. 2nd APV Conference on Continuous Manufacturing, February 18, 2020; Freiburg im Breisgau, Germany.
35. Garcia T. Industry experiences with continuous manufacturing. FDA/Xavier PharmaLink Conference, March 13, 2019; Cincinnati, OH, USA.
36. U.S. Food and Drug Administration. Daurismo summary review. 2018. https://www.accessdata.fda.gov/drugsatfda_docs/nda/2018/210656Orig1s000SumR.pdf. Accessed 04.08.2020.
37. Portier C, Pandelaere K, Delaet U, Vigh T, Kumar A, Di Pretoro G, De Beer T, Vervaet C and Vanhoorne V. Continuous twin screw granulation: Influence of process and formulation variables

on granule quality attributes of model formulations. Int J Pharm. 2020;576:118981. doi:https://doi.org/10.1016/j.ijpharm.2019.118981.
38. Krishnan H. ConsiGma continuous manufacturing OSD - road to operational excellence & accelerated drug development. 2019. https://www.ipa-india.org/static-files/pdf/event/gmp2019d.pdf. Accessed 11.08.2020.
39. Pfizer Inc. Highlights of prescribing information Lorbrena. 2018. https://www.accessdata.fda.gov/drugsatfda_docs/label/2018/210868s000lbl.pdf. Accessed 03.08.2020.
40. Laske S, Paudel A, Scheibelhofer O, Sacher S, Hoermann T, Khinast J, Kelly A, Rantanen J, Korhonen O, Stauffer F and De Leersynder F. A review of PAT strategies in secondary solid oral dosage manufacturing of small molecules. J Pharm Sci. 2017;106(3):667-712. doi:https://doi.org/10.1016/j.xphs.2016.11.011.
41. Fonteyne M, Vercruysse J, De Leersnyder F, Van Snick B, Vervaet C, Remon JP, and De Beer T. Process analytical technology for continuous manufacturing of solid-dosage forms. Trac-Trend Anal Chem. 2015;67:159-66. doi:https://doi.org/10.1016/j.trac.2015.01.011.
42. Nicolaï N, Nopens I, Verstraeten M, De Beer T. Process control levels for continuous pharmaceutical tablet manufacturing. In: Mary T. am Ende David Jam E, editor. Chemical Engineering in the Pharmaceutical Industry: Drug Product Design, Development, Modeling. 2nd ed. Hoboken, NJ, USA2019. p. 561-84.
43. Allen T. Powder sampling and particle size determination. 1 ed. Amsterdam: Elsevier; 2003.
44. Shah S, Shridhar P, Gohil D. Control chart: A statistical process control tool in pharmacy. Asian J Pharm Sci. 2014;4(3). doi:https://doi.org/10.4103/0973-8398.72116
45. Agachi PS, Cristea MV. Basic process engineering control. Berlin/Boston: Walter de Gruyter; 2014.
46. Ang KH, Chong G, Yun L. PID control system analysis, design, and technology. IEEE T Contr Sys T. 2005;13(4):559-76. doi:https://doi.org/10.1109/TCST.2005.847331.
47. The International Council for Harmonisation. ICH Q8 Pharmaceutical development. 2017. https://www.ema.europa.eu/en/documents/scientific-guideline/international-conference-harmonisation-technical-requirements-registration-pharmaceuticals-human-use_en-11.pdf. Accessed 03.08.2020.
48. Myerson AS, Krumme M, Nasr M, Thomas H, Braatz RD. Control systems engineering in continuous pharmaceutical manufacturing May 20–21, 2014 Continuous Manufacturing Symposium. J Pharm Sci. 2015;104(3):832-9. doi:https://doi.org/10.1002/jps.24311.
49. Lakerveld R, Benyahia B, Braatz RD, Barton PI. Model-based design of a plant-wide control strategy for a continuous pharmaceutical plant. AIChE J. 2013;59(10):3671-85. doi:https://doi.org/10.1002/aic.14107.
50. Lakerveld R, Benyahia B, Heider PL, Zhang H, Wolfe A, Testa CJ et al. The application of an automated control strategy for an integrated continuous pharmaceutical pilot plant. Org Process Res Dev. 2015;19(9):1088-100. doi:https://doi.org/10.1021/op500104d.
51. Reimers T, Thies J, Stöckel P, Dietrich S, Pein-Hackelbusch M, Quodbach J. Implementation of real-time and in-line feedback control for a fluid bed granulation process. Int J Pharm. 2019;567:118452. doi:https://doi.org/10.1016/j.ijpharm.2019.118452.
52. Roggo Y, Pauli V, Jelsch M, Pellegatti L, Elbaz F, Ensslin S, Kleinebudde P and Krumme M. Continuous manufacturing process monitoring of pharmaceutical solid dosage form: A case study. J Pharmaceut Biomed. 2020;179:112971. doi:https://doi.org/10.1016/j.jpba.2019.112971.
53. Van Snick B, Kumar A, Verstraeten M, Pandelaere K, Dhondt J, Di Pretoro G, De Beer T, Vervaet C and Vanhoorne V. Impact of material properties and process variables on the residence time distribution in twin screw feeding equipment. Int J Pharm. 2019;556:200-16. doi:https://doi.org/10.1016/j.ijpharm.2018.11.076.

54. Engisch W, Muzzio F. Using residence time distributions (RTDs) to address the traceability of raw materials in continuous pharmaceutical manufacturing. J Pharm Innov. 2016;11(1):64-81. doi:https://doi.org/10.1007/s12247-015-9238-1.
55. Levenspiel O. Mixed models to represent flow of fluids through vessels. Can J Chem Eng. 1962;40(4):135-8. doi:https://doi.org/10.1002/cjce.5450400402.
56. Kruisz J, Rehrl J, Sacher S, Aigner I, Horn M, Khinast JG. RTD modeling of a continuous dry granulation process for process control and materials diversion. Int J Pharm. 2017;528(1-2):334-44. doi:https://doi.org/10.1016/j.ijpharm.2017.06.001.
57. Martinetz MC, Karttunen AP, Sacher S, Wahl P, Ketolainen J, Khinast JG and Korhonen O. RTD-based material tracking in a fully-continuous dry granulation tableting line. Int J Pharm. 2018;547(1):469-79. doi:https://doi.org/10.1016/j.ijpharm.2018.06.011.
58. Kleinebudde P. Roll compaction/dry granulation: pharmaceutical applications. Eur J Pharm Biopharm. 2004;58(2):317-26. doi:https://doi.org/10.1016/j.ejpb.2004.04.014.
59. Malkowska S, Khan K. Effect of re-compression on the properties of tablets prepared by dry granulation. Drug Dev Ind Pharm. 1983;9(3):331-47. doi:https://doi.org/10.3109/03639048309044678
60. Sun C, Himmelspach MW. Reduced tabletability of roller compacted granules as a result of granule size enlargement. J Pharm Sci. 2006;95(1):200-6. doi:https://doi.org/10.1002/jps.20531.
61. Mosig J, Kleinebudde P. Critical evaluation of root causes of the reduced compactability after roll compaction/dry granulation. J Pharm Sci. 2015;104(3):1108-18. doi:https://doi.org/10.1002/jps.24321.
62. Sun C, Kleinebudde P. Mini review: Mechanisms to the loss of tabletability by dry granulation. Eur J Pharm Biopharm. 2016;106:9-14. doi:https://doi.org/10.1016/j.ejpb.2016.04.003.
63. Patel S, Dahiya S, Sun CC, Bansal AK. Understanding size enlargement and hardening of granules on tabletability of unlubricated granules prepared by dry granulation. J Pharm Sci. 2011;100(2):758-66. doi: https://doi.org/10.1002/jps.22315.
64. Mangal H, Derksen E, Lura A, Kleinebudde P. In-line particle size measurement in dry granulation: evaluation of probe position [conference poster]. 10th World Meeting on Pharmaceutics, Biopharmaceutics and Pharmaceutical Technology, April 4 - 7, 2016; Glasgow, UK.
65. Wiedey R, Kleinebudde P. Infrared thermography — a new approach for in-line density measurement of ribbons produced from roll compaction. Powder Technology. 2018;337:17-24. doi:https://doi.org/10.1016/j.powtec.2017.01.052.
66. Freitag F, Reincke K, Runge J, Grellmann W, Kleinebudde P. How do roll compaction/dry granulation affect the tableting behaviour of inorganic materials?: Microhardness of ribbons and mercury porosimetry measurements of tablets. Eur J Pharm Sci. 2004;22(4):325-33. doi:https://doi.org/10.1016/j.ejps.2004.04.001.
67. Wiedey R, Šibanc R, Wilms A, Kleinebudde P. How relevant is ribbon homogeneity in roll compaction/dry granulation and can it be influenced? Eur J Pharm Biopharm. 2018;133:232-9. doi:https://doi.org/10.1016/j.ejpb.2018.10.021.
68. Freeman T, Vom Bey H, Hanish M, Brockbank K, Armstrong B. The influence of roller compaction processing variables on the rheological properties of granules. Asian J Pharm Sci. 2016;11(4):516-27. doi:https://doi.org/10.1016/j.ajps.2016.03.002.
69. Kazemi P, Khalid MH, Gago AP, Kleinebudde P, Jachowicz R, Szlęk J and Medyk A. Effect of roll compaction on granule size distribution of microcrystalline cellulose–mannitol mixtures: computational intelligence modeling and parametric analysis. Drug Des Devel Ther. 2017;11:241. doi:https://doi.org/10.2147/DDDT.S124670.
70. Hopkins M. Loss in weight feeder systems. Meas Control. 2006;39(8):237-40. doi:https://doi.org/10.1177/002029400603900801

71. Blackshields CA, Crean AM. Continuous powder feeding for pharmaceutical solid dosage form manufacture: a short review. Pharm Dev Technol. 2018;23(6):554-60. doi:https://doi.org/10.1080/10837450.2017.1339197.
72. Mangal H, Kleinebudde P. Is the adjustment of the impeller speed a reliable attempt to influence granule size in continuous dry granulation? Adv Powder Technol. 2018;29(6):1339-47. doi:https://doi.org/10.1016/j.apt.2018.02.029.
73. Fassihi A, Kanfer I. Effect of compressibility and powder flow properties on tablet weight variation. Drug Dev Ind Pharm. 1986;12(11-13):1947-66. doi:https://doi.org/10.3109/03639048609042619
74. Tan S, Newton J. Powder flowability as an indication of capsule filling performance. Int J Pharm. 1990;61(1-2):145-55. doi:https://doi.org/10.1016/0378-5173(90)90053-7.
75. European Pharmacopoeia. 2.9.16 Flowability. 9th ed. Strasbourg: Councel of Europe; 2017.
76. Shekunov BY, Chattopadhyay P, Tong HH, Chow AH. Particle size analysis in pharmaceutics: principles, methods and applications. Pharm Res. 2007;24(2):203-27. doi:https://doi.org/10.1007/s11095-006-9146-7.
77. Arndt O-R, Baggio R, Adam AK, Harting J, Franceschinis E, Kleinebudde P. Impact of different dry and wet granulation techniques on granule and tablet properties: a comparative study. J Pharm Sci. 2018;107(12):3143-52. doi:https://doi.org/10.1016/j.xphs.2018.09.006.
78. Wikberg M, Alderborn G. Compression characteristics of granulated materials. IV. The effect of granule porosity on the fragmentation propensity and the compatibility of some granulations. Int J Pharm. 1991;69(3):239-53. doi:https://doi.org/10.1016/0378-5173(91)90366-V.
79. Ansari MA, Stepanek F. The effect of granule microstructure on dissolution rate. Powder Technol. 2008;181(2):104-14. doi:https://doi.org/10.1016/j.powtec.2006.12.012.
80. Gupta A, Peck GE, Miller RW, Morris KR. Real-time near-infrared monitoring of content uniformity, moisture content, compact density, tensile strength, and young's modulus of roller compacted powder blends. J Pharm Sci. 2005;94(7):1589-97. doi:https://doi.org/10.1002/jps.20375.
81. Jaminet F, Hess H. Studies on compacting and dry granulation. Pharm Acta Helv. 1966;41:39-58.
82. Wiedey R, Šibanc R, Kleinebudde P. Laser based thermo-conductometry as an approach to determine ribbon solid fraction off-line and in-line. Int J Pharm. 2018;547(1):330-7. doi:https://doi.org/10.1016/j.ijpharm.2018.06.014.
83. Wiedey R, Kleinebudde P. Potentials and limitations of thermography as an in-line tool for determining ribbon solid fraction. Powder Technol. 2018. doi:https://doi.org/10.1016/j.powtec.2018.03.047.
84. Gupta A, Peck GE, Miller RW, Morris KR. Nondestructive measurements of the compact strength and the particle-size distribution after milling of roller compacted powders by near-infrared spectroscopy. J Pharm Sci. 2004;93(4):1047-53. doi:https://doi.org/10.1002/jps.20003.
85. Gupta A, Peck GE, Miller RW, Morris KR. Influence of ambient moisture on the compaction behavior of microcrystalline cellulose powder undergoing uni-axial compression and roller-compaction: a comparative study using near-infrared spectroscopy. J Pharm Sci. 2005;94(10):2301-13. doi:https://doi.org/10.1002/jps.20430.
86. Khorasani M, Amigo JM, Sun CC, Bertelsen P, Rantanen J. Near-infrared chemical imaging (NIR-CI) as a process monitoring solution for a production line of roll compaction and tableting. Eur J Pharm Biopharm. 2015;93:293-302. doi:https://doi.org/10.1016/j.ejpb.2015.04.008.
87. Khorasani M, Amigo JM, Bertelsen P, Sun CC, Rantanen J. Process optimization of dry granulation based tableting line: extracting physical material characteristics from granules, ribbons and tablets using near-IR (NIR) spectroscopic measurement. Powder Technol. 2016;300:120-5. doi:https://doi.org/10.1016/j.powtec.2016.03.004.

88. Hakanen A, Laine E. Acoustic emission during powder Compaction and its frequency spectral analysis. Drug Dev Ind Pharm. 1993;19(19):2539-60. doi:https://doi.org/10.3109/03639049309047200.
89. Hakanen A, Laine E. Acoustic characterization of a microcrystalline cellulose powder during and after its compression. Drug Dev Ind Pharm. 1995;21(13):1573-82. doi:https://doi.org/10.3109/03639049509069247.
90. Salonen J, Salmi K, Hakanen A, Laine E, Linsaari K. Monitoring the acoustic activity of a pharmaceutical powder during roller compaction. Int J Pharm. 1997;153(2):257-61. doi:https://doi.org/10.1016/S0378-5173(97)00086-0.
91. Müller N. Untersuchungen zur Prozessüberwachung und - regulierung bei der Walzenkompaktierung mittels Drehmomenterfassung an der Granuliereinheit. PhD thesis (in german), title translates to "Investigations on process monitoring and control during roll compaction using the torque of the granulation unit.": Universitäts - und Landesbibliothek Bonn; 2012.
92. Schorr F. Walzenkompaktierung: Untersuchungen zur in-line Überwachung der Schülpenfestigkeit mittels Vibrations - und Schalldruckanalyse im Bereich der Zerkleinerungseinheit. PhD thesis (in german), title translates to "Roll compaction: Investigations for an in-line control tool of ribbon hardness using vibration and acoustics analysis in the granulation unit.": Rheinische Friedrich-Wilhelms-Universität Bonn; 2016.
93. Lim H, Dave VS, Kidder L, Lewis EN, Fahmy R, Hoag SW. Assessment of the critical factors affecting the porosity of roller compacted ribbons and the feasibility of using NIR chemical imaging to evaluate the porosity distribution. Int J Pharm. 2011;410(1-2):1-8. doi:https://doi.org/10.1016/j.ijpharm.2011.02.028.
94. Souihi N, Nilsson D, Josefson M, Trygg J. Near-infrared chemical imaging (NIR-CI) on roll compacted ribbons and tablets–multivariate mapping of physical and chemical properties. Int J Pharm. 2015;483(1-2):200-11. doi:https://doi.org/10.1016/j.ijpharm.2015.02.006.
95. Austin J, Gupta A, McDonnell R, Reklaitis GV, Harris MT. The use of Near-Infrared and microwave resonance sensing to monitor a continuous roller compaction process. J Pharm Sci. 2013;102(6):1895-904. doi:https://doi.org/10.1002/jps.23536.
96. Mangal H. Implementierung der Trockengranulierung in eine kontinuierliche Produktionsanlage für feste Arzneiformen. PhD thesis (in german), title translates to "Implementation of dry granulation in a continuous manufacturing line for solid oral dosage forms". PhD thesis Heinrich Heine University Düsseldorf. 2018.
97. Acevedo D, Muliadi A, Giridhar A, Litster JD, Romañach R. Evaluation of three approaches for real-time monitoring of roller compaction with near-infrared spectroscopy. AAPS PharmSciTech. 2012;13(3):1005-12. doi:https://doi.org/10.1208/s12249-012-9825-0.
98. Patel S, Sun CC. Macroindentation hardness measurement—modernization and applications. Int J Pharm. 2016;506(1-2):262-7. doi:https://doi.org/10.1016/j.ijpharm.2016.04.068.
99. Mangal H, Kleinebudde P. Experimental determination of residence time distribution in continuous dry granulation. Int J Pharm. 2017;524(1-2):91-100. doi:https://doi.org/10.1016/j.ijpharm.2017.03.085.
100. Madarasz L, Nagy ZK, Hoffer I, Szabo B, Csontos I, Pataki H et al. Real-time feedback control of twin-screw wet granulation based on image analysis. Int J Pharm. 2018;547(1-2):360-7. doi:https://doi.org/10.1016/j.ijpharm.2018.06.003.
101. Madarász L, Köte Á, Gyürkés M, Farkas A, Hambalkó B, Pataki H et al. Videometric mass flow control: a new method for real-time measurement and feedback control of powder micro-feeding based on image analysis. Int J Pharm. 2020:119223. doi:https://doi.org/10.1016/j.ijpharm.2020.119223.
102. Naidu VR, Deshpande RS, Syed MR, Wakte PS. Real-time imaging as an emerging process analytical technology tool for monitoring of fluid bed coating process. Pharm Dev Technol. 2018;23(6):596-601. doi:https://doi.org/10.1080/10837450.2017.1287730

103. Možina M, Tomaževič D, Leben S, Pernuš F, Likar B. Digital imaging as a process analytical technology tool for fluid-bed pellet coating process. Eur J Pharm Sci. 2010;41(1):156-62. doi:https://doi.org/10.1016/j.ejps.2010.06.001.
104. Medendorp J, Bric J, Connelly G, Tolton K, Warman M. Development and beyond: strategy for long-term maintenance of an online laser diffraction particle size method in a spray drying manufacturing process. J Pharmaceut Biomed. 2015;112:79-84. doi:https://doi.org/10.1016/j.jpba.2015.04.019.
105. Ma Z, Merkus HG, van der Veen HG, Wong M, Scarlett B. On-line Measurement of Particle Size and Shape using Laser Diffraction. Part Part Syst Char. 2001;18(5-6):243-7. doi:https://doi.org/10.1002/1521-4117(200112)18:5/6<243::AID-PPSC243>3.0.CO;2-4.
106. Ma Z, van der Veen H, G. Merkus H, Scarlett B. In-line Particle Size Measurement for Control of Jet Milling. Part Part Syst Char. 2001;18(2):99-106. doi:https://doi.org/10.1002/1521-4117(200107)18:2<99::AID-PPSC99>3.0.CO;2-4.
107. Reimers T, Thies J, Dietrich S, Quodbach J, Pein-Hackelbusch M. Evaluation of in-line particle measurement with an SFT-probe as monitoring tool for process automation using a new time-based buffer approach. Eur J Pharm Sci. 2019;128:162-70. doi:https://doi.org/10.1016/j.ejps.2018.11.026.
108. Reimers T. Entwicklung einer Regelstrategie für die Partikelgrößenregelung während des Wirbelschichtgranulationsprozesses und Implementierung für einen effizienten Prozess. PhD thesis in german, title translates to "Development of a control strategy for particle size control during fluidized bed granulation and its implementation for an efficient process.": Heinrich Heine University Düsseldorf; 2020.
109. Närvänen T, Lipsanen T, Antikainen O, Räikkönen H, Heinämäki J, Yliruusi J. Gaining fluid bed process understanding by in-line particle size analysis. J Pharm Sci. 2009;98(3):1110-7. doi:https://doi.org/10.1002/jps.21486.
110. Burggraeve A, Monteyne T, Vervaet C, Remon JP, De Beer T. Process analytical tools for monitoring, understanding, and control of pharmaceutical fluidized bed granulation: a review. Eur J Pharm Biopharm. 2013;83(1):2-15. doi:https://doi.org/10.1016/j.ejpb.2012.09.008.
111. Hu X, Cunningham JC, Winstead D. Study growth kinetics in fluidized bed granulation with at-line FBRM. Int J Pharm. 2008;347(1-2):54-61. doi:https://doi.org/10.1016/j.ijpharm.2007.06.043.
112. Paul Findlay W, Peck GR, Morris KR. Determination of fluidized bed granulation end point using near-infrared spectroscopy and phenomenological analysis. J Pharm Sci. 2005;94(3):604-12. doi:https://doi.org/10.1002/jps.20276.
113. Rantanen J, Yliruusi J. Determination of particle size in a fluidized bed granulator with a near infrared set-up. Pharm Pharmacol Commun. 1998;4(2):73-5. doi:https://doi.org/10.1111/j.2042-7158.1998.tb00509.x.
114. Alcalà M, Blanco M, Bautista M, González JM. On-line monitoring of a granulation process by NIR spectroscopy. J Pharm Sci. 2010;99(1):336-45. doi:https://doi.org/10.1002/jps.21818. .
115. Nieuwmeyer FJ, Damen M, Gerich A, Rusmini F, van der Voort Maarschalk K, Vromans H. Granule characterization during fluid bed drying by development of a near infrared method to determine water content and median granule size. Pharm Res. 2007;24(10):1854-61. doi:https://doi.org/10.1007/s11095-007-9305-5.
116. Rosas JG, Blanco M, Gonzalez JM, Alcalà M. Real-time determination of critical quality attributes using near-infrared spectroscopy: a contribution for Process Analytical Technology (PAT). Talanta. 2012;97:163-70. doi:https://doi.org/10.1016/j.talanta.2012.04.012.
117. Pauli V, Roggo Y, Kleinebudde P, Krumme M. Real-time monitoring of particle size distribution in a continuous granulation and drying process by near infrared spectroscopy. Eur J Pharm Biopharm. 2019;141:90-9. doi:https://doi.org/10.1016/j.ejpb.2019.05.007.

118. Yu W, Hancock BC. Evaluation of dynamic image analysis for characterizing pharmaceutical excipient particles. Int J Pharm. 2008;361(1):150-7. doi:https://doi.org/10.1016/j.ijpharm.2008.05.025.
119. Sparks DL. Advances in agronomy. 1st ed. Cambridge, MA, USA: Academic Press; 2018.
120. de Boer GB, de Weerd C, Thoenes D, Goossens HW. Laser diffraction spectrometry: Fraunhofer diffraction versus Mie scattering. Part Part Syst Char. 1987;4(1-4):14-9. doi:https://doi.org/10.1002/ppsc.19870040104.
121. Ma ZH, Merkus HG, Scarlett B. Extending laser diffraction for particle shape characterization: technical aspects and application. Powder Technol. 2001;118(1-2):180-7. doi:https://doi.org/10.1016/S0032-5910(01)00309-6.
122. Heffels CM, Heitzmann D, Dan Hirleman E, Scarlett B. The use of azimuthal intensity variations in diffraction patterns for particle shape characterization. Part Part Syst Char. 1994;11(3):194-9. doi:https://doi.org/10.1002/ppsc.19940110305.
123. Xu R. Particle characterization: light scattering methods. New York, NY, USA: Springer Science & Business Media; 2001.
124. Malvern Panalytical. Mastersizer 3000 - Smarter Particle sizing. https://www.malvernpanalytical.com/en/products/product-range/mastersizer-range/mastersizer-3000. Accessed 04.08.2020.
125. Ator J. Image-velocity sensing with parallel-slit reticles. JOSA. 1963;53(12):1416-22. doi:https://doi.org/10.1364/JOSA.53.001416
126. Petrak D. Simultaneous measurement of particle size and particle velocity by the spatial filtering technique. Part Part Syst Char. 2002;19(6):391-400. doi:https://doi.org/10.1002/ppsc.200290002.
127. Petrak D, Dietrich S, Eckardt G, Köhler M. In-line particle sizing for real-time process control by fibre-optical spatial filtering technique (SFT). Adv Powder Technol. 2011;22:203-8. doi:https://doi.org/10.1016/j.apt.2010.11.002.
128. Malvern Panalytical. Inline Particle Measurement Valuable Insight in your process. https://www.malvernpanalytical.com/en/products/product-range/parsum-range. Accessed 04.08.2020.
129. Sankaranarayanan S, Likozar B, Navia R. Real-time particle size analysis using the focused beam reflectance measurement probe for in situ fabrication of polyacrylamide–filler composite materials. Sci Rep. 2019;9(1):1-12. doi:https://doi.org/10.1038/s41598-019-46451-x.
130. Broitman E. Indentation hardness measurements at macro-, micro-, and nanoscale: a critical overview. Ribol Lett. 2017;65:article number 23. doi:https://doi.org/10.1007/s11249-016-0805-5.
131. Walley SM. Historical origins of indentation hardness testing. J Mater Sci Technol. 2012;28(9-10):1028-44. doi:https://doi.org/10.1179/1743284711Y.0000000127
132. DIN EN ISO 14577 - 1:2015-11 Metallic materials - Instrumented indentation test for hardness and materials parameters - Part 1: Test method (ISO 14577-1:2015).
133. Aulton M. Indentation hardness profiles across the faces of some compressed tablets. Pharma Acta Helv. 1981;56(4-5):133-6.
134. Duncan-Hewitt WC, Weatherly GC. Modeling the uniaxial compaction of pharmaceutical powders using the mechanical properties of single crystals. I: ductile materials. J Pharm Sci. 1990;79(2):147-52. doi:https://doi.org/10.1002/jps.2600790214.
135. Wöll F. Entwicklung von Methoden zur Charakterisierung von Schülpen. PhD thesis (in german), title tranlates to "Development of methods to charaterize ribbons": Martin-Luther-University Halle-Wittenberg; 2003.
136. Freitag F. Walzenkompaktieren und Trockengranulieren zur Verbesserung des Tablettierverhaltens anorganischer Hilfsstoffe am Beispiel von Magnesiumcarbonat und Calciumcarbonat. PhD thesis in german, title translates to "Roll compaction/dry granulation in

order to improve the tabletting behaviour of anorganic excipients, exemplarily on magnesium- and calciumcarbonate.": Martin-Luther-University Halle-Wittenberg; 2004.
137. Oliver WC, Pharr GM. An improved technique for determining hardness and elastic modulus using load and displacement sensing indentation experiments. Mater Res. 1992;7(6):1564-83. doi:https://doi.org/10.1557/JMR.1992.1564.
138. Mallick S, Anoop MB, Balaji Rao K. Early age creep of cement paste - governing mechanisms and role of water - a microindentation study. Cement Concrete Res. 2019;116:284-98. doi:https://doi.org/10.1016/j.cemconres.2018.12.004.
139. Griepentrog M, Ullner C, Duck A. Instrumented indentation test for hardness and materials parameter from millinewtons to kilonewtons. VDI Berichte. 2002;1685:105-12.
140. Salako M, Podczeck F, Newton JM. Investigations into the deformability and tensile strength of pellets. Int J Pharm. 1998;168(1):49-57. doi:https://doi.org/10.1016/S0378-5173(98)00077-5.
141. Adams MJ, Mullier MA, Seville JPK. Agglomerate strength measurement using a uniaxial confined compression test. Powder Technol. 1994;78(1):5-13. doi:https://doi.org/10.1016/0032-5910(93)02777-8.
142. Dunstan T, Arthur J, Dalili A, Ogunbekun O, Wong R. Limiting mechanisms of slow dilatant plastic shear deformation of granular media. Nature. 1988;336(6194):52-4. doi:https://doi.org/10.1038/336052a0.
143. Labuz JF, Zang A. Mohr–Coulomb failure criterion. Rock Mech Rock Eng. 2012;45(6):975-9. doi:https://doi.org/10.1007/s00603-012-0281-7.
144. Mohr O. Welche Umstände bedingen die Elastizitätsgrenze und den Bruch eines Materials. Zeitschrift des VDI. 1900;46(1524-1530):1572-7.
145. Feng X-T, Kong R, Yang C, Zhang X, Wang Z, Han Q et al. A three-dimensional failure criterion for hard rocks under true triaxial compression. Rock Mech Rock Eng. 2020;53(1):103-11. doi:https://doi.org/10.1007/s00603-019-01903-8.

2 Combination of a rotating tube sample divider and dynamic image analysis for continuous on-line determination of granule size distribution

Annika Wilms[a,b], Klaus Knop[a], Peter Kleinebudde[a]

[a] Institute of Pharmaceutics and Biopharmaceutics, Heinrich Heine University, Universitaetsstrasse 1, 40225 Duesseldorf, Germany

[b] INVITE GmbH, Drug Delivery Innovation Center (DDIC), CHEMPARK Building W32, 51364 Leverkusen, Germany

2.1 Pretext

The following research paper has been published by the International Journal of Pharmaceutics: X in Volume 1 (2019).

https://doi.org/10.1016/j.ijpx.2019.100029

Evaluation of authorship:

author	idea [%]	study design [%]	experimental [%]	evaluation [%]	manuscript [%]
Annika Wilms	40	70	90	80	60
Klaus Knop	30	20	10	20	20
Peter Kleinebudde	30	10	0	0	20

Evaluation of Copyright permission:

Combination of a rotating tube sample divider and dynamic image analysis for continuous on-line determination of granule size distribution

Annika Wilms[a,b], Klaus Knop[a], Peter Kleinebudde[a]

[a] Institute of Pharmaceutics and Biopharmaceutics, Heinrich Heine University, Universitaetsstrasse 1, 40225 Duesseldorf, Germany

[b] INVITE GmbH, Drug Delivery Innovation Center (DDIC), CHEMPARK Building W32, 51364 Leverkusen, Germany

International Journal of Pharmaceutics: X 1 (2019): 100029.

https://doi.org/10.1016/j.ijpx.2019.100029

Abstract

The granule size distribution is a critical quality attribute of granules. It has a great impact on further packaging or processing. Due to increasing interest in continuous manufacturing techniques, it is of high interest to develop an in-line or on-line tool to monitor the granule size distribution. However, development of an in-line measurement tool for granule size distribution was challenging since large throughput and inhomogeneous product stream are limiting factors for current particle size analyzers. In this study, continuous sampling was tested in conjunction to a continuous on-line method of size determination using dynamic image analysis. A rotating tube sample divider was used to split previously compacted material in representative samples at different ratios and the sample was directly conveyed to the particle size analyzer where the granule size distribution was determined. The method was tested for different granule sizes to determine limits of detection and its ability to detect these changes immediately, as this enables real-time monitoring of the process. This research is the base for development of control tools concerning the granule size distributions for continuous granulation processes.

Keywords

Granule size distribution; Representative sampling; Process analytical technologies; Dynamic image analysis; Continuous manufacturing; Process monitoring

Abbreviations

CQA - critical quality attribute(s); CM - continuous manufacturing; PAT - process analytical technologies; FDA - U.S. Food and Drug Administration; RCDG - roll compaction/dry granulation; TSG - Twin Screw granulation; GSD - granule size distribution; SY - symmetry factor; DIA - dynamic image analysis; Q3 - volume-based cumulative undersized curve

Graphical abstract

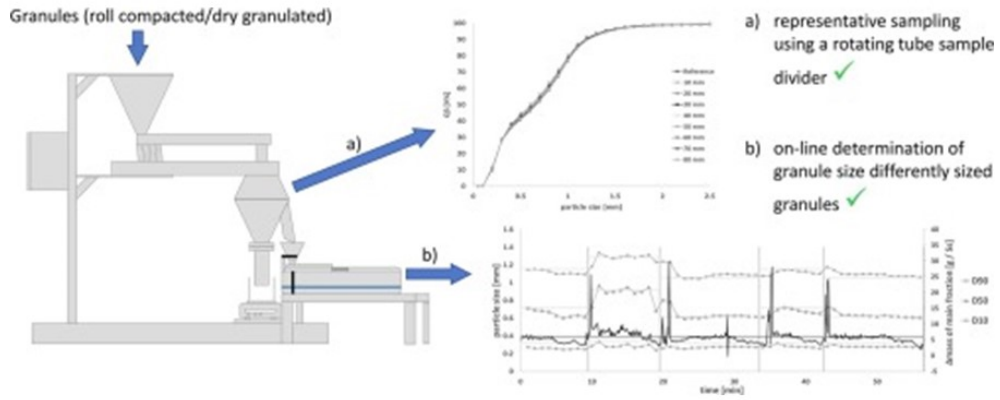

1. Introduction

1.1. Continuous manufacturing of solid oral dosage forms

Batch processes are defined as processes, in which material is loaded, processed and stored until the next manufacturing step. During storage time, critical quality attributes (CQA) are measured, evaluated and the batch is released for further processing. Disadvantages of batch manufacturing include the necessity to discard the whole batch if a CQA does not match the requirements, that the time to produce a final market form can take several weeks and scale-up may be challenging (Plumb, 2005).

Currently most pharmaceutical products are produced in batch processes, even though numerous benefits of a continuous manufacturing (CM) approach, as commonly seen in food production, are already well known (Plumb, 2005, Rantanen and Khinast, 2015). The interest in CM was furthermore increased by the FDA promoting incorporation of continuous processes in pharmaceutical manufacture (Lee, 2016).

Process analytical technologies (PAT) – tools are aiming to ensure that the CQA's are met during manufacturing (Lee, 2016). If the CQA's do not match the requirements only the material that showed insufficient parameters has to be discarded (Singh et al., 2012). If a deviation from the target values is detected, the process should be adapted to match the target values using control loops. The implementation of PAT is of great importance in order to test the intermediates and ensure quality. The aim is a CM line with sufficient process and product control tools to allow a real-time release of the final drug product.

1.2. Granulation

Granulation is one of the most important processes in manufacturing of solid oral dosage forms. With growing interest in CM, granulation processes in which material is fed, processed and discharged continuously are in focus of developmental efforts. Two granulation processes that have gained interest rapidly are roll compaction/dry granulation (RCDG) and twin-screw wet granulation (TSG).

RCDG is a well-established granulation process used in pharmaceutical manufacturing (Kleinebudde, 2004). It has retained its relevance through various innovations due to a number of advantages. These include the ability to process moisture-sensitive active pharmaceutical ingredients and economic benefits through its high energy efficiency (Parikh, 2016, Shlieout et al., 2000). Furthermore, it is exceptionally well-suited for continuous manufacturing (Fonteyne et al., 2015).

Use of an extruder to granulate was published in 1986 (Gamlen and Eardley, 1986). In contrast to other methods of wet granulation, twin-screw granulation (TSG) allows continuous inlet of powder and granulation liquid, processing and discharge (Vercruysse et al., 2012). In contrast to RCDG, drying of the granules is necessary. The dryer can be linked to the outlet of the extruder or incorporated into it (QbCon®, L.B. Bohle, Germany). With growing interest, there is an increasing number of publications on the development of in-line process control tools for TSG (e.g. Harting and Kleinebudde, 2018, Madarász et al., 2018).

Whether granules are packaged or further processed, the granule size distribution (GSD) is a critical quality attribute. The GSD affects the granules flow properties as well as its compaction behavior. Different granule sizes correspond to different particle volumes that can change the fill of tablet press dies and therefore change the resulting tablet strength,

disintegration and dissolution. For solely filling processes (e.g. as commonly seen in stick pack or sachet manufacture) a varying particle volume can interfere with volumetric filling and affect the product uniformity of mass and content of single dose preparations (Shekunov et al., 2007). Therefore, it is of great interest to monitor key parameters of the GSD during continuous granulation.

1.3. Granule size analysis

There is a variety of analytical tools to measure particle size distributions that can be applied to granules (size ranges e.g. 20–3000 µm (Almeida-Prieto et al., 2004)). There have been multiple efforts to develop monitoring tools of particle size distributions for various pharmaceutical processes. Well-established technologies that have been applied are laser diffraction (Chan et al., 2008) and dynamic image analysis (Madarász et al., 2018, Nalluri et al., 2010). Newer technologies include focused beam reflectance (Greaves et al., 2008) and spatial filter velocimetry (Mangal et al., 2016, Närvänen et al., 2009, Petrak, 2002).

Difficulties occurring specifically in RCDG processes are the high product throughput and the broad, bimodal GSD of the granules (Parikh, 2016). Therefore, direct measurements of the GSD could not be applied to a RCDG process so far. Published efforts to determine the GSD in a RCDG process include correlating the particle size to the slope of in-line obtained NIR spectra (Gupta et al., 2004), off-line use of the Eyecon system (McAuliffe et al., 2015) and spatial filter velocimetry (Mangal et al., 2016).

Dynamic image analysis (DIA) is a valuable tool to determine the GSD of various products. Additionally to the particle size measurement, various particle shape parameters can be monitored. With an appropriate measurement size range, the bimodal GSD curve of dry granulated material can be measured.

1.4. Representative sampling

The product stream of a RCDG process can be inhomogeneous (Mangal et al., 2016) and the typical throughput of a roll compaction process is high. The high throughput was found to exceed the capacity of established particle size analyzers (Wilms et al., 2019). Therefore, obtaining a representative sample is necessary in the development of an on-line direct GSD measurement system. This sample should be of adequate size to ensure a representative particle size distribution.

In theory, it is recommended to sample from a powder when it is in motion and to take samples from the complete powder stream (Allen, 2003). Most commonly used is a sample divider in which the sampling vessels rotate underneath a constant stream of product (e.g. PT100, Retsch, Germany). Small quantities of product are thereby split evenly among the mounted number of sampling vessels. Although this system is suitable for lab scale applications, it cannot be applied to a continuous sampling regime. An opposite approach, a rotating product stream and a static sample exit is also commercially available (e.g. PT35-K, Vock Maschinen- und Stahlbau GmbH, Germany) but has not been used in pharmaceutical applications yet.

Another commercially available approach for in-line sampling is the "TWISTER" system (Sympatec GmbH, Germany). In this system, a sampling tip facing the opposite direction of the product stream is placed in the product stream. Therefore, product is collected if it falls directly on the sampling tip. To ensure the whole cross section of the product stream is sampled the sample tip is driven along defined trajectories around the product stream tube (Witt et al., 2004). However, there are no publications confirming the representative sampling of pharmaceutical bulk products in peer-reviewed journals so far.

1.5. Objectives

The aim of this study was to implement an in-line rotating tube sample divider to representatively split granules that were produced using RCDG and to determine the particle size of the sample on-line in real-time. It should be shown, whether the sample splitter can split representatively at various sampling ratios. The material throughput should be at least 5 kg/h in total to ensure relevance for pharmaceutical production. The focus was to obtain reliable data of the GSD and to investigate, whether the system is sensitive to changes in the material granule size. The tools settings were optimized for use in continuous manufacturing of pharmaceutical products. The method should then be universally applicable to continuous granulation processes.

2. Materials and methods

2.1. Materials

Dibasic calciumphosphate anhydrous (=DCPA) (DiCaFos® A150, Budenheim, Germany) was used for all experiments. The particle size distribution of the excipient measured with

laser diffraction (Mastersizer 3000, Malvern Panalytical, United Kingdom) is shown in Fig. 1a).

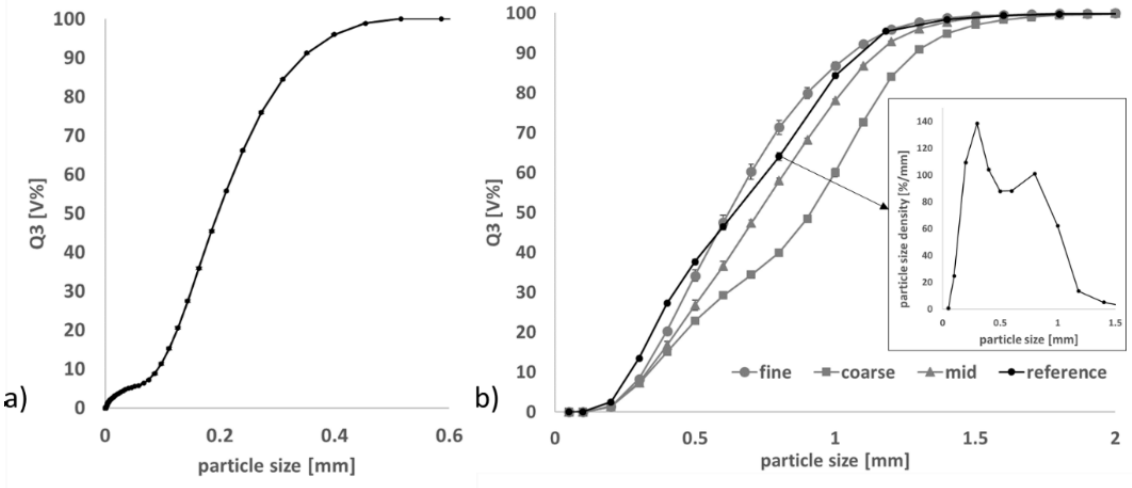

Fig. 1. Cumulative size distribution a) DCPA excipient b) DCPA granules produced using BRC 25. Measured with Haver CPA 2-1. In box: particle size density distribution of reference granules. n = 3; mean ± sd.

2.2. Roll compaction/dry granulation

DCPA was used for RCDG on a BRC 25 (LB Bohle GmbH, Germany). The roll compactor was equipped with smooth surfaced rolls, rim roll sealing system and a 360° rotating turbo sieve (BTS, LB Bohle GmbH, Germany). The specific compaction force was varied to obtain granules of different granule size distributions (Fig. 1b)). Granules were produced at specific compaction forces between 5 kN/cm and 18 kN/cm. As a correlation between the specific compaction force and respective granule size is of no importance for this work, the granules are hereafter referred to as fine grade, coarse grade, mid grade (Fig. 1b)). Reference granules were used for initial set-up of the equipment, confirming the representative sampling and evaluating measurement settings.

2.3. In-line representative sampling of granules produced using RCDG

PT35-K (Vock Maschinen- und Stahlbau GmbH, Germany), a rotating tube sample divider, was used for all experiments. The divider tube rotates at a speed of 29 rpm. It moves closely along the wall of the lower cone. An adjustable gap that can be closed or opened up to 80 mm is located inside the lower cone (Fig. 2).

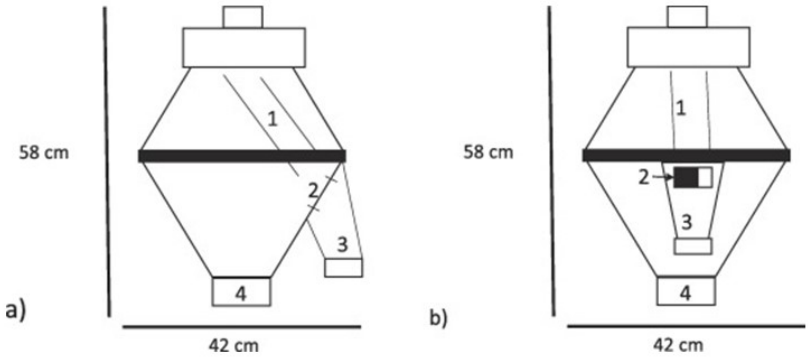

Fig. 2. Rotating tube sample divider PT35-K. 1 – divider tube, 2 – adjustable gap, 3 – sample outlet, 4 – main product outlet a) gap at the side b) gap at the front (black = closed; white = open).

The PT35-K was instrumented with a control unit (Fig. 3).

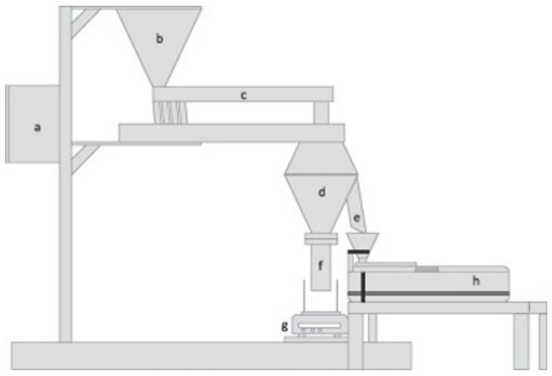

Fig. 3. Setup of PT35-K for off-line measurements. a) control unit b) input funnel c) vibration chute d) biconical sample splitter e) sample outlet f) main fraction outlet g) balance h) Haver CPA 2-1.

It had to be confirmed whether the PT35-K splits representative samples from a bulk of granules that was produced using RCDG. The adjustable gap includes a scale of 10 mm steps. Therefore, to ensure consistent sampling gap widths, experiments were conducted increasing the gap width 10 mm for each setting (0–80 mm). A bulk of reference granules (approximately 2 kg) was split and the GSD of the sample was determined off-line using Haver CPA 2-1 at an optical density range of 0.8–3. The GSD was determined in triplets and the sample was reunited with the main fraction in order to reobtain the complete bulk. To determine the GSD of the total bulk it was split using an established rotary sample divider (PT 100, Retsch, Germany). The GSD of the bulk was determined at three points during the experiment to evaluate whether mechanical stress causes breakage of the granules during the experiment.

2.4. Granule size determination

The Haver CPA 2-1 (Haver & Boecker, Germany) determines granule size based on a CCD line scan camera that scans particles in backlight of a LED light source. The line scan camera records with a frequency of up to 50 million pixel-scans per second. The scanned lines will then be joined to a dataset (picture) and evaluated in real-time. Further technical information is presented in Table 1. Particles are transported and separated using a vibration chute and, if needed, additional ultrasound. The separated particles pass through the sight of the line camera in free fall. This analysis is a non-destructive measurement method and the measured sample can be reunited with the main fraction afterwards.

Table 1. Haver CPA 2-1 technical information.

Feature	Haver CPA 2-1
Measurement range	34 µm–25 mm
Sensor	CCD line scan camera
Pixel count	2048
Feeder width	65 mm
Pixel frequency	50 MHz
Light source	LED, red
L × W × H	800 mm × 200 mm × 355 mm
Environment temperature	5–40 °C
Maximum surrounding humidity	85%

Granule size calculation was based on the equivalent diameter. Each pixel has a height and width of 34 µm. For every experiment and product, the optical density range was evaluated. The optical density range chosen was 0.8–3.0. The optimal optical density range of 0.8–3.0 originates from recommendations from the analyser manufacturer for usage of the system in lab scale experiments. A low optical density range will result in a slower feed rate and less particles will be delivered to the measurement area. A higher optical density however allows to deliver more particles to the measurement zone in the same time interval. After measurements in triplets the optical density range was increased step-wise until significant differences in GSD were recorded. During optimizing of the measurement settings, the mass of the sample and the measurement time was noted. This allowed calculation of the measurement speed.

Haver CPA 2-1 analyses the shape of each individual particle and calculates a symmetry value (SY). It is calculated using the smallest ratio of all symmetry axes that run through the gravimetrical centre of the particle projection area. Register a SY value of one ("1") is a characteristic of a perfect sphere and will also for a particle that has the size of one pixel. Therefore, the SY value is also dependent on the resolution. If two particles are not separated sufficiently, there is a possibility of them touching during their free fall through the sight of the camera. Hence, they will be treated as one particle with a bigger size for analysis. If the common area, in which two particles overlap is small, the recognized particle will show a low symmetry factor. In the following experiments, results were recorded using no SY restrictions or filters. Afterwards, to evaluate the impact of introducing a minimal SY requirement (filter), the Haver CPA raw-data was recalculated to include only particles with a SY of 0.5 or more.

2.5. On-line analytics

The input funnel of the Haver CPA 2-1 was positioned underneath the sample outlet of the PT35-K (Fig. 3) for on-line experiments. The granules were poured in the PT35-K input funnel, split in the PT35-K and subsequently measured using Haver CPA 2-1. All settings were chosen prior to starting the measurement and could not be adjusted during the measurement. Temporary measurements were conducted for one minute each. A lab scale balance (CPA5201, Sartorius AG, Germany) was placed underneath the outlet of the main fraction. The mass is tracked (Sartorius connect, Sartorius AG, Germany) in 5 s intervals.

2.6. Statistical analysis

All off-line measurements were conducted at least threefold. To determine, whether different samples show the same GSD, their D10, D50 and D90 values were compared. An F-test was executed to compare the variances. Depending on the outcome of the F-test a two-sided t-test ($\alpha = 0.05$) was conducted for either equal or unequal variances.

3. Results and discussion

3.1. In-line representative sampling of granules produced using RCDG

It had to be verified whether PT35-K splits representative samples from a bulk of RCDG granules. The GSD of the reference and the samples, depending on gap width and thereby

the split ratio, is displayed in Fig. 4. Furthermore, the split ratios were determined and compared to the values provided by the manufacturer (Table 2).

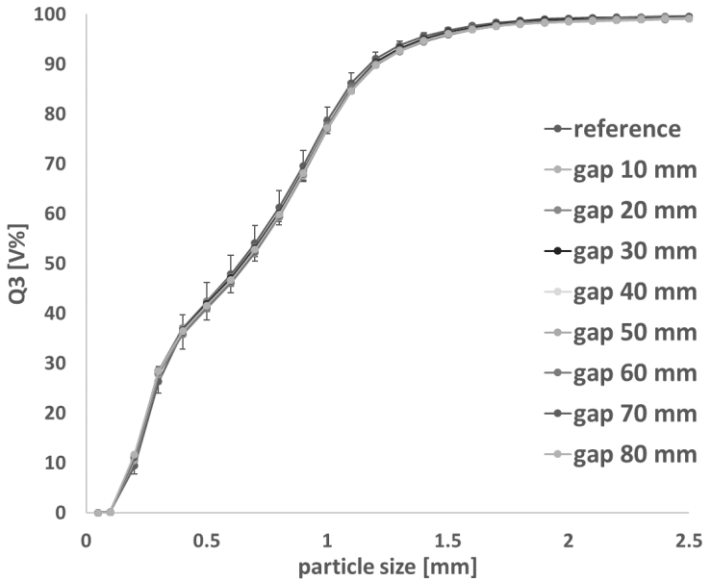

Fig. 4. Cumulative size distributions of DCPA granules. Optical density = 0.8 – 3.0; n = 3; mean ± sd. reference: n = 3 × 3; mean ± sd.

Table 2. Split ratios PT35-K.

gap opening [mm]	split ratio (stated in handbook)	split ratio (measured)
10	1:80	1:66
20	N/A	1:37
30	1:41	1:27
40	1:28	1:21
50	1:16.5	1:17
60	1:14	1:14
70	1:12	1:12
80	1:10	1:11

It was observed that the split ratios differ from the values stated in the PT35-K handbook. For further experiments, the determined values were used.

The reference was measured in triplets at three time points during the experiment. The resulting mean GSD curve did not differ significantly to the GSD curves of the samples. However, the reference showed larger standard deviations (Fig. 4). A decrease in particle size during the experiment was observed. This was expected, as the same granules were

stressed repeatedly in conveying and rotating tube sample dividing as well as conventional sample splitting. Regarding the amount of stress on the granules, the decline in granule size is negligible. For regular application, a single mechanical stress is not regarded as problematic. This proved representative sampling for granules obtained using RCDG at different gap widths and split ratios between 1:66 and 1:11 (Table 2).

3.2. Off-line determination of measurement settings

The critical measurement setting of optical density range was defined in the Haver CpaServ software prior to starting the measurement. No adjustments to the predefined range could be made after the measurement had started. Therefore, it was critical to define this range carefully. Two major factors were considered. The first factor was the significant shift in GSD parameters that could be observed when the optical density range was increased (Fig. 5). Secondly, a high throughput of material, which correlates to an increased optical density and a high measurement speed, was desirable in order to ensure relevance for pharmaceutical production. The aim was to measure as much material as possible without results deviating significantly from the reference recorded at an optical density of 0.8–3.0. The settings for on-line experiments were determined using the reference granules shown in Fig. 1b).

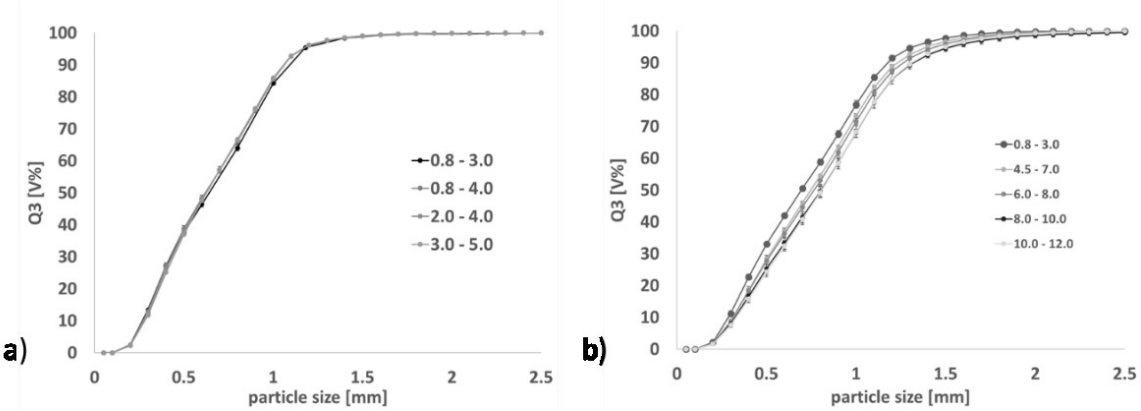

Fig. 5. Cumulative size distributions of reference granules. Varying optical density. No symmetry restriction. a) Experiment A b) Experiment B. n = 3; mean ± sd.

3.2.1. Deviation from reference measurement at increasing optical densities

GSD curves obtained using varying optical density ranges are shown in Fig. 5. The granules measured in Fig. 5a) were the reference granules for in-line experiments (Fig. 1b)). Optical density could be increased from 0.8–3.0 to 3.0–5.0 without significant differences (experiment A). In a second experiment (experiment B) the optical density was increased

until a significant deviation from the reference was observed (Fig. 5b)). Unfortunately, before these measurements were conducted the granules were also used for further preliminary testing and, as a result from repeated mechanical stress, the particle size had decreased. The results are however indicating that starting from an optical density of 4.5 – 7.0 the GSD curve shows a significant shift compared to the reference measurement. As expected, the granule size is overestimated at high optical densities due to more particle overlapping and agglomerates in the measurement channel.

3.2.2. Determination of measurement duration

Samples were measured at different optical densities and the measurement time was recorded to determine the measurement speed (Table 3). Each sample was measured threefold for each setting. Knowledge of the measurement speed was critical as the system parameters are evaluated for this throughput of material. The complete product conveyance and the sampling ratio should then provide a sample input into Haver CPA 2-1 equal to the previously determined measurement speed.

In Fig. 6a), the total number of particles, that were analysed are plotted against the optical density setting chosen. Although the number of particles in the sample was not changed, the number of particles measured varied significantly. Less particles were registered at increasing optical density ranges. A high optical density required more particles in each picture taken by the analyser. To achieve this, the increased mass flow also increased chances of two or more particles touching, overlapping or agglomerating. They were then analysed as one particle and the total number of particles decreased. Experiments A and B were conducted with samples of different masses and hence differ in total amount of particles.

The measurement speed plotted against the optical density is shown in Fig. 6b). As expected, an increase in measuring speed could be observed with increasing optical density ranges. It is important to note, that two experiments using granules of different granule sizes and sample masses led to similar results and trends. In the future, this should be confirmed for different materials and granule sizes. This could then allow prediction of the measurement speed depending on optical density settings and material properties.

Table 3. Speed of measurement. No asterisk marks results from experiment A, the asterisk indicates results from experiment B. n = 3; mean ± sd.

Optical density	Sample mass [g]	Time of measurement [s]	Speed of measurement [g/min]	Number of particles [*10^6]
0.8–3.0*	37.7	536 ± 35	4.22 ± 0.28	1.53 ± 0.06
0.8–3.0	76.3	1034 ± 138	4.43 ± 0.60	3.10 ± 0.04
0.8–4.0	76.3	829 ± 96	5.52 ± 0.65	3.18 ± 0.05
2.0–4.0	76.3	661 ± 5	6.93 ± 0.05	3.10 ± 0.00
3.0–5.0	76.3	486 ± 8	9.42 ± 0.15	3.06 ± 0.04
4.5–7*	36.8	154 ± 3	14.37 ± 0.28	1.25 ± 0.01
6.0–8.0*	36.7	135 ± 9	16.27 ± 1.08	1.07 ± 0.05
8.0–10.0*	35.5	100 ± 2	21.30 ± 0.96	0.78 ± 0.09
10.0–12.0*	35.6	82 ± 1	26.05 ± 0.19	0.67 ± 0.1

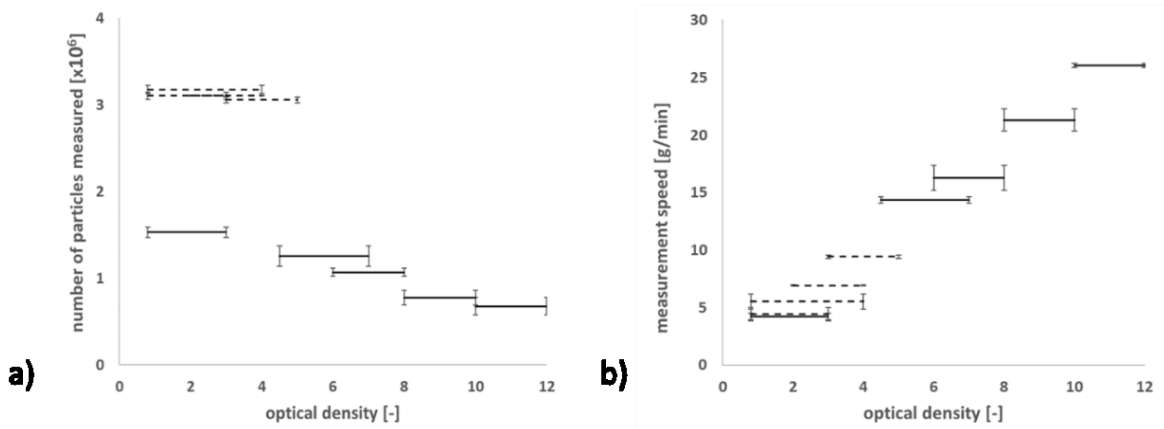

Fig. 6. a) Total number of analysed particles and b) measurement speed plotted against the bottom (black) and top (grey) optical density range, experiment A (dashed line), experiment B (solid line) n = 3; mean ± sd.

3.2.3. Symmetry settings

The influence of varying the symmetry setting was evaluated (Fig. 7). As expected, the GSD curve was shifted to larger granule sizes with increasing optical density ranges. Introducing a minimal symmetry factor of 0.5 adjusted the GSD curves to smaller sizes, however, the effect was not large enough to correct the curves to the reference

measurement. After addition of symmetry limitation, the curves still varied significantly from their reference. For all further experiments, no symmetry restrictions were applied.

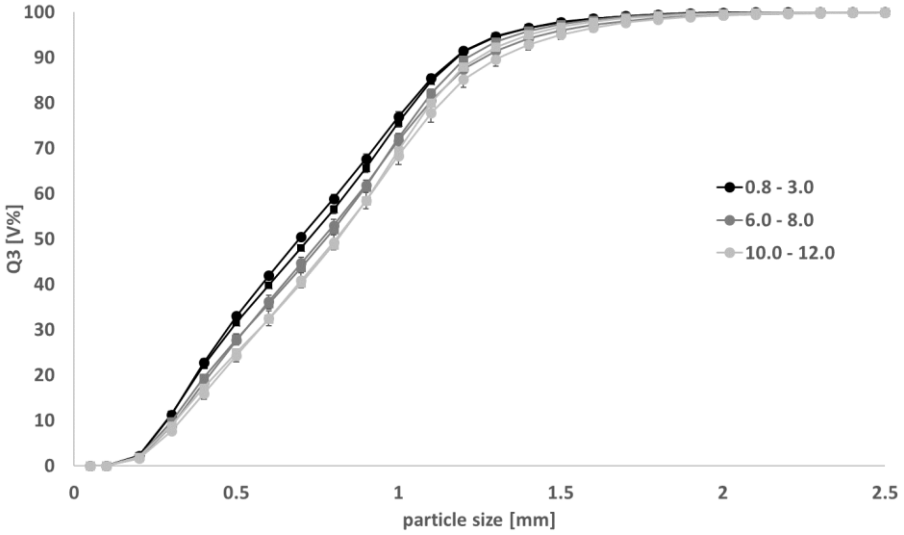

Fig. 7. Cumulative size distributions of reference DCPA granules, n = 3; mean ± sd. Varying optical density. Symmetry restriction: circle = no restriction, square = minimum SY of 0.5.

Using this data, the expected throughput for the main fraction was calculated. Taking the data of the optical density setting 2.0–4.0 (Table 3) into account, a measurement speed of 7.2 g/min was determined. For a gap width of 80 mm the sampling ratio was determined to be 1/11 (Table 2). Throughput was calculated to be 79.2 g/min (≈4.75 kg/h) and is in relevant production throughputs of commercial roll compactors. However, the mass that was tracked during the experiments was solely the mass of the main fraction (72.0 g/min). As the mass was tracked every 5 s, the desired mass signal resulted in 6.3 g/5s.

3.3. On-line determination of GSD using DIA

Fig. 8 shows results of an on-line measurement (off-line results of the used granules can be seen in Fig. 1b)). The fine and the coarse grade of granules were separated representatively into two batches. When all material was transferred on the vibrating chute, no more material was present in the input funnel, the granules were brushed forward. This was done in order to avoid a decline in throughput based on low fill-level of the chute and mixing of the different grades when the new grade was poured in the funnel. However, both factors could not be eliminated completely. Hence, they were expected to influence the measurements and lead to disturbances after changing the granule type. Brushing forward the material also had an impact on the feed rate and should be avoided in future experimental set-ups.

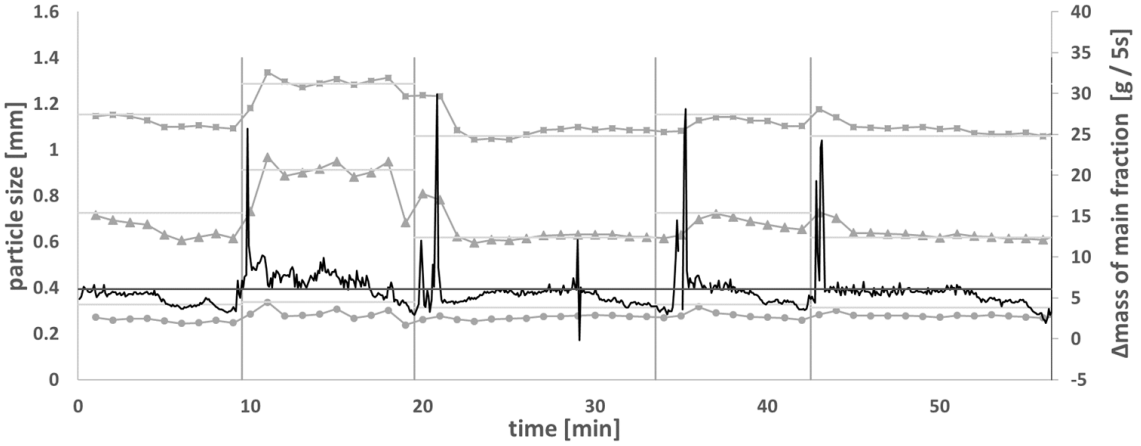

Fig. 8. Measured GSD quantiles. squares = D90, triangles = D50, circles = D10. Roman numbers indicate the sample that was measured at the given time period. I = mid, II = coarse, III = fine. Measurement duration = 1 min. Dark black = feed rate.

The vertical lines in Fig. 8 indicate the time points at which the new grade of granules was filled into the input funnel. The horizontal lines indicate the off-line determined reference values for D90, D50 and D10.

Based on the GSD measurements, it was possible to distinguish the differently sized granules. The time needed until changes in the GSD quantiles could be recorded was less than two minutes. This is understandable as the granules did not reach the sample splitter directly but were conveyed in the vibration chute of the PT35-K instrumentation and in the vibration chute of Haver CPA 2-1 first. Residence time in the splitter was negligible. Therefore, the differences in GSD could be observed close to real-time.

Compared to off-line measurements, the D10 value was underestimated for most measurements. This could be explained based on the settings that were chosen. As big granules and fines require different settings (namely optical density) the chosen settings were a compromise in which all key quantiles can be measured in realistic scales. A lower optical density range, as the fine fraction would require for measurement, would also require a lower material throughput. The material throughput however, is crucial for ensuring this measurement system is relevant for pharmaceutical production. As the D50 is, arguably, the most important parameter it was important to measure the D50 precisely. The slight underestimation of the D10 was assessed as less critical.

Fluctuations were detected during the measurements of the GSD quantiles. Plotting of the mass flow (secondary y-axis) against the time shows the mass flow throughout the whole experiment (Fig. 8). It can be seen that the mass flow fluctuated frequently, especially in

the beginning and at the end of a new bulk that was conveyed. Comparing these trends, e.g. a decrease in mass flow at minutes 6–10 lead to fluctuations in the GSD parameters. As previously discussed, the expected feed rate based on the main fraction mass was 6.3 g/5s (black horizontal line, Fig. 8). If this throughput was reached, the measurements correlated well with the reference values (see minute 25–30). The settings were optimized for a certain throughput (7–9 g/min sample and 72–92.4 g/min bulk). A deviation from this throughput changed the requirements for the optical settings and lead to different results. An option to adjust the settings with a varying throughput would be beneficial for these measurements.

4. Conclusions

Representative sampling of granules produced by RCDG was successfully implemented using a rotating tube sample divider. This enables on-line characterizations that could not be conducted previously due to limited operational capacity of the measurement or due to the inhomogeneity of the RCDG-product stream. The sampling procedure can be integrated in a bypass solution for an on-line measurement.

The sampling was joined to a particle size analyzer based on dynamic image analysis, which measured every granules size and shape. In future, monitoring of the granule size can be enhanced further by development of control tools. Real-time adjustments to the measurement settings according to the current product mass flow could enhance this set-up.

RCDG was simulated to produce granules at a throughput of 5 kg/h and with sampling an amount of 10%. As the sample divider allows for smaller splitting ratios even higher throughputs can be aimed at using this system.

The experimental system can be transferred to a RCDG process and validated.

Funding

This research did not receive any specific grant from funding agencies in the public, commercial or not-for-profit sectors. This work was supported by the Drug Delivery Innovation Center (DDIC), INVITE GmbH, Leverkusen.

Declaration of Competing Interest

The authors declare that they have no known competing financial interests or personal relationships that could have appeared to influence the work reported in this paper.

References

Allen, 2003 - T. Allen; Powder Sampling and Particle Size Determination (first ed.), Elsevier B.V, Amsterdam (2003)

Almeida-Prieto et al., 2004 - S. Almeida-Prieto, J. Blanco-Méndez, F. Otero-Espinar; Image analysis of the shape of granulated powder grains; J. Pharm. Sci., 93 (2004), pp. 621-634

Chan et al., 2008 - L.W. Chan, L.H. Tan, P.W.S. Heng; Process analytical technology: application to particle sizing in spray drying; AAPS PharmSciTech, 9 (2008), pp. 259-266

Fonteyne et al., 2015 - M. Fonteyne, J. Vercruysse, F. De Leersnyder, B. van Snick, C. Vervaet, J. Remon, T. De Beer; Process analytical technology for continuous manufacturing of solid-dosage forms; Trends Anal. Chem., 67 (2015), pp. 159-166

Gamlen and Eardley, 1986 - M.J. Gamlen, C. Eardley; Continuous extrusion using a Baker Perkins MP50 (multipurpose) extruder; Drug Dev. Ind. Pharm., 12 (1986), pp. 1701-1713

Greaves et al., 2008 - D. Greaves, J. Boxall, J. Mulligan, A. Montesi, J. Creek, E.D. Sloan, C. Koh; Measuring the particle size of a known distribution using the focused beam reflectance measurement technique; Chem. Eng. Sci., 63 (2008), pp. 5410-5419

Gupta et al., 2004 - A. Gupta, G.E. Peck, R.W. Miller, K.R. Morris; Nondestructive measurements of the compact strength and the particle-size distribution after milling of roller compacted powders by near-infrared spectroscopy; J. Pharm. Sci., 93 (2004), pp. 1047-1053

Harting and Kleinebudde, 2018 - J. Harting, P. Kleinebudde; Development of an in-line Raman spectroscopic method for continuous API quantification during twin-screw wet granulation; Eur. J. Pharm. Biopharm., 125 (2018), pp. 169-181

Kleinebudde, 2004 - P. Kleinebudde; Roll compaction/dry granulation: pharmaceutical applications; Eur. J. Pharm. Biopharm., 58 (2004), pp. 317-326

Lee, 2016 - S.L. Lee; Current FDA perspective for continuous manufacturing; US FDA Center for Drug Evaluation and Research, MIT-CMAC 2nd International Symposium on Continuous Manufacturing of Pharmaceuticals (2016)

Madarász et al., 2018 - L. Madarász, Z.K. Nagy, I. Hoffer, B. Szabó, I. Csontos, H. Pataki, B. Démuth, B. Szabó, K. Csorba, G. Marosi; Real-time feedback control of twin-screw wet granulation based on image analysis; Int. J. Pharm., 547 (2018), pp. 360-367

Mangal et al., 2016 - H. Mangal, E. Derksen, A. Lura, P. Kleinebudde; In-line particle size measurement in dry granulation: evaluation of probe position; 10th World Meeting on Pharmaceutics, Biopharmaceutics and Pharmaceutical Technology (2016)

McAuliffe et al., 2015 - M.A.P. McAuliffe, G.E. O'Mahony, C.A. Blackshields, J.A. Collins, D.P. Egan, L. Kiernan, E. O'Neill, S. Lenihan, G.M. Walker, A.M. Crean; The use of PAT and off-line methods for monitoring of roller compacted ribbon and granule properties with a view to continuous processing; Org. Process Res. Dev., 19 (2015), pp. 158-166

Nalluri et al., 2010 - V.R. Nalluri, P. Schirg, X. Gao, A. Virdis, G. Imanidis, M. Kuentz; Different modes of dynamic image analysis in monitoring of pharmaceutical dry milling process; Int. J. Pharm., 391 (2010), pp. 107-114

Närvänen et al., 2009 - T. Närvänen, T. Lipsanen, O. Antikainen, H. Räikkönen, J. Heinämäki, J. Yliruusi; Gaining fluid bed process understanding by in-line particle size analysis; J. Pharm. Sci., 98 (2009), pp. 1110-1117

Parikh, 2016 - D.M. Parikh; Handbook of Pharmaceutical Granulation Technology; CRC Press, Boca Raton (2016)

Petrak, 2002 - D. Petrak; Simultaneous measurement of particle size and particle velocity by the spatial filtering technique; Part. Part. Syst. Charact., 19 (2002), pp. 391-400

Plumb, 2005 - K. Plumb; Continuous processing in the pharmaceutical industry: changing the mind set; Chem. Eng. Res. Des., 83 (2005), pp. 730-738

Rantanen and Khinast, 2015 - J. Rantanen, J. Khinast; The future of pharmaceutical manufacturing sciences; J. Pharm. Sci., 104 (2015), pp. 3612-3638

Shekunov et al., 2007 - B.Y. Shekunov, P. Chattopadhyay, H.H.Y. Tong, A.H.L. Chow Particle size analysis in pharmaceutics: principles, methods and applications; Pharm. Res., 24 (2007), pp. 203-227

Shlieout et al., 2000 - G. Shlieout, R.F. Lammens, P. Kleinebudde; Dry granulation with a roller compactor Part I: The functional units and operation modes; Pharm. Technol. Eur., 12 (2000), pp. 24-35

Singh et al., 2012 - R. Singh, M. Ierapetritou, R. Ramachandran; An engineering study on the enhanced control and operation of continuous manufacturing of pharmaceutical tablets via roller compaction; Int. J. Pharm., 438 (2012), pp. 307-326

Vercruysse et al., 2012 - J. Vercruysse, D. Córdoba Díaz, E. Peeters, M. Fonteyne, U. Delaet, I. Van Assche, T. De Beer, J.P. Remon, C. Vervaet; Continuous twin screw granulation: influence of process variables on granule and tablet quality; Eur. J. Pharm. Biopharm., 82 (2012), pp. 205-211

Wilms et al., 2019 - A. Wilms, K. Knop, P. Kleinebudde; In-line determination of granule size distribution during continuous roll compaction/dry granulation by laser diffraction; Nuremberg; PARTEC, 9–11 (04) (2019), p. 2019

Witt et al., 2004 - W. Witt, M. Heuer, M. Schaller; In-line particle sizing for process control in new dimensions; China Particuol., 2 (2004), pp. 185-188

3 Development and Evaluation of an In-line and On-line Monitoring System for Granule Size Distributions in Continuous Roll Compaction/Dry Granulation Based on Laser Diffraction

Annika Wilms[a,b], Robin Meier[c], Peter Kleinebudde[a]

[a] Institute of Pharmaceutics and Biopharmaceutics, Heinrich Heine University, Universitaetsstrasse 1, 40225 Duesseldorf, Germany

[b] INVITE GmbH, Drug Delivery Innovation Center, Chempark Building W32, 51364 Leverkusen, Germany

[c] L.B. Bohle Maschinen + Verfahren GmbH, Industriestrasse18, 59320, Ennigerloh

3.1 Pretext

The following research paper has been published in the Journal of Pharmaceutical Innovation (2020). https://doi.org/10.1007/s12247-020-09443-3

Evaluation of authorship:

author	idea [%]	study design [%]	experimental [%]	evaluation [%]	manuscript [%]
Annika Wilms	40	70	100	80	60
Robin Meier	30	20	0	20	20
Peter Kleinebudde	30	10	0	0	20

Development and Evaluation of an In-line and On-line Monitoring System for Granule Size Distributions in Continuous Roll Compaction/Dry Granulation Based on Laser Diffraction

Annika Wilms[a,b],Robin Meier[c], Peter Kleinebudde[a]

[a] Institute of Pharmaceutics and Biopharmaceutics, Heinrich Heine University, Universitaetsstrasse 1, 40225 Duesseldorf, Germany

[b] INVITE GmbH, Drug Delivery Innovation Center (DDIC), CHEMPARK Building W32, 51364 Leverkusen, Germany

[c] L.B. Bohle Maschinen + Verfahren GmbH, Industriestrasse 18, 59320 Ennigerloh, Germany

Journal of Pharmaceutical Innovation (2020)

https://doi.org/10.1007/s12247-020-09443-3

Abstract

Purpose Roll compaction/dry granulation is established in manufacturing of solid oral dosage forms and, within the context of continuous manufacturing, it has sparked interest as material is fed, processed, and ejected continuously while also providing large possible throughputs. However, this amount of material has to be adequately controlled in real time to assure quality.

Methods This research aimed at monitoring the critical quality attribute granule size distribution in continuous roll compaction/dry granulation (QbCon®; L.B. Bohle, Ennigerloh, Germany) using in-line and on-line laser diffraction. The influence of varying process parameters and excipient formulations was studied and evaluated with the prospect of using this technique to develop control loops. For this purpose, residence time parameters were assessed. In- and on-line data was compared with off-line laser diffraction and dynamic image analysis data.

Results The system successfully monitored the granule size distribution in a variety of process parameters and throughputs (up to 27.5 kg/h). It was sensitive to changes in process parameters and changes in material blends, which could pose a potential threat to the final drug products' quality. Average event propagation time from the compaction zone to the laser diffraction system of 17.7 s demonstrates the systems' fast reaction time.

Conclusion Results highlight laser diffraction as a valuable method of in- and on-line size determination and allow for the development of a control strategy using this principle.

Keywords

Continuous manufacturing; Roll compaction/dry granulation; Process analytical technologies; Laser diffraction; Process monitoring

Introduction

Shifting the mindset from batch to continuous manufacturing (CM), the pharmaceutical industry is rather slow, compared with, e.g., the food industry, as the highest standard of quality must be met and documented for every product [1, 2]. However, the advantages of CM have been recognized and academic and industrial research efforts have increased [3,4,5,6]. Issues like proposing a new definition of a "batch" and traceability have been addressed [7]. Early in CM initiatives, proposals for continuous granulation were published [8]. The Food and Drug Administration (FDA) has been especially supportive of the CM approach [3, 5] and the International Council of Harmonization published quality guidance to help introducing advanced concepts [9, 10]. ICH Guideline Q13, Continuous Manufacturing, was also announced and is currently under construction. Currently, six small-molecule drug products are on the market that, at least to some extent, incorporate CM approaches [11].

An integral part of a functional CM manufacturing line is a detailed control strategy to assure that the resulting final drug product is matching all necessary quality requirements and to separate out-of-specification product from in-specification product. To achieve this, process analytical technologies (PAT) can be implemented. PAT tools are developed to monitor critical quality attributes (CQA) [12] of the intermediates and the final product and use these results to control the process in real time. The aim is to minimize the amount of product that is out-of-specification and, if all necessary CQAs can be controlled, real-time release of the final drug product. Various guidelines and experimental approaches to implementing PAT tools have been described in literature [3, 13,14,15,16,17].

Roll compaction/dry granulation (RCDG) is the favored continuous dry granulation method while twin-screw granulation is chosen if a wet granulation process is desired [18, 19]. RCDG is known for its high potential material throughput, comparably low production cost

and the granulation method of choice if the bulk density of the material needs to be significantly increased [20,21,22]. The granule size distribution (GSD) of the resulting granules is a CQA [23, 24]. Therefore, development of in-line or on-line particle size measurements are of interest. Numerous techniques (e.g., dynamic image analysis (DIA), laser diffraction, focused beam reflectance measurement, spatial filtering technique) have been reported to be implemented in discontinuous or continuous processing of pharmaceuticals [25,26,27,28,29,30]. GSD monitoring for RCDG is impeded by the high throughput of the process, resulting in a high number of granules, and the broad size distribution that typically results from dry granulation. This results in difficulties to measure the full product flow as well as obtaining a representative sample to measure [20]. Therefore, limited research has been published on RCDG and in-line/on-line particle sizing [31,32,33].

Laser diffraction as means of particle size determination is based on the different behaviors of laser light that is diffracted at the surface of a particle. Larger particles diffract light at smaller angles and different intensities compared with smaller particles. The scattered light intensity is measured by circular detector plates and used to calculate the size of the particle that would be responsible for this scattering under certain assumptions (e.g., a spherical particle shape) [34]. Laser diffraction is widely used for off-line analytics in batch mode manufacturing, has been intensively studied [35,36,37], and was explored for process monitoring in pharmaceutical applications [26].

The aim of this study was to implement laser diffraction as a tool to monitor GSD in-line or on-line. The sensitivity of the tool with regard to a change in process parameters, excipients, and reproducibility was studied. Off-line laser diffraction was performed and compared with in-line/on-line data. In general, the applicability of the PAT tool with regard to continuous manufacturing of solid oral dosage forms with a throughput up to 27.5 kg/h was to be explored.

Materials and Methods

Materials

Microcrystalline cellulose (MCC, Vivapur® 102, JRS Pharma, Germany) was used as primary excipient in experiments studying varying process parameters.

Different placebo formulations were prepared. Excipients used were lactose (Granulac® 200, Meggle, Germany) and magnesium stearate (Parteck® LUB MST, Merck, Germany).

Continuous Roll Compaction/Dry Granulation

RCDG was performed on a QbCon® dry continuous manufacturing line using a commercially available roll compactor (BRC 25, L.B. Bohle GmbH, Germany). Filling of material, either pure MCC or a preblend, was conducted manually. The roll compactor was equipped with knurled surfaced rolls, a hybrid sealing system and a 360° rotating conical sieve (BTS 100, L.B. Bohle GmbH, Germany) equipped with a 1.0-mm rasp sieve. Specific compaction forces (SCF) between 2 and 7 kN/cm were applied. If not mentioned otherwise, the default gap width was 2.0 mm and the roll speed setting was 2 rpm. Below the sieve, a small buffer vessel was mounted with a suction shoe. On the other side, a plastic hose was attached (Fig. 1a). The hose was then attached either to the laser diffraction system itself or to a T-piece, if the bypass system was used. At the outlet of the laser diffraction system, a plastic hose was attached and connected to a vacuum receiver (Volkmann GmbH, Soest, Germany). If the fill grade of the vessel exceeded a certain level, the pump stopped for 10 s and the container was emptied. Afterwards, conveyance restarted.

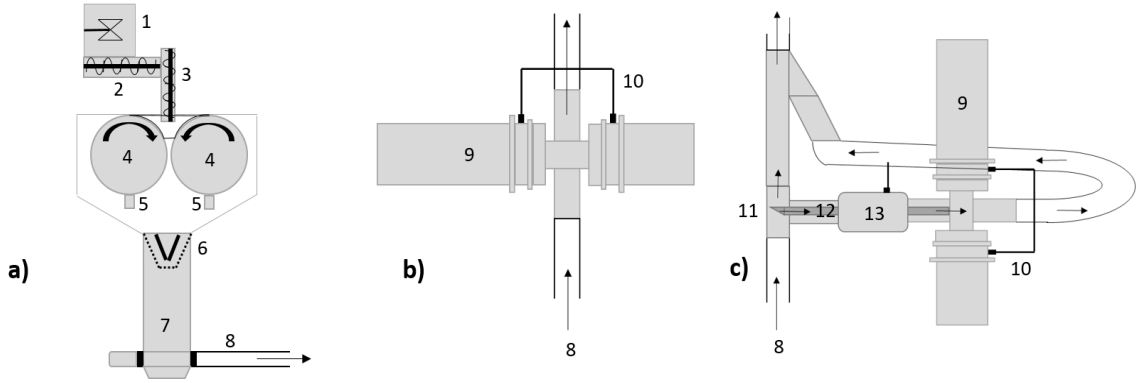

Fig. 1 Scheme of a RCDG, b in-line laser diffraction, c on-line laser diffraction. (1) powder inlet, (2) feeding auger, (3) tamping auger, (4) rolls, (5) scrapers, (6) conical sieve, (7) vessel, (8) hose, (9) laser diffraction system, (10) inlet for scavenging air, (11) T-piece, (12) pipe with angled opening, (13) venturi nozzle

Granule Size Determination Using Laser Diffraction

The granule size distribution was determined using Insitec® T laser diffraction system (Malvern Panalytical, United Kingdom). The system was equipped with a lens of 500-mm focal length, allowing the measurements of particles' equivalence diameters up to 1600 µm. It consists of a red diode laser (670 nm), a 10.0-mm beam waist, and a circular detector

with 33 detector plates. The scan rate was 2000 Hz. GSD parameters and transmission data were exported. The transmission is a value that describes how much of laser light passes through the measurement zone onto the detector. At 100% transmission, all laser light reaches the detector, while at 0% transmission, none of the laser light reaches the detector. It is therefore a value that can be used to estimate how many particles are in the measurement zone at a certain time frame. An initial update time of 5 s was chosen. Scavenging air of 10 Nm^3/h was used to protect the lenses from window fouling and inserted on both, the laser and the detector lens. Window fouling was evaluated daily, as a blank measurement with a fouled window will lead to a decreased transmission and recording of granule size, while no particles are transported through the measurement zone. Measurements were performed only if the transmission during the blank was 100%. RTSizer® (Malvern Panalytical, United Kingdom) software was used to track and export GSD and transmission data.

For in-line laser diffraction, the whole product stream was passing the laser diffraction installation (Fig. 1b). For on-line measurements, the product stream was directed through a T-piece, in which a metal pipe (10 mm) with an angled opening was inserted. The pipe was linked to a venturi nozzle to disperse the sample through the laser diffraction measurement zone with additional compressed air (4 Nm^3/h). After measurement, the sample was reunited with the main fraction and conveyed into the storage vessel (Fig. 1c).

Off-line laser diffraction was conducted using the Mastersizer® 3000 (Malvern Panalytical, United Kingdom). Samples for off-line analysis were taken without the hose and vessel (nos. (7) and (8) in Fig. 1). Every sample was taken for 1 min, resulting in a sample mass between 50 and 275.8 g. Samples were split using a rotational sample divider (PT100, Retsch, Germany). They were measured at 0.8-bar dispersion pressure. The dispersion pressure was chosen to ensure that no granules are destroyed during dispersion based on expertise on laser diffraction measurement of dry granulated product. All off-line samples were measured at least in threefold.

In-line/On-line Data Analysis

For figures that show the granule size development over time, the key parameters D25, D50, and D75 are plotted instead of a full GSD curve. In all cases, the moving average over

30 s was calculated and plotted. Transmission values were plotted as individual values every 5 s. Process parameters were plotted as individual values every 10 s.

Detailed analysis of GSD curves is also included in this work. Data was only included in this analysis, if it was measured, when the system was in equilibrium. More specifically, if the set-specific compaction force (SCF) was met and the gap width only fluctuated between set gap width ± 0.1 mm. When the system was in equilibrium, the average of the last 30 s was taken as data point every minute.

Granule Size Determination Using Dynamic Image Analysis

There are many different methods to determine particle size. It is therefore interesting to compare the method of choice with at least one other method that provides additional information. A distinctive difference between laser diffraction and DIA is the role of particle shape and morphology. Laser diffraction does not provide information about particle shape and irregularly shaped particles will generate signals that might under- or overestimate their size. DIA typically records two-dimensional projections that are subsequently evaluated. It is possible to choose from a plethora of different size descriptors. It was therefore chosen as a comparative technique of size determination.

DIA was conducted using Haver CPA 2-1 (Haver&Boecker, Oelde, Germany). It scans the particle projection in free fall through a measurement zone that is equipped with a red LED light source and a CCD line scan camera. With a pixel size of 34 µm × 34 µm, it can measure particles between 24 µm (67% obscuration needed to measure a signal) and 25 mm. To allow a comparison to laser diffraction results, the equivalent diameter was chosen as a size descriptor. The equivalent diameter was calculated by measuring the projected area of each particle and determining the radius of a circle that would generate the same projected area.

Results and Discussion

GSD Determination at Varying SCF and Determination of Residence Time

Figure 2 displays results from two experiments with the same experimental scheme. GSD was determined in-line (Fig. 2a and b) and on-line (Fig. 2c and d) at four different SCFs. All three GSD parameters react to a change in SCF. They seem to reach a constant value, albeit fluctuations can be seen, especially in the D75 values. This constant level is reached after the SCF and gap width (see Fig. 2b and d) have reached an equilibrium. For both, in- and on-line analysis, returning to a SCF led to GSD parameters that do not differ significantly from different experiment timings in which the same parameters were chosen (e.g., 2 kN/cm at minutes 6–12 and 24–30). In this example, the average D25, D50, and D75 values were evaluated statistically. The arithmetic mean was chosen as parameter every 30 s. As stated before, data was only included in this analysis if the process was in equilibrium. In this example, 6 values for D25, D50, and D75 were taken into account for minutes 6–12 and 8 values for minutes 24–30. An F test was conducted comparing the variances of the recorded data ($\alpha = 0.05$). Variances were similar for D25 and D50 (F values of 1.19 and 1.66 accordingly compared with the table value of $F = 3.97$) but varied for D75 (F value of 8.87). Afterwards, a t test (either for similar variances or varying variances) was conducted ($\alpha = 0.05$). In all cases, the t test confirmed that the arithmetic means do not differ significantly (t value of 0.44 (D25), 1.77 (D50), and 2.05 (D75) were calculated and compared with the table values of t (2.18 for D25 and D50; 2.36 for D75). In both experiments, approximately at minutes 8.5 and 22.5 (Fig. 2a and b) and 8.5 and 23.5 (Fig. 2c and d), the collecting vessel was emptied, which can be seen in abrupt stop of all measurements. Afterwards, the conveying system restarted.

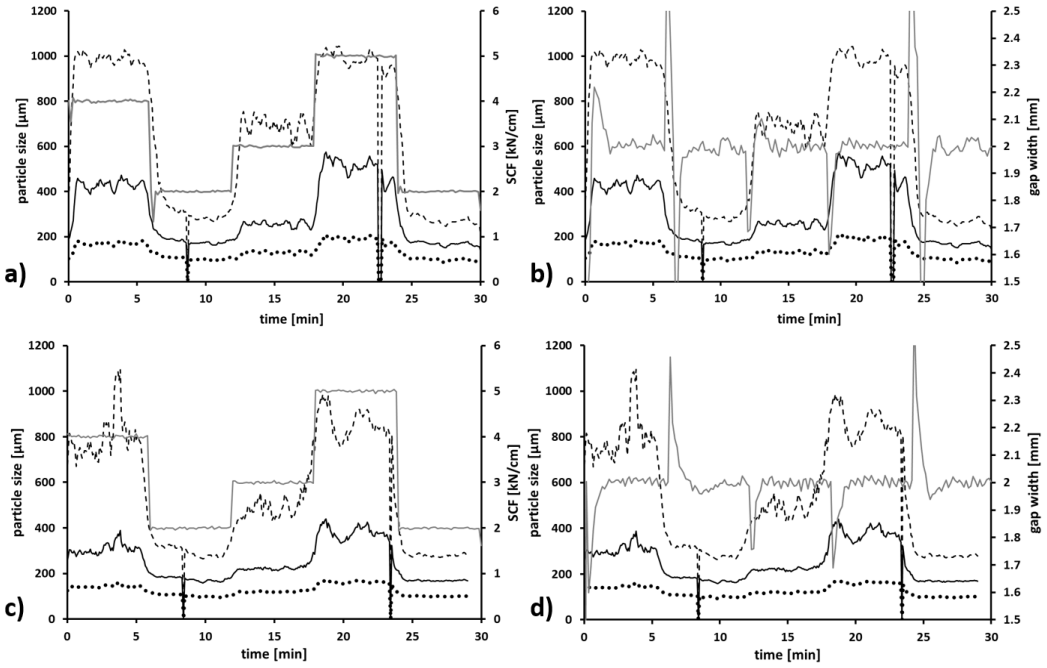

Fig. 2 Plot of GSD parameters (dashed, D75; full, D50; dotted, D25) against time. a and c SCF is plotted in gray. b and d Gap width is plotted in gray. Constant settings: gap width 2 mm and roll speed 2 rpm. a and b In-line measurement, n = 1. c and d On-line measurement, n = 1. GSD data in moving average over 30 s

Using these results (Fig. 2), an analysis of the residence time from between the two rolls to the analysis in the laser diffraction system was performed. It has to be noted that this residence time does not only include the time a particle needs to move from the tightest place in the compaction gap to the laser diffraction measurement zone. It furthermore includes the time the roll compaction process needs to reach the equilibrium after the SCF was adjusted. The combination of particle movement and process equilibration was measured in this experiment. A change in specific compaction force was the step change input while the D50 value was chosen as response parameter. The defining D50 value for each step was calculated by averaging the D50 values of the last 20 s of each run (individual measurements), assuming the values are in equilibrium right before changing the SCF. Event propagation time (EPT) was determined by calculating the time in which 5% (EPT5), 50% (EPT50), and 95% (EPT95) of the step change were reached and were calculated for every step change (n = 4) and averaged (Table 1).

Table 1 event propagation times (EPT) and mean residence time determination. n = 4; mean ± sd

EPT5	EPT50	EPT95
5.8 ± 4.0 s	17.7 ± 10.3 s	46.1 ± 13.4 s

Despite the time delay implied by using the moving average, it can be seen that with a mean EPT50 of 17.7 s, the time between changing SCF and reaching a GSD plateau is short. The SCF is measured between the rolls while the GSD is measured in the laser diffraction setup. Although the distance was about 2 m, the pneumatic conveyance was fast. The slowest step is supposedly the milling process. As shown in literature, the MRT of the milling process varies with different SCF [38]. Therefore, a fluctuation in residence time parameters can be reasoned by varying residence time of the ribbons in the milling unit. Furthermore, to obtain reliable granule size, both, the SCF and the gap width, must be in equilibrium. A change in SCF results in fluctuating gap widths (Fig. 2b and d). The time that is needed to reach a constant gap width also influences the time that is needed to reach the plateau. Despite relevant standard deviations, the calculated residence time parameters underline a fast adaption of the system to changes in particle size generated by process parameters.

For both setups, the effect of a change in SCF was seen. Changing back to a previously used SCF leads to comparable GSD results (see also the “In-line vs. on-line GSD determination and repeatability of measurements” section). Concerning a change in SCF, laser diffraction is an appropriate monitoring tool. Residence times of under a minute highlight that the system is fast in measuring differences in particle size if they appear in the process and are therefore favorable if a control strategy is to be developed.

GSD Determination at Increasing Throughput

In Fig. 3, GSD data recorded at 2 kN/cm SCF, 2.0-mm gap width, and increasing roll speed is displayed. The GSD parameters fluctuate around a constant value. For in-line measurements (Fig. 3a), the fluctuation is higher at low roll speeds while it decreases with increasing roll speed. This could be true for on-line measurements as well; however, judgment here is impeded by the higher frequency of emptying the collection vessel. After each emptying, the recorded transmission (Fig. 3d) is zero, indicating an overload of material passing through the laser beam. The material that was produced in about 10 s (up to 76 g) is collected just below the compactor outlet and transported in a bulk when the conveying is restarted. The dispersion might not be sufficient to separate those granules. This could explain increased recorded particle size at low-transmission values. These disturbances are visible in the data and complicate the analysis.

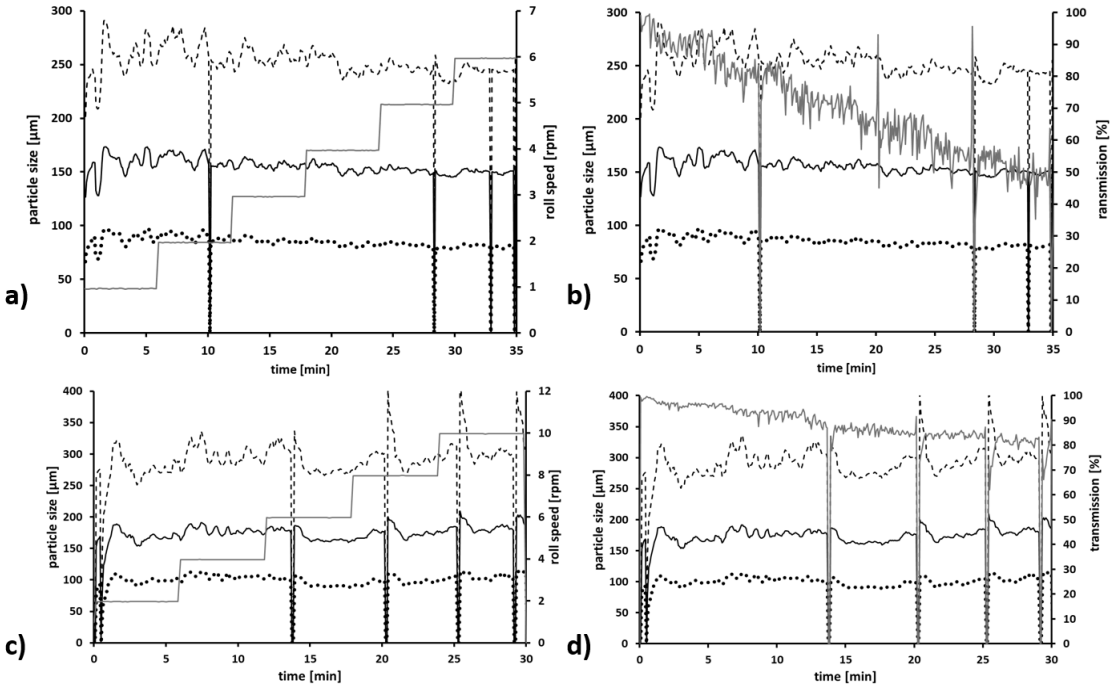

Fig. 3 Plot of GSD parameters (dashed, D75; full, D50; dotted, D25) against time. a and c Roll speed is plotted in gray. b and d Transmission is plotted in gray. Constant settings: gap width 2 mm and SCF 2 kN/cm. a and b In-line measurement, n = 1. c and d On-line measurement, n = 1. Transmission data in single values; GSD data in moving average over 30 s

Figure 3b additionally shows the current transmission every 5 s. The value of transmission depends on the size and number of particles in the measurement zone. As size is constant in this experiment, it is a measure of throughput. The actual throughput was determined off-line (Table 2).

Table 2 Throughputs at varying roll speed. SCF and gap width constant (2 kN/cm and 2 mm)

Roll speed [rpm]	Throughput [kg/h]
1	3.0
2	5.6
3	8.3
4	11.5
5	13.6
6	16.6
8	20.7
10	27.5

With increasing roll speed and throughput, the transmission is lowered. This is in accordance with the basic principle of laser diffraction. A decline in transmission can be a warning for the chances of multiple scattering increasing. This would be seen in varying GSD data. As the GSD data up to 16.6 kg/h is constant for the experiment, it can be concluded that no relevant multiple scattering effects take place. The in-line system can, in this case, be used for throughputs up to 16.6 kg/h (for pure MCC).

The on-line setup utilizes a bypass and, as not all material is conducted through the measurement zone, the transmission is higher for similar throughputs (Fig. 3d). Comparing the concentration values recorded by the laser diffraction system in parts per million, about 50% of material are directed through the bypass. Therefore, higher throughputs can be aimed at. Up to 27.5 kg/h, the measurements are fluctuating around similar values. A further increase of the throughput was feasible; however, the collection vessel filled up fast and the pneumatic conveyance was frequently stopped to empty the vessel so a continuous process with stable measurements was not possible.

In Fig. 3a and b, it can be seen that with increasing roll speed, fluctuations in the measurement seem to diminish. An explanation can be found in the hybrid sealing system that was implemented. Comparable with cheek plate sealing systems commonly found in RCDG, the hybrid sealing system leads to ribbons not sticking to the rolls after leaving the compaction zone. The ribbon is usually one continuous piece until it touches the milling unit and breaks. A slow roll speed leads to longer time between ribbon breakage than a high roll speed. Therefore, it could be observed that at 1 rpm, the mill is not filled with material constantly. A broken piece of the ribbon is completely milled down and before the next ribbon enters the milling unit, there is a certain time in which the mill is empty. This results in a fluctuating concentration of particles (Cv (ppm)) that is detected by the laser diffractometer (Fig. 4a).

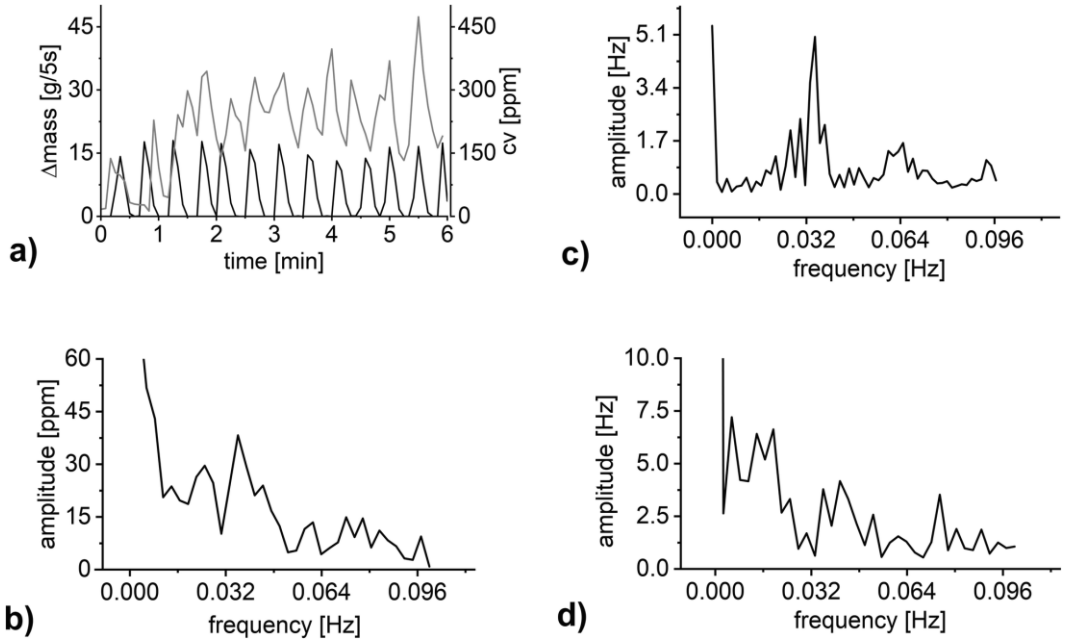

Fig. 4 Plot of mass variation (g/5 s) (black) and concentration of particles (ppm) (gray), value saved every 10 s, against production time; n = 1. b Amplitude against frequency plot of the mass variation (fast Fourier transformation). c Amplitude against frequency plot of the Cv fluctuations (fast Fourier transformation) d Amplitude against frequency plot of the D50 fluctuations (fast Fourier transformation). Roll speed = 1 rpm; throughput = 3.0 kg/h

In a separate experiment, the mass produced using a BRC25 with similar setup and 1 rpm roll speed was tracked every 10 s. The fluctuations in the output of the sieve are evident (Fig. 4a). Both fluctuations show peaks in dominant frequencies after a fast Fourier transformation (FFT) (Fig. 4b and c) that lay around 0.035 Hz (≈ a surge of material output every 28 s). This fluctuation of material can be one reason for fluctuations in measured GSD. Another point that has to be considered is that a ribbon entering the milling unit will be milled down over a certain time. Thereby, there is an initial breakage of ribbons that has to be differentiated from breakage occurring later in the milling process. Milling of a single ribbon over a time period can lead to resulting granule sizes that differ in the beginning and in the end. This phenomenon disappears at higher throughput as ribbons are produced faster and an equilibrium fill level is reached in the mill. Granule sizes can be expected to show less fluctuations in these cases as shown in Fig. 3a minutes 20–35. Figure 4d shows FFT results of the D50 parameter. It was tracked every 5 s over a period of 1895 s (equaling 379 individual measurement points). There is a peak at 0.036 Hz indicating that the mass fluctuation in ribbon production is noticeable in the D50 variation. Further dominant frequencies exist and could indicate effects of the differing fill level in the sieve or further, so far undescribed, effects.

GSD determination can therefore be done in adequate throughputs for pharmaceutical manufacturing. For high throughputs, the on-line setup could be favorable. To reach constant granule sizes (produced and measured), a roll speed of 3 rpm and above is favorable. It is also possible to develop a bypass system in which the material is not continuously conveyed in the manufacturing line. Instead, the material could be collected in a vessel below the compactor outlet and then conveyed in bulk at predefined time points. Measurement details have to be adapted in such a system.

In-line vs. On-line GSD Determination and Repeatability of Measurements

Figure 5 shows a comparison of full GSD curves between in- and on-line measurements at various SCFs. The data is obtained partly from the experiment shown in Fig. 2. However, the experiment was repeated on a different day following the same experimental procedure. For Fig. 5, results of both experiments were merged. As 2 kN/cm was also the SCF used for further experiments (e.g., also part of the data shown in Fig. 3), there are additional measurements that were also taken into consideration for this specific SCF (also shown in Fig. 6). Judging from the low standard deviations in all cases, the repeatability of the system can be regarded as high.

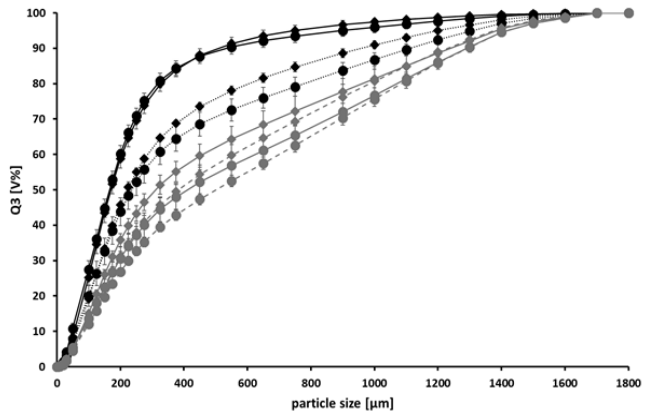

Fig. 5 GSD plot of in-line (circle) and on-line (diamond) data. Full black = 2 kN/cm, dotted black = 3 kN/cm, full gray = 4 kN/cm, dashed gray = 5 kN/cm. n ≥ 4, mean ± sd

Concerning the comparison of in-line and on-line measurements, at 2 kN/cm, the curves align well (full black lines). At higher SCFs, the on-line measurements repeatedly record smaller granule sizes compared with the same measurements in-line (in-line curves shifted to the left). Potentially, this difference is a product of non-representative sampling in the on-line setup that can only be seen for larger, more sluggish granules with a broader size distribution than that of the granules at 2 kN/cm. The fact that at increasing SCF, the size

distributions get wider and the difference in D50 increases (4 µm at 2 kN/cm, 14.2 µm at 3 kN/cm, 100.1 µm at 4 kN/cm, and 219.2 µm at 5 kN/cm) supports this. The angled pipe might not isokinetically sample the granule stream representatively, as larger granules with a higher mass require a stronger intervention than the pressured air of the venturi nozzle to be distracted from their flow pattern.

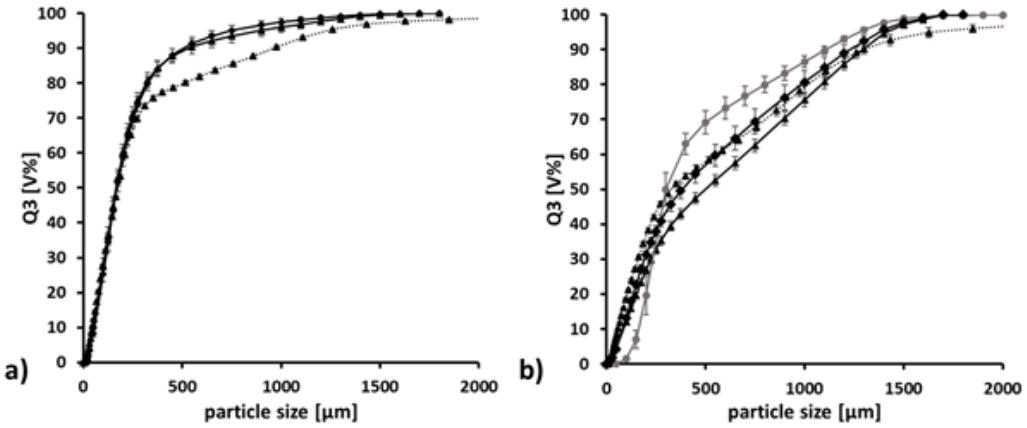

Fig. 6 GSD curves in-line (full black, triangle), on-line (full black, diamond), off-line (dotted line, triangle), and measured using dynamic image analysis (gray, circle). a 2 kN/cm: in-line, n = 17; on-line, n = 14; off-line, n = 3. b 5 kN/cm: in-line, n = 4; on-line, n = 5; off-line, n = 3. Mean ± sd

Granules obtained at low SCF can be representatively separated using the bypass setup. For bigger granules and broader size ranges, the bypass does not sample representatively but favors the extraction of smaller granules (shift to the left in the GSD curve). In- and on-line data therefore show differences. The sensitivity of the system to changes in process parameters is not diminished. If key GSD parameters can be determined representatively, it can therefore still be used as a parameter for a control strategy.

Comparison to Off-line Data

Figure 6 shows exemplary full GSD data for granules produced at 2 kN/cm and 5 kN/cm. As previously discussed, the in- and on-line measurements match well at 2 kN/cm but for larger SCF, they vary, with on-line data measuring smaller granule sizes. In the case of 2 kN/cm, off-line measurements match well with in/on-line data up to the D70 value. At higher size quantiles, off-line measurements record larger granule sizes. As a 1000-µm rasp sieve was used and granulation was performed at low SCF, it is unlikely that granules up to over 2000 µm were produced. Similar observations can be made for higher SCF (e.g., 5 kN/cm). The off-line measurement matches well with the on-line measurements up to 750 µm equaling about 60% of all material. Afterwards, it records larger granules up to a D99

of 2830 µm. About 10% of all granules are measured off-line with a granule size of 1600 µm and above. As mentioned above, this amount of granules larger than the rasp sieve size can be regarded as questionable.

Exemplarily, dynamic image analysis was conducted for the 5 kN/cm granules. The granule size distribution measured using DIA of the same material used for off-line laser diffraction is shown in Fig. 6b) (gray curve). A different curve shape when comparing laser diffraction and image analysis was expected and can be seen. However, the in/on-line laser diffraction data and image analysis data agree on a maximum granule size between 1400 and 1600 µm (D99). Larger granules (10% above 1600 µm in case of off-line laser diffraction) cannot be found by any other technique. As DIA also provides information on particle shape, the roundness according to DIN ISO 9276-6 ("Representation of results of particle size analysis – Part 6: Descriptive and quantitative representation of particle shape and morphology") was evaluated. Ninety percent of all measured particles show a roundness of 0.65 or less (with 1.00 indicating a perfect circle projection of a particle). The particles are therefore irregularly shaped, which can shift laser diffraction particle size results and explain the observed deviations. It has to be kept in mind that the dispersion is 0.8 bar for off-line measurements. As the dispersion pressure is relatively low (up to 4 bars are possible), destruction of granules can be avoided. There was no hint of measuring agglomerates. It is however difficult to decide, whether smaller particle sizes are recorded at larger dispersion pressure due to destruction of granules or due to a previous lack of dispersion. As the 0.8-bar dispersion pressure is chosen routinely for characterization of dry granulated product [39], it was chosen for this study as well.

As expected, it is not possible to transfer GSD information from one analyzing system to another without any adjustments. This is also true for in/on-line and off-line laser diffraction. Since repeatability for in/on-line measurements is high (see Figs. 6 and 7), it might be advisable to conduct reference measurements in the same setup as used in development/manufacturing to avoid the usage of off-line measurement systems.

Ability of the System to Detect Faulty Excipient Blends

The ability to detect changes in the granule sizes, if process parameters do not adhere, is important to judge the system's usefulness. Process parameters should themselves be monitored and incorporated into a control strategy. The information about GSD in this case

is valuable to determine whether the product is still suitable for further processing despite an unexpected event in process parameters. It could avoid unnecessary discarding of material, however, especially unexpected events that might not be visible directly in the process parameters should be detectable by monitoring the granule size of the resulting granules.

In the following experiments, no process parameters were changed. However, excipient blends were fed into the system that were produced differently.

Figure 7 shows results of two experiments in which the same formulation (MCC 79%, lactose 20%, magnesium stearate 1%) was used. However, the material was prepared differently according to Table 3.

Table 3 Formulation and preparation of experiments

Blend A	**Blend B**
microcrystalline cellulose – 79 % lactose – 20 % magnesium stearate – 1%	
Blending of MCC and lactose for 20 minutes. Afterwards, addition of magnesium stearate for an additional 3 minutes.	Blending of MCC, lactose and magnesium stearate for 20 minutes.
Correct procedure	Blend resulting in an over lubricated mixture

In the first experiment (Fig. 7a), blend B was compacted at a constant 7 kN/cm specific compaction force (minutes 0 to 11). Without any adjustments, at minute 11, blend A was manually fed into the inlet of the roll compactor. The material was introduced as soon as the feeding screw was visible. Immediate blending of the two materials in the feeding unit could not be inhibited, as the material could not be fed into the compaction zone directly. Therefore, a delay in response was expected. As expected, the over lubricated material led to smaller granules compared with the correctly blended mixture. All GSD key parameters (D25, D50, and D75) increase after the blend was switched.

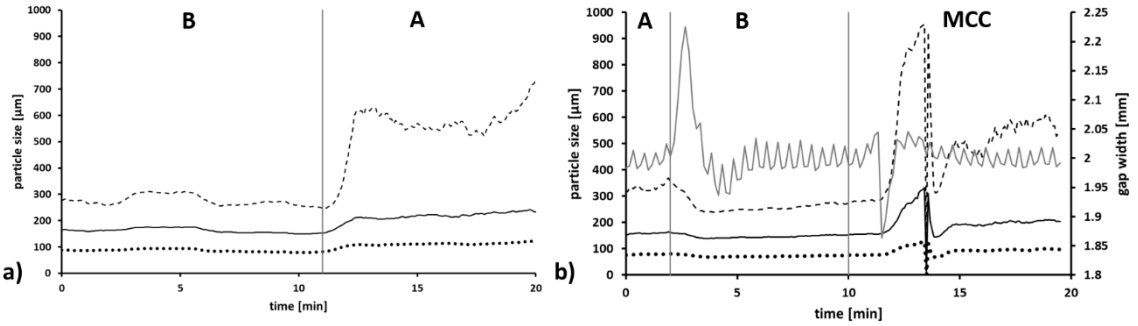

Figure 7. Plot of GSD parameters (dashed, D75; full, D50; dotted, D25) against time. a Gray vertical bar = addition of different excipients or blends and b also shows gap width in gray. n = 1, in-line measurement. Blend A = A; blend B = B; MCC= microcrystalline cellulose. GSD data in moving average over 30 s

Figure 7b shows results of a similar experiment in which at first blend A was compacted at 3 kN/cm and at minute two blend B was added. GSD parameters of blend A are well below the ones in the experiment shown in Fig. 7a. This can be explained by different applied SCFs. The resulting granules of blend B show smaller particle sizes. They are comparable with the granulation behavior at 7 kN/cm which can be reasoned by the impact of magnesium stearate as lubricant in compaction processes. At minute 10, pure MCC was added as excipient. About 30 s after addition, the gap width decreased as not enough material was fed into the gap to reach 3 kN/cm at a constant gap width. This resulted in a strong initial increase in granule size. Afterwards, the gap equilibrated around the desired 2 mm. The D75 was significantly increased compared with the over lubricated formulation as larger granules were produced. A high amount of fine material is typical for RCDG, especially at low SCF of 3 kN/cm. This amount is comparable with particle sizes resulting from an over lubricated formulation (D25 and D50).

The laser diffraction system was able to determine differences in GSD, if over lubricated material was delivered to the process. This should simulate a user error of incorrect blending of materials. A time delay was noticed as the material was fed into the hopper and not directly into the compaction zone.

Conclusions

An in- and on-line GSD monitoring system based on laser diffraction was implemented successfully in a RCDG process with up to 27.5 kg/h of material throughput. No window fouling was observed over the experiment time span of 2 weeks. The system detected changes in granule size based on varying process parameters or blend preparation methods.

This can be utilized as the base to develop an integrated control strategy for continuous RCDG. Knowledge about possible parameters that can be used to control (feedback or feedforward control loops) needs to be identified and linked to information obtained by GSD measurements. Also, information about RTD in the RCDG needs to be cumulated and put into practice. On-line laser diffraction measurements are based on non-representative sampling; however, sensitivity of and relevance in measured GSD data is similar to in-line data. A control strategy could be based on this bypass setup if measurements are reproducible or the bypass could be improved in future research.

References

1.Plumb K. Continuous processing in the pharmaceutical industry - changing the mind set. Chem Eng Res Des. 2005;83(A6):730–8. https://doi.org/10.1205/cherd.04359.

2. Rantanen J, Khinast J. The future of pharmaceutical manufacturing sciences. J Pharm Sci. 2015;104(11):3612–38. https://doi.org/10.1002/jps.24594.

3. Lee SL. Current FDA Perspective for Continuous Manufacturing. US FDA Center for Drug Evaluation and Research, MIT-CMAC 2nd International Symposium on Continuous Manufacturing of Pharmaceuticals. 2016. http://iscmp.mit.edu/sites/default/files/documents/ISCMP%202016%20-%20FDA%20MIT-CMAC%20for%20CM%202016%20Ver6.pdf.

4. Lee SL, O'Connor TF, Yang XC, Cruz CN, Chatterjee S, Madurawe RD, et al. Modernizing pharmaceutical manufacturing: from batch to continuous production. J Pharm Innov. 2015;10(3):191–9. https://doi.org/10.1007/s12247-015-9215-8.

5. Lee SL. Quality Considerations for Continuous Manufacturing Guidance for Industry. Food and Drug Administration, Silver Spring. 2019. https://www.fda.gov/media/121314/download. Accessed 14.11.2019 14:48.

6. Garcia T, Cook G, Nosal R. PQLI key topics-criticality, design space, and control strategy. J Pharm Innov. 2008;3(2):60–8.

7. Engisch W, Muzzio F. Using residence time distributions (RTDs) to address the traceability of raw materials in continuous pharmaceutical manufacturing. J Pharm Innov. 2016;11(1):64–81. https://doi.org/10.1007/s12247-015-9238-1.

8. Betz G, Junker-Burgin P, Leuenberger H. Batch and continuous processing in the production of pharmaceutical granules. Pharm Dev Technol. 2003;8(3):289–97. https://doi.org/10.1081/pdt-120022157.

9. ICH Q8 (R2) Pharmaceutical development, (2014).

10. ICH Q10 Pharmaceutical Quality System, (2008).

11. Badman C, Cooney CL, Florence A, Konstantinov K, Krumme M, Mascia S, et al. Why we need continuous pharmaceutical manufacturing and how to make it happen. J Pharm Sci. 2019;108(11):3521–3. https://doi.org/10.1016/j.xphs.2019.07.016.

12. Hlinak AJ, Kuriyan K, Morris KR, Reklaitis GV, Basu PK. Understanding critical material properties for solid dosage form design. J Pharm Innov. 2006;1(1):12–7. https://doi.org/10.1007/bf02784876.

13. Laske S, Paudel A, Scheibelhofer O, Author T. A review of PAT strategies in secondary solid oral dosage manufacturing of small molecules. J Pharm Sci. 2017;106(3):667–712. https://doi.org/10.1016/j.xphs.2016.11.011.

14. U.S. Food & Drug Administration. Guidance for Industry, PAT - A Framework for Innovative Pharmaceutical Development, Manufacturing and Quality Assurance. 2004. https://www.fda.gov/media/71012/download.

15. Singh R, Ierapetritou M, Ramachandran R. An engineering study on the enhanced control and operation of continuous manufacturing of pharmaceutical tablets via roller compaction. Int J Pharm. 2012;438(1–2):307–26. https://doi.org/10.1016/j.ijpharm.2012.09.009.

16. Fonteyne M, Vercruysse J, De Leersnyder F, Van Snick B, Vervaet C, Remon JP, et al. Process analytical technology for continuous manufacturing of solid-dosage forms. Trac-Trend Anal Chem. 2015;67:159–66. https://doi.org/10.1016/j.trac.2015.01.011.

17. Tok AT, Goh X, Ng WK, Tan RB. Monitoring granulation rate processes using three PAT tools in a pilot-scale fluidized bed. AAPS PharmSciTech. 2008;9(4):1083–91. https://doi.org/10.1208/s12249-008-9145-6.

18. Leuenberger H. New trends in the production of pharmaceutical granules: batch versus continuous processing. Eur J Pharm Biopharm. 2001;52(3):289–96. https://doi.org/10.1016/s0939-6411(01)00199-0.

19. Vervaet C, Remon JP. Continuous granulation in the pharmaceutical industry. Chem Eng Sci. 2005;60(14):3949–57. https://doi.org/10.1016/j.ces.2005.02.028.

20. Parikh DM. Handbook of pharmaceutical granulation technology. Boca Raton: CRC Press; 2016.

21. Kleinebudde P. Roll compaction/dry granulation: pharmaceutical applications. Eur J Pharm Biopharm. 2004;58(2):317–26. https://doi.org/10.1016/j.ejpb.2004.04.014.

22. Shlieout G, Lammens RF, Kleinebudde P. Dry granulation with a roller compactor part I: the functional units and operation modes. Pharm Technol Eur. 2000;12(11):24–35.

23. Shekunov BY, Chattopadhyay P, Tong HH, Chow AH. Particle size analysis in pharmaceutics: principles, methods and applications. Pharm Res. 2007;24(2):203–27. https://doi.org/10.1007/s11095-006-9146-7.

24. Alderliesten M. Mean particle diameters. Part IV: empirical selection of the proper type of mean particle diameter describing a product or material property. Part Part Syst Charact. 2004;21(3):179–96. https://doi.org/10.1002/ppsc.200400917.

25. Madarasz L, Nagy ZK, Hoffer I, Szabo B, Csontos I, Pataki H, et al. Real-time feedback control of twin-screw wet granulation based on image analysis. Int J Pharm. 2018;547(1–2):360–7. https://doi.org/10.1016/j.ijpharm.2018.06.003.

26. Chan LW, Tan LH, Heng PWS. Process analytical technology: application to particle sizing in spray drying. AAPS PharmSciTech. 2008;9(1):259–66. https://doi.org/10.1208/s12249-007-9011-y.

27. Nalluri VR, Schirg P, Gao X, Virdis A, Imanidis G, Kuentz M. Different modes of dynamic image analysis in monitoring of pharmaceutical dry milling process. Int J Pharm. 2010;391(1–2):107–14. https://doi.org/10.1016/j.ijpharm.2010.02.027.

28. Greaves D, Boxall J, Mulligan J, Montesi A, Creek J, Sloan ED, et al. Measuring the particle size of a known distribution using the focused beam reflectance measurement technique. Chem Eng Sci. 2008;63(22):5410–9. https://doi.org/10.1016/j.ces.2008.07.023.

29. Närvänen T, Lipsanen T, Antikainen O, Räikkönen H, Heinämäki J, Yliruusi J. Gaining fluid bed process understanding by in-line particle size analysis. J Pharm Sci. 2009;98(3):1110–7.

30. Petrak D. Simultaneous measurement of particle size and particle velocity by the spatial filtering technique. Part Part Syst Charact. 2002;19(6):391–400. https://doi.org/10.1002/ppsc.200290002.

31. Mangal H, Derksen E, Lura A, Kleinebudde P. In-line particle size measurement in dry granulation: Evaluation of probe position. 10th World Meeting on Pharmaceutics, Biopharmaceutics and Pharmaceutical Technology. 2016.

32. Wilms A, Knop K, Kleinebudde P. Combination of a rotating tube sample divider and dynamic image analysis for continuous on-line determination of granule size distribution. Int J Pharm X. 2019;1:100029. https://doi.org/10.1016/j.ijpx.2019.100029.

33. McAuliffe MAP, O'Mahony GE, Blackshields CA, Collins JA, Egan DP, Kiernan L, et al. The use of PAT and off-line methods for monitoring of roller compacted ribbon and granule properties with a view to continuous processing. Org Process Res Dev. 2015;19(1):158–66. https://doi.org/10.1021/op5000013.

34. Allen T. Powder sampling and particle size determination. 1st ed. Amsterdam: Elsevier B.V; 2003.

35. Ma ZH, Merkus HG, de Smet JGAE, Verheijen PJT, Scarlett B. Improving the sensitivity of forward light scattering technique to large particles. Part Part Syst Charact. 1999;16(2):71–6. https://doi.org/10.1002/(Sici)1521-4117(199906)

36. Ma ZH, Merkus HG, Scarlett B. Extending laser diffraction for particle shape characterization: technical aspects and application. Powder Technol. 2001;118(1–2):180–7. https://doi.org/10.1016/S0032-5910(01)00309-6.

37. Ma Z, Merkus HG, van der Veen HG, Wong M, Scarlett B. On-line measurement of particle size and shape using laser diffraction. Part Part Syst Charact. 2001;18(5–6):243–7.

38. Mangal H, Kleinebudde P. Experimental determination of residence time distribution in continuous dry granulation. Int J Pharm. 2017;524(1–2):91–100. https://doi.org/10.1016/j.ijpharm.2017.03.085.

39. Wiedey R, Šibanc R, Wilms A, Kleinebudde P. How relevant is ribbon homogeneity in roll compaction/dry granulation and can it be influenced? Eur J Pharm Biopharm. 2018;133:232–9. https://doi.org/10.1016/j.ejpb.2018.10.021.

Acknowledgments

This work was supported by the Drug Delivery Innovation Center (DDIC), INVITE GmbH, Leverkusen.

Funding

Open Access funding provided by Projekt DEAL.

4 Implementing Feedback Granule Size Control in a Continuous Dry Granulation Line Using Controlled Impeller Speed of the Granulation Unit, Compaction Force and Gap Width

Annika Wilms[a,b], Andreas Teske[c], Robin Meier[c], Raphael Wiedey[a], Peter Kleinebudde[a]

[a] Heinrich Heine University Düsseldorf, Universitätsstraße 1, 40225 Düsseldorf, Germany

[b] INVITE GmbH, Drug Delivery Innovation Center, Chempark Building W32, 51368 Leverkusen, Germany

[c] L.B. Bohle Maschinen + Verfahren GmbH, Industriestrasse18, 59320 Ennigerloh, Germany

4.1 Pretext

The following research paper has been published in the Journal of Pharmaceutical Innovation (2020). https://doi.org/10.1007/s12247-020-09524-3

Evaluation of authorship:

author	idea [%]	study design [%]	experimental [%]	evaluation [%]	manuscript [%]
Annika Wilms	40	50	85	70	65
Andreas Teske	20	20	15	10	5
Robin Meier	20	15	0	0	10
Raphael Wiedey	0	0	0	20	10
Peter Kleinebudde	20	15	0	0	10

Implementing Feedback Granule Size Control in a Continuous Dry Granulation Line Using Controlled Impeller Speed of the Granulation Unit, Compaction Force and Gap Width

Annika Wilms[a,b], Andreas Teske[c], Robin Meier[c], Raphael Wiedey[a], Peter Kleinebudde[a]

[a] Heinrich Heine University Düsseldorf, Universitätsstraße 1, 40225 Düsseldorf, Germany

[b] INVITE GmbH, Drug Delivery Innovation Center, Chempark Building W32, 51368 Leverkusen, Germany

[c] L.B. Bohle Maschinen + Verfahren GmbH, Industriestrasse18, 59320, Ennigerloh

Journal of Pharmaceutical Innovation (2020)

https://doi.org/10.1007/s12247-020-09524-3

Abstract

Purpose In continuous manufacturing of pharmaceuticals, dry granulation is of interest because of its large throughput capacity and energy efficiency. In order to manufacture solid oral dosage forms continuously, valid control strategies for critical quality attributes should be established. To this date, there are no published control strategies for granule size distribution in continuous dry granulation.

Methods In-line laser diffraction was used to determine the size of granules in a continuous roll compaction/dry granulation line (QbCon® dry). Different process parameters were evaluated regarding their influences on granule size. The identified critical process parameters were then incorporated into control strategies. The uncontrolled and the controlled processes were compared based on the resulting granule size. In both processes, a process parameter was changed to induce a shift in median particle size and the controller had to counteract this shift.

Results In principle, all process parameters that affect the median particle size could also be used to control the particle size in a dry granulation process. The sieve impeller speed was found to be well suited to control the median particle size as it reacts fast and can be controlled independently of the throughput or material.

Conclusion

Themedianparticlesizeincontinuousrollcompactioncanbecontrolledbyadjustingprocesspara metersdepending on real-time granule size measurements. The method has to be validated

and explored further to identify critical requirements to the material and environmental conditions.

Keywords

Continuous manufacturing, roll compaction/dry granulation, process analytical technologies, laser diffraction, process control, feedback control

I. Introduction

Continuous manufacturing(CM) in the production of pharmaceutical solid oral dosage forms is characterized by the connection of individual processes into one line, ideally from raw excipients and active pharmaceutical ingredient (API) to final dosage form. Potentials of this production concept include higher flexibility of production volume and time as well as increased quality due to tight monitoring and control strategies [1,2,3,4]. Regulatory agencies and the International Council of Harmonization (ICH) have shown support of this approach [5,6,7,8,9,10,11]. A new guideline, ICH Q13, is currently developed for continuous manufacturing processes [12]. However, monitoring and control strategies have to be developed by the manufacturers prior to taking advantage of this manufacturing technique. High priority is set to process-analytical technologies (PAT) which aim at executing timely (in-line or on-line) measurements and determining critical quality attributes (CQA) [13]. As described by the U.S. FDA, in-line measurements are characterized by the sample not being removed from the process [6]. Using this concept, time and resources can be drastically reduced. As a necessary premise, traditional characterization techniques (e.g. particle size or API concentration determination) have to be transferred to robust real-time measurements [14].

While direct compression is the favorable process in continuous manufacturing, it is not always possible due to the raw materials properties (especially poor flow properties or segregation issues of powder material). Therefore, a granulation step might be needed prior to tableting. The manufacturing classification system (MCS) is a joint effort from academic and industrial technology experts to rank the feasibility of pharmaceutical processing routes for solid dosage forms. It ranks roll compaction/dry granulation (RCDG) as the granulation method of choice, if direct compression is not possible [15]. It is favorable due to its natural continuity, large throughput possibilities and energy efficiency [16]. It is however not suitable for all formulations as the capability of improving the flow properties is limited

based on the large amount of fines in the final granules and the undesired effect of reduced tabletability that is well described in literature [17 - 19]. A CQA in granulation is the granule size distribution (GSD) of the granulated material [20, 21]. While there are multiple measurement principles and apparatuses, most of them are set up in a discontinuous way and do not allow continuous GSD-determination. However, due to the growing interest there have been reports of continuous size determination in the production of pharmaceuticals [22 - 27]. Size determination has proven to be challenging in continuous RCDG due to the high throughput, the bimodal size distribution with a large fraction of fines and the inhomogeneous product stream [28 - 32]. The use of laser diffraction, as a non-invasive, in- and on-line technique to monitor the GSD during continuous RCDG was recently published [33].

However, monitoring is only the first step to a process control strategy. To develop a control strategy, a CQA has to be adequately measured first. Afterwards, it is necessary to determine a specification window for the CQA and to find a process parameter that can be controlled which affects the CQA in a desired way. It is well known that the specific compaction force (SCF) and gap width affect the GSD of dry granulated material [34]. However, especially the SCF is a key critical process parameter (CPP) that affects further properties (e.g. hardness [35], porosity [36, 37] and throughput [38] if only the SCF is changed).

Singh et al. (2012) [39] mentioned that the particle size in continuous RCDG could be controlled by adjusting the milling speed of the granulation unit. This claim was statistically analyzed by Mangal and Kleinebudde in 2018 [40]. The group confirmed that the impeller speed of a conical sieve in the milling unit of a roll compactor has significant impact on the median particle size and the amount of fines. This was evaluated for three different raw materials and two formulations containing ibuprofen and acetaminophen as active pharmaceutical ingredient (API). Mangal and Kleinebudde claimed that high impeller speeds should be avoided as it could lead to large amount of fines and slow speeds could bear issues in milling the material in adequate time. However, these claims were not backed with data and should be evaluated further.

For a CPP that influences the granule size, it should be possible to program a controller to react to changes in the desired CQA by adjusting the chosen process parameter. Examples

of PAT-controllers in pharmaceutical manufacturing, e.g. in fluidized bed processes, can be found in literature [41, 42].

The aim of this study was to advance the previously published monitoring strategy for GSD in continuous dry granulation to a control strategy [33]. The proof of principle was supposed to be given for various parameters to be controlled. Therefore, process parameters in RCDG were evaluated for their suitability as control valves. Controller parameters and data analysis were optimized to evaluate the applicability in industrial manufacturing. Implementing a control strategy for granule size in continuous granulation is the next step in the continuous process of implementing advanced manufacturing techniques in the pharmaceutical industry.

II. Material and Methods

II.1. Materials

Microcrystalline cellulose (MCC, Vivapur® 102, JRS Pharma, Germany) was used as a plastically deforming excipient in experiments studying varying process parameters.

For various experiments, magnesium stearate (Parteck LUB MST, Merck, Germany) was added at 1% for lubrication. To avoid sticking of the material to the rolls, magnesium stearate was mixed with formulation components in a bin blender (LM 40, L.B. Bohle Maschinen + Verfahren GmbH, Germany) for 3 min at 20 rpm. In some experiments the behavior of over-lubricated mixtures was studied. These were produced by increasing the mixing time to 20 min.

For studies using an API in a formulation, 25% Diclofenac (Amoli Organics Pvt. Ltd., India), 60% MCC and 14% anhydrous β-lactose (SuperTab® 21AN, DFE Pharma, Germany) were blended for 20 min at 20 rpm. Afterwards, 1% magnesium-stearate was added and blended for another 3 min.

II.2. Continuous roll compaction/dry granulation

A QbCon© dry CM-line was used for all experiments. It was equipped with a small-scale roll compactor (BRC 25, L.B. Bohle Maschinen + Verfahren GmbH, Germany). A 360° rotating conical sieve was implemented as granulation unit and comprised a 1.0 mm rasp sieve (BTS 100, L.B. Bohle Maschinen + Verfahren GmbH, Germany). Knurled surface

rolls and a hybrid sealing system were used for all experiments. 2 rpm roll speed was set for all experiments. Material was refilled manually. A suction shoe was mounted below the roll compactor outlet and attached to a plastic hose (see Fig. 1, points 7 and 8). The hose was linked to a vacuum receiver (Volkmann GmbH, Soest, Germany) and the applied vacuum continuously transported the granules through the laser diffraction system into a collection vessel. If the fill volume exceeded a capacity maximum, the vacuum receiver stopped for ten seconds, the vessel was emptied and afterwards conveyance continued.

II.3. Granule size determination using laser diffraction

An in-line laser diffraction system (Insitec© T, Malvern Panalytical, UK) was instrumented. The hose attached to the outlet of the roll compactor lead the material through the installation before reaching the collection vessel. The system can analyze particles up to a diameter of 1600 µm. It contains a lens of 500 mm focal length, a laser (red, 670 nm) with a 10.0 mm beam waist, a circular detector comprising 33 detector plates and a scan rate of 2000 Hz. The system logged the GSD data with a frequency of 0.2 Hz equaling to a displayed value every 5 seconds, which comprised 10 000 individual scans. Raw data was tracked and exported using RTSizer© software (Malvern Panalytical, UK). To avoid lens fouling a constant stream of pressured air was inserted on both lenses (10 Nm^3/h) and drained off together with the material stream.

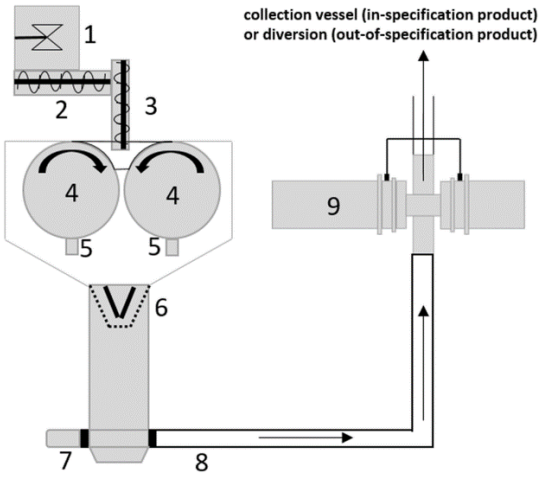

Fig. 1 Experimental set-up 1) powder inlet, 2) feeding auger, 3) tamping auger, 4) rolls, 5) scraper, 6) conical sieve, 7) suction shoe, 8) plastic hose, 9) laser diffraction system

II.4. Process control

The granule size data was logged with MalvernLink© software (MalvernPanalytical, UK) and synchronized via OPC UA to a SCADA server (L.B. Bohle Maschinen + Verfahren

GmbH, Germany). Individual values of transmission as well as characteristic quantiles (D25, D50, D75, D90) were transmitted. Furthermore, moving average (90 s) values were transmitted for all of the named parameters. The moving average over 90 s was chosen as GSD parameter to be controlled in order to smoothen the natural fluctuations.

A proportional-integral (PI) controller was programmed to compare the current value with the set-point value, calculate the error and generate a response. The formula of a PI-controller is shown in eq. 1. The control signal addressed to the actuator (c) is calculated [43].

$$c = c_0 + K_c \left(e(t) + \frac{1}{T_i} \int_0^1 e(\tau) d\tau \right) \quad (1)$$

c_0 is a constant controller bias (or null signal) which assures a smooth transition from turning on the controller. Typically, it equals c at the time point of turning on the controller. e represents the current error (current value – set point) at time point τ. K_c (gain-factor) and T_i (integral time) could be varied for optimization of the controller. They characterize the proportional and integral part of the controller respectively [43]. The desired particle size value was entered in the software. Three controllers were programmed, each controlling a different process parameter (SCF, gap width and impeller speed of the milling unit). K_c and T_i values are listed with every experiment in the Results section.

II.5. Data treatment

For evaluation of possible control variables, GSD data was logged every 5 s. Depending on run-time during the experiment, 48 to 72 values were logged corresponding to experimental run times between 4 to 6 min. If a run was executed 3 times and lasted 6 min each, the amount of data points is specified as $n = 3 \times 72$.

For analysis of a continuous process, the RCDG process parameters and the GSD data were logged together every second. For time against parameter graphs the 90 s moving average for GSD data is plotted. The process parameters are plotted as individual, non-smoothed values ($n = 1$).

To evaluate the distribution of GSD values in one process, a density against particle size plot was chosen. All GSD values recorded over the time span of the experiment were normalized to the desired set-point that was chosen for the experiment. Afterwards, the

density of each relative particle size (D50/D50mean) was estimated using kernel density estimation and plotted. The data analysis was performed using functions of Pythons Pandas library (python 3.8, python.org; Pandas 1.1.0, pandas.pydata.org).

III. Results and Discussion

III.1. Determination of suitable control variables for different material types

The effect of varying CPPs on GSD was evaluated using MCC and a formulation containing Diclofenac. As mentioned in the introduction, Mangal et al. reported that increasing the impeller speed decreases the particle size of granules [40]. In their work, the factor space was limited to 300, 600 and 900 rpm impeller speed. To develop a control strategy based on this effect, it was analyzed in more detail for this work. Therefore, the impeller speed was increased from 100 rpm to 900 rpm in 100 rpm intervals and the resulting granule size was measured. Before each measurement, the sieve was vacuumed to be empty and the measurement was started when the system was in equilibrium. Every individual measurement lasted 4–6 min (48–72 individual values). Results are shown in Fig. 2.

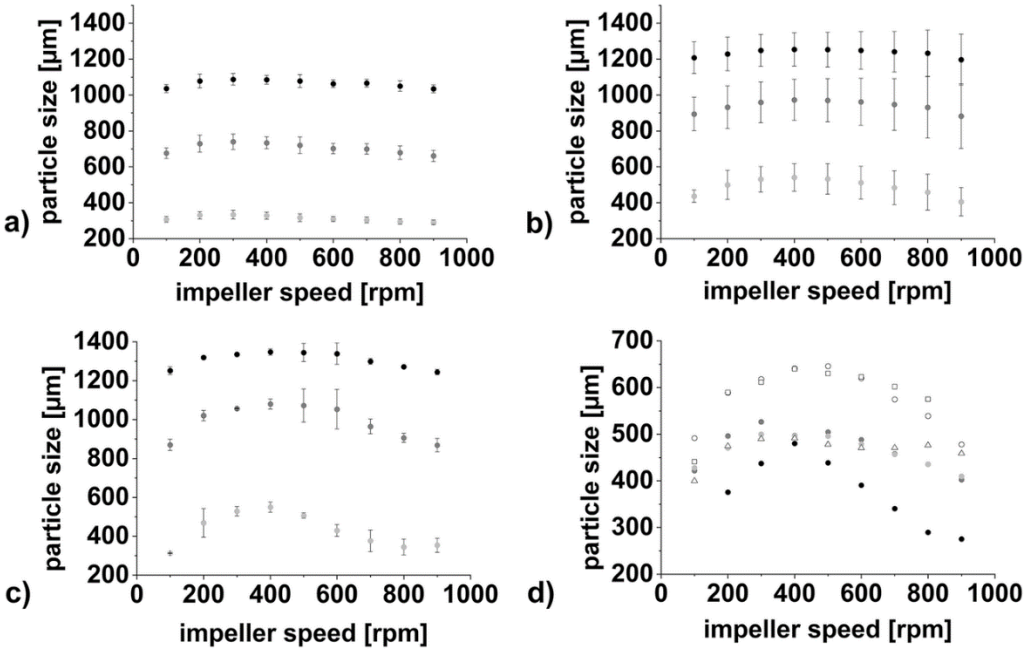

Fig. 2 GSD parameters against impeller speed. a), b) and c): black = D90; gray = D75; light gray = D50. a) MCC, 2 kN/cm; n = 3 × 72; mean ± sd. b) MCC, 4 kN/cm; n = 6 × 48–72; mean ± sd. c) Diclofenac formulation, 7 kN/cm; n = 3 × 48; mean ± sd. d) individual D50-values for MCC at 4 kN/cm. Each symbol represents an individual experiment. Each data point n = 48–72; mean

In contrast to Mangal [40], the effect of the impeller speed on particle size was not found to be solely a decrease in particle size at increasing impeller speeds. A maximum in particle size was observed at 300–500 rpm. Decreasing and increasing the impeller speed from there decreased the granule size parameters. With the experimental settings chosen by Mangal, this effect could not be visible in the statistical design of experiment chosen.

Figure 2 b) clearly shows a large variation at different impeller speeds for MCC compacted at 4 kN/cm. In Fig. 2 d), the 6 repetitions are shown individually. For every individual measurement, the curve has an inverted u-shape with a maximum for D50. However, the absolute values differ.

A possible explanation, as MCC is a hygroscopic material, could be the varying air humidity in the laboratory facility. The effect of moisture content on MCC characteristic properties was extensively studied by Sun [44, 45]. In one of the studies, MCC was equilibrated between 0 and 84.3% RH. Afterwards, compressibility plots of the materials were compared. If the monolayer water coverage was exceeded (26% RH at 25 °C), the compressibility plots depended on water content of MCC. A higher water content of MCC led to a reduced porosity and a faster approach to zero porosity at increasing pressure [44].

As the compressibility plot describes the change in porosity upon pressure, this variety can also be applicable to the roll compaction process. The temperature was controlled at 23 °C. However, air humidity was not controlled. In Fig. 2 d), the empty triangles were recorded at 37% RH while the results plotted as empty circles were recorded at 50% RH. It is possible that the monolayer water coverage was exceeded for parts or all of the material, however, measurements were not performed. Therefore, in accordance with the research by Sun, during the experiment at 50% RH, MCC was compressed to a ribbon showing less porosity compared to the experiment conducted at 37% RH. The observed differences in resulting granule sizes are then plausible [34]. For the results plotted as filled circles, the relative humidity was not tracked. It is recommended to perform experiments in a temperature and air humidity-controlled environment and track these values if they cannot be controlled. For the research presented in this work, the results meant that absolute particle sizes registered have to be analyzed in accordance with the day experiments were conducted. Figure 2 c) shows the results for a formulation containing Diclofenac as API. The curves have a similar shape as those of pure MCC. The values in Fig. 2 c) were, opposed to Fig. 2 a) and b), recorded on a single day.

ANOVA was performed and results are shown in Table 1. For MCC compacted at 2 and 4 kN/cm trends were observed, but it could not be stated with statistical significance that the impeller speed has any effect on granule size. For the Diclofenac formulation, all three granule size values are significantly impacted by impeller speed. For individual measurement runs (Fig. 4 d)) the statistical analysis could not be performed as individual values of n = 1 cannot be statistically analyzed comparably. The insufficient repeatability for MCC compacted at 4 kN/cm has to be evaluated further in future research.

Table 1. Results of ANOVA for data shown in Fig. 2 a) – c). Diclo = Diclofenac formulation; DF = degrees of freedom; SSQ = sum of squares; Mean Sq = mean sum of squares; F emp = calculated F-value; p value = calculated p value

SCF [kN/cm]	**Material**	**Dx [µm]**	**DF**	**SSQ**	**Mean Sq**	***F emp***	***p value***
2	MCC	50	8	576.5	720.2	2.236	0.0745
		75		19 051.3	2 381.4	1.755	0.1531
		90		9 538.6	1 192.3	1.515	0.2204
4		50		95 940.5	11 992.6	1.775	0.1088
		75		45 001.6	5 625.2	0.315	0.9563
		90		17 437.3	2 179.7	0.193	0.9904
7	Diclo	50		158 137.5	19 767.2	13.626	< 0.00001
		75		163 348.6	20 418.6	6.936	0.0007
		90		35 913.9	4 489.2	5.480	0.0023

For controlling the granule size by adjusting the impeller speed of the milling unit, a direction of action has to be defined. Therefore, the impeller speed controller was limited to either 100–400 rpm or 400–900 rpm and the direction (increasing or decreasing the impeller speed at deviation from set-point) was defined by using a positive or a negative K_c-value.

It can be seen in Fig. 2 that the impact of impeller speed on particle size is limited, as the slopes of the increasing and decreasing part of the curve are small. As known from literature, the CPPs SCF and gap width have an impact on the resulting granule sizes. In scope of this work, the impact of both parameters on the resulting median particle size (D50) was measured using in-line laser diffraction for MCC as excipient (Fig. 3).

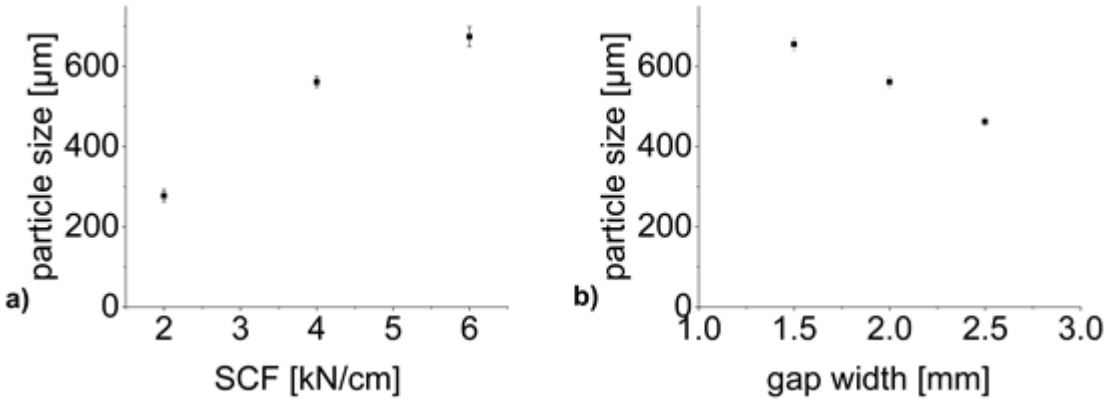

Fig.3 Median particle size (D50) against a) SCF (constant roll speed = 2 rpm, gap width = 2.0 mm and impeller speed = 800 rpm) and b) gap width (constant roll speed = 2 rpm, SCF = 4.0 kN/cm and impeller speed = 800 rpm) for MCC. Each point n = 1 × 72; mean ± sd

In conclusion, impeller speed, gap width and SCF are CPP that impact the resulting granule size. Based on these results, there needs to be a proof that this behavior can be used to control a process in accordance with granule size. There was no impact of impeller speed on the granule size at low SCF (2 kN/cm, see Table 1). At 4 kN/cm, the impact was visible for individual measurement runs, however, insufficient repeatability impacts a general conclusion. The decision, which process parameter is suited to control the granule size must be evaluated carefully prior to implementing the control loop.

III.2. Controlling a process with an unstable gap width – impeller speed controller

A change in gap width leads to a change in resulting particle size (Fig. 3 b). An unstable gap can be the result of poorly flowing materials for which even feeding is difficult. It was evaluated whether the control tool can counteract the changes in GSD caused by an unstable gap. Therefore, in a reference experiment, MCC was compacted at 2 kN/cm SCF, 800 rpm impeller speed and 2 mm gap width for 15 min. After 15 min the gap width was increased to 2.5 mm at otherwise constant process parameters. Results can be seen in Fig. 4 a). As expected, the D50 values that are registered dropped after an increase in gap width. During the first 15 min, at 2.0 mm gap width, the average D50 value recorded was 440 µm. Therefore, 440 µm was chosen as set-point for the experiments under controlled conditions (horizontal dashed lines in Fig. 4). Figures 4 b) and c) show results of the same experimental set-up but with a controlled impeller speed. The two experiments differ in the proportional controller gain (Kc). The controller set at Kc = −1.0 is more aggressive than the one set at $K_c = -0.5$.

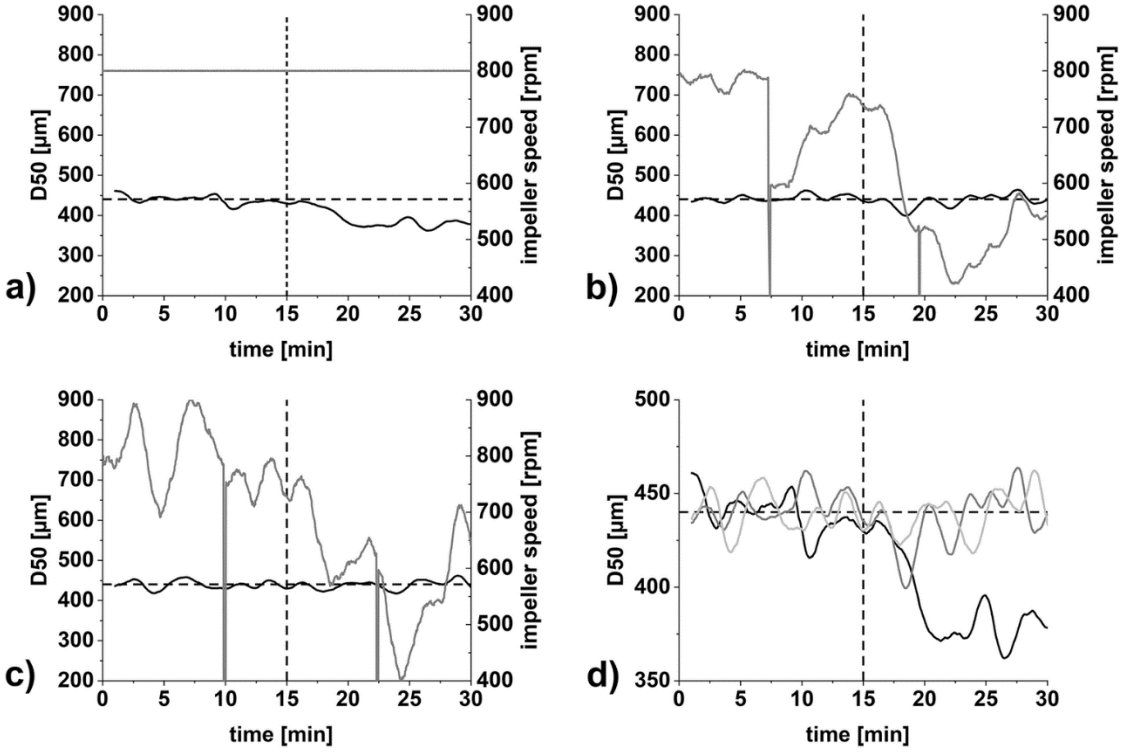

Fig. 4 Plot of D50 and impeller speed against time. a) uncontrolled process b) controlled at 440 µm, $K_c = -0.5$, $T_i = 10.0$ s c) controlled at 440 µm, $K_c = -1.0$, $T_i = 10.0$ s d) D50 values of experiments a) – c) combined. a) – c) black = D50, gray = impeller speed, horizontally dashed = 440 µm set-point, vertically dashed = gap width change d) black = uncontrolled, dark gray = controlled, $K_c = -0.5$, $T_i = 10.0$ s, light gray = controlled, Kc = −0.5, Ti = 10.0 s. Each data point n = 1; in-line data

In both cases, the drop in particle size can be counteracted by the controller adjusting the impeller speed (Fig. 4 d)). To evaluate the effect in more detail, the density against relative particle size plot is shown in Fig. 5. In the uncontrolled process, the density curve shows a bimodal shape indicating that two particle sizes are dominant. One is located at 1 (= 440 µm) and the second one is located at about 0.86 (≈ 378 µm). Based on the experimental procedure and results (Fig. 4 a)) it is obvious that the first peak at 1 indicates the average particle size at 2.0 mm gap width while the second peak can be attributed to compacting the material at 2.5 mm gap width. When the process is controlled, the peak at 0.86 relative particle size is no longer visible. The curves show a slightly different shape, as the more aggressive controller tends to over- and under-shoot leading to a bimodal shape slightly above and below 1. The less aggressive controller has a mono-modal curve shape centered at 1, as desired. However, it has a broader distribution ranging from 0.85 to 1.13. The initial drop in particle size that triggered the controller response can be seen approximately at 0.95 relative particle size.

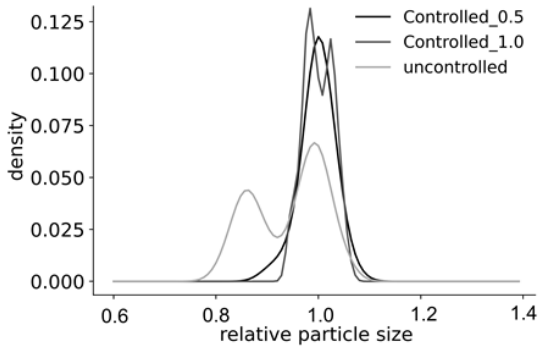

Fig.5 Density against relative particle size for the experiments shown in Fig. 4 a) – c). Each plot n = 1; in-line data

In Fig. 4 b) and c), the sieve speed drops to the minimum of 400 rpm on two occasions each. This is a result of the experimental set-up (see section II.2. Continuous roll compaction/dry granulation) and the collection vessel in which all material is collected. If the fill level of the vessel reaches a threshold, the vessel is emptied. For this process, the pneumatic transport of material is interrupted for approximately 10 s. Therefore, for two individual measurements, no granule sizes can be measured, as no granules pass through the laser beam. Unfortunately, on these occasions, a D50 value of 0 µm is transmitted to the SCADA server. The sudden decrease is D50 value leads to an increased error e and triggers a large control signal c to the actuator. In this case, a sudden drop in impeller speed occurs (see eq. 1). As pneumatic conveyance restarts after emptying of the vessel, the impeller speed recovers. However, this sudden change in impeller speed can trigger a change in particle size. Therefore, the system is not directly in equilibrium after conveyance restarts. This issue was also addressed in previous research [33]. Programming the software to transmit a blank value instead of 0 µm when no particles were measured, a larger collection vessel or implementing a rotary valve instead of the vessel are reasonable adjustments that will solve the current issue and should be implemented in further experiments.

III.3. Controlling a process with an unstable gap width – SCF controller

It was assumed that an increase in gap width and the following drop in granule size can also be counteracted by controlling the SCF. This was proven by repeating the experiments as shown in section II.2 (Controlling a process with an unstable gap width – impeller speed

controller) and utilizing an SCF controller instead of an impeller speed controller. The impeller speed was constant at 800 rpm. Results are shown in Fig. 6.

As experiments were conducted on the same day, the same data for the uncontrolled process could be used (Fig. 6 a) and Fig. 4 a)). As expected, after increasing the gap width, the SCF of the systems needs to be increased in order to counteract the drop in granule size. The effect of the controller is clearly visible (Fig. 6 b) - d)). As explained in the introduction, changing the SCF during the process is not favorable. In this experiment, the SCF was varied between approximately 4 and 5.8 kN/cm. This will impact other CQA of the granules, which is not intended.

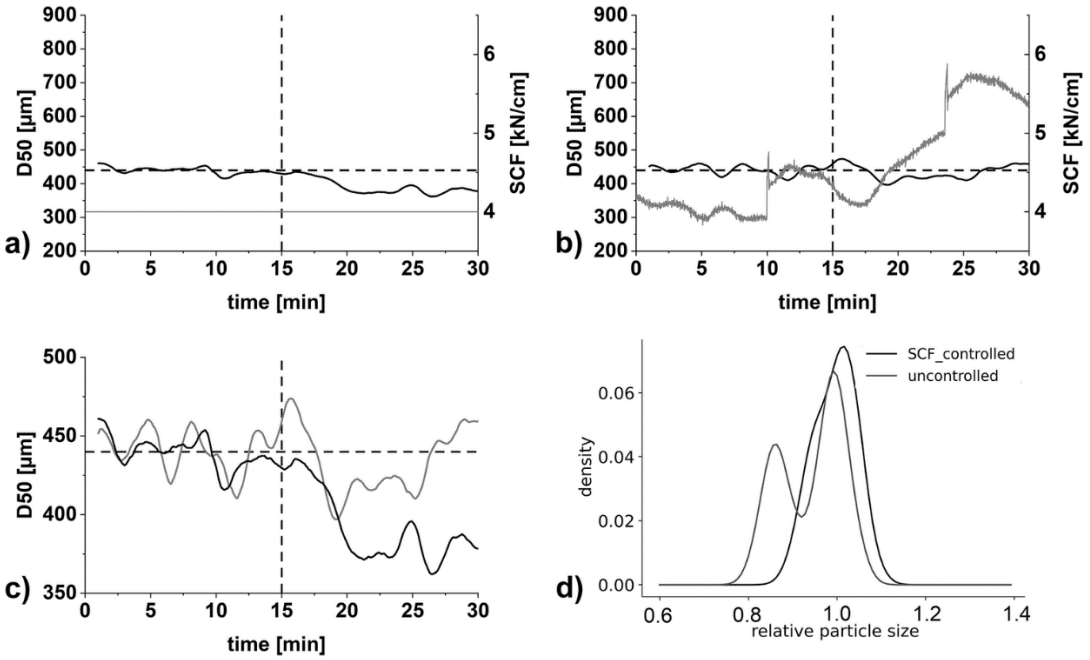

Fig. 6 Plot of D50 and SCF against time. a) uncontrolled process b) controlled at 440 µm, K_c = 0.001, T_i = 10.0 s c) D50 values of experiments a) and b) combined. d) density against relative particle size plot for uncontrolled (gray) and SCF controlled (black) experiments a) and b) black = D50, gray = SCF, horizontally dashed = 440 µm set-point, vertically dashed = gap width change. Each data point n = 1; in-line data

III.4. Controlling a process with an unstable SCF – gap width controller

To evaluate the gap width controller, the experiment had to be adjusted. In a similar manner as discussed before, the SCF was changed after 15 min to stimulate a drop in particle size. As the SCF is a tightly controlled CPP, a drop in SCF is unusual during granulation. However, it was used in this case to generate a drop in granule size and to test the principle of using a gap width controller to control the GSD. To evaluate the results in comparison

with another control valve, the drop in SCF was also counteracted by using a impeller speed controller as presented in section III.2 (controlling a process with an unstable gap width – impeller speed controller). Results are shown in Figs. 7 and 8.

Changing the SCF from 4 to 3.5 kN/cm led to a drop in the D50 parameter. However, the drop was not as pronounced as in the previous experiments (median particle size decreased from approximately 430 µm to 400 µm). The density distribution of the uncontrolled process (gray in Fig. 8 a) shows a peak at 1.0 relative particle size and then a crooked curve along lower relative particle sizes but no sharp second peak. The controlled process was able to produce granules with a mono-modal D50-density curve. Controlling the gap width (Fig. 7 c) and d)) led to satisfying results using a controller with a K_c value of −0.0003 and T_i value of 10.0 s. The phase shift in reaction is visible in the D50/gap width against time plot (Fig. 7 c) and d)). This shift is visible due to the comparably longer time the change in gap width needs to have an effect on the D50 value. At more aggressive controller settings (K_c = −0.0006 and T_i = 10.0 s), this led to large over and undershoots of gap width and particle size (Fig. 7 d) and a density curve that is similarly crooked than the uncontrolled one (Fig. 8 b), medium gray curve).

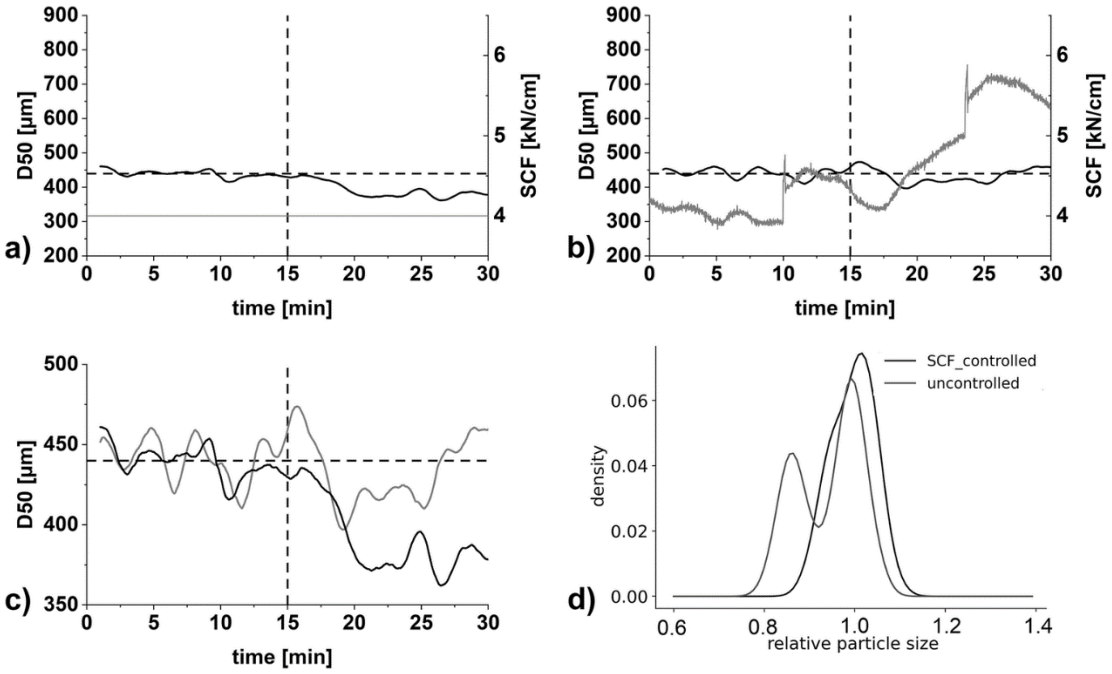

Fig. 7 Plot of D50 and impeller speed or gap width against time. a) uncontrolled process b) impeller speed controlled at 440 µm, K_c = −0.5, T_i = 10.0 s c) gap width controlled at 440 µm, K_c = −0.0003, T_i = 10.0 s d) gap width controlled at 440 µm, K_c = −0.0006, T_i = 10.0 s. black line = D50, a) and b) gray = impeller speed c) and d) gray = gap width, a) - d) black = D50, horizontal dashed line = set-point (440 µm), vertical dashed line = change in SCF (4 to 3.5 kN/cm). Each data point n = 1; in-line data

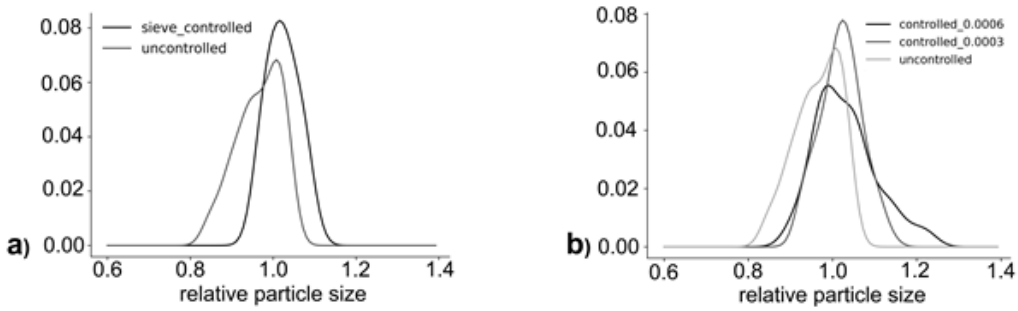

Fig. 8 Density against relative particle size for the experiments shown in Fig. 9 a) – d). a) uncontrolled and sieve-speed controlled density distribution b) uncontrolled and gap width controlled density distribution. Each plot n = 1; in-line data

In principle, the gap width can be used to control the D50 parameter in continuous RCDG. However, due to a long response time the controller settings must be carefully evaluated and the risk of over and undershooting is potentially larger than for the impeller speed and SCF controller. This is underlined by the fact that the impeller speed controller generates D50-density curves with a monomodal shape that is distinctively narrower than both gap width controllers. Furthermore, in controlling the SCF of the roller compactor, the gap width is used as control valve (PID controller, $K_c = 0.0072$, $T_i = 2.0$ s, $T_d = 0.007$). Using the gap width as a control valve for two parameters could lead to conflicts of interest (setting the desired SCF and desired granule size at the same time). Based on this and the results presented, it appears unfavorable to utilize the gap width as control valve albeit it was proven that in principle it is possible.

III.5. Controlling a process with a properly lubricated and an over-lubricated excipient blend

It was previously reported that granulating an over-lubricated formulation significantly decreases the particle size compared to the same formulation with proper lubrication [33]. Within the scope of this work, it was evaluated whether the controllers can counteract this drop in particle size. Therefore, MCC was blended with 1% Magnesium-stearate, 3 min at 20 rpm to form a properly lubricated mixture and 20 min at 20 rpm to form an over-lubricated mixture. The properly lubricated material was granulated first. Then, the over-lubricated mixture was poured into the powder inlet unit. It was waited until the hopper was almost completely empty and the feeding screw of the roll compactor was visible

before the over-lubricated mixture was added. That way the extent of back-mixing between two different materials was minimized.

Results are shown in Fig. 9. It is visible that shortly after the over-lubricated mixture was poured into the roll compactor the D50 value decreased. If the impeller speed controller was turned on, it reacted to the decreased particle size by lowering the impeller speed until the minimum of 400 rpm was reached. For two SCFs, no effect of impeller speed on the particle size could be registered. Therefore, in both cases, the impeller speed controller was turned off and the SCF controller was turned on. It reacted to the difference between set-point and current value by increasing the SCF. In both cases, the particle size then increased (Table 2).

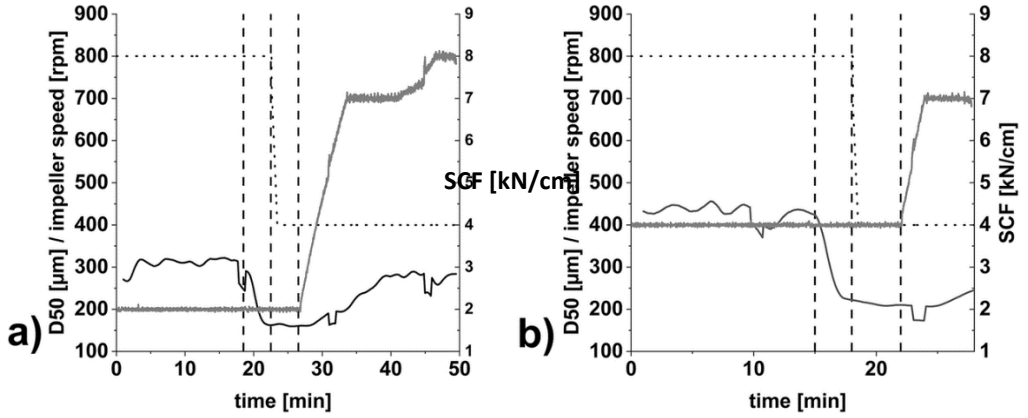

Fig. 9 Plot of D50 (black), impeller speed (black dotted) and SCF (gray) against time. a) SCF = 2 kN/cm b) SCF = 4 kN/cm. First vertical dashed line = addition of the over lubricated mixture, second vertical line = the controller of the impeller speed was turned on, third vertical dashed line = the impeller speed controller was turned off and the SCF controller was turned on. Each data point n = 1; in-line data

Table 2. D50-values during granulation of correct and over-lubricated MCC. n = 1; mean

SCF	**Average D50 with correct lubrication**	**Average D50 with over-lubrification**	**Max D50 at increased SCF**
2 kN/cm	313 µm	162 µm	286 µm / 8 kN/cm
4 kN/cm	429 µm	208 µm	246 µm / 7 kN/cm

In both cases, both controllers were unable to shift the granule size back to its original value (Fig. 9 and Table 2). The impeller speed controller had no effect on the granule size of the over-lubricated formulation. The effect of magnesium stearate in over-lubrication is well described in literature, although to this day not fully understood [46,47,48]. During over-

lubrication, its main effect is the formation of friable ribbons which show poor mechanical strength and almost disintegrate to powder during milling. It is reasonable to assume that the impeller speed has no effect on the particle size and that the over-lubrication in itself determines the resulting particle size. At increased SCF, the ribbon itself is compacted differently and thereby a certain effect on the resulting granule size is understandable. The large increase of SCF needed to increase the D50-value relevantly underlines this.

Overall, granules that were produced from an over lubricated powder mixture will not be suitable for further processing. The principle of using an SCF controller to counteract the drop in particle size further proofs the controller principle. It also showed that not every excipient and formulation can be controlled by adjusting the impeller speeds. Therefore, recording the particle size at different impeller speeds (as shown in Fig. 2) is an important preliminary experiment to determine a formulations suitability to be impeller-controlled.

IV. Conclusions

CPP that have an effect on the GSD can be used to control the resulting granule size using feedback control loops. The impeller speed is well suited to be used in control loops as it can be directly set itself, independent from further process parameters and has limited effect on further CQA apart from the granule size. SCF and gap width are parameters that, in principle, can be used to control a granulation process. However, their impact on further CQA and the fact that they are controlled themselves impede this usage. To determine, whether a material can be controlled, it has to be checked, how sensitive the granule size reacts to changes in the chosen control valve process parameter. Limits of this control strategy include the large variability that was seen experimentally and the limited impact of the impeller speed on the granule size. The impact of air humidity on various excipients in the laser diffraction system should be evaluated. Additional experiments should be conducted to evaluate, if there are additional factors that could lead to insufficient reproducibility. Furthermore, advanced strategies to tune the controller should be implemented to optimize the reaction and minimize material out of the desired specification.

V. Disclosure of potential conflicts of interest The authors declare that they have no conflict of interest.

VI. References

1. Lee SL, O'Connor TF, Yang XC, Cruz CN, Chatterjee S, Madurawe RD et al. Modernizing Pharmaceutical Manufacturing: from Batch to Continuous Production. J Pharm Innov. 2015;10(3):191-9. doi:https://doi.org/10.1007/s12247-015-9215-8

2. Lee SL. Current FDA Perspective for Continuous Manufacturing. US FDA Center for Drug Evaluation and Research, MIT-CMAC 2nd International Symposium on Continuous Manufacturing of Pharmaceuticals. 2016. http://qbdworks.com/wp-content/uploads/2014/06/FDA-on-Continuous-Manufacturing-Lee-2016.pdf. Accessed 03.08.2020 08:22.

3. Plumb K. Continuous processing in the pharmaceutical industry - Changing the mind set. Chem Eng Res Des. 2005;83(A6):730-8. doi:https://doi.org/10.1205/cherd.04359.

4. Rantanen J, Khinast J. The Future of Pharmaceutical Manufacturing Sciences. J Pharm Sci. 2015;104(11):3612-38. doi:https://doi.org/10.1002/jps.24594

5. Lee SL. Quality Considerations for Continuous Manufacturing Guidance for Industry. Food and Drug Administration. 2019. https://www.fda.gov/media/121314/download. Accessed 03.08.2020 08:27.

6. U.S. Food and Drug Administration. Guidance for Industry, PAT-A Framework for Innovative Pharmaceutical Development, Manufacturing and Quality Assurance. 2004. https://www.fda.gov/media/71012/download. Accessed 03.08.2020 08:30.

7. U.S. Food and Drug Administration. Advancement of emerging technology applications for pharmaceutical innovation and modernization: guidance for industry. 2017. https://www.fda.gov/files/drugs/published/Advancement-of-Emerging-Technology-Applications-for-Pharmaceutical-Innovation-and-Modernization-Guidance-for-Industry.pdf. Accessed 03.08.2020 08:35.

8. European Medicines Agency. Guideline on real-time release testing (formerly guideline on parametric release) - Revision 1. 2012. https://www.ema.europa.eu/en/documents/scientific-guideline/guideline-real-time-release-testing-formerly-guideline-parametric-release-revision-1_en.pdf. Accessed 03.08.2020 08:36.

9. European Medicines Agency. Guideline on manufacture of the finished dosage form 2017. https://www.ema.europa.eu/en/documents/scientific-guideline/guideline-manufacture-finished-dosage-form-revision-1_en.pdf. Accessed 03.08.2020 08:37.

10. The International Council for Harmonisation. ICH Q10 Pharmaceutical Quality System. 2015. https://www.ema.europa.eu/en/documents/scientific-guideline/international-conference-harmonisation-technical-requirements-registration-pharmaceuticals-human_en.pdf.

11. The International Council for Harmonisation. ICH Q8 Pharmaceutical development. 2017. https://www.ema.europa.eu/en/documents/scientific-guideline/international-conference-harmonisation-technical-requirements-registration-pharmaceuticals-human-use_en-11.pdf. Accessed 03.08.2020 08:44.

12. Zwolensky-Lambert W. Update on ICH Q13. 2nd Continuous Manufacturing Conference; February 18, 2020; Freiburg im Breisgau.

13. Hlinak AJ, Kuriyan K, Morris KR, Reklaitis GV, Basu PK. Understanding critical material properties for solid dosage form design. J Pharm Innov. 2006;1(1):12-7. https://doi:10.1007/bf02784876

14. Fonteyne M, Vercruysse J, De Leersnyder F, Van Snick B, Vervaet C, Remon JP et al. Process Analytical Technology for continuous manufacturing of solid-dosage forms. Trac-Trend Anal Chem. 2015;67:159-66. https://doi.org/10.1016/j.trac.2015.01.011

15. Leane M, Pitt K, Reynolds G. A proposal for a drug product Manufacturing Classification System (MCS) for oral solid dosage forms. Pharm Dev Technol. 2015;20(1):12-21. https://doi.org/10.3109/10837450.2014.954728

16. Kleinebudde P. Roll compaction/dry granulation: pharmaceutical applications. Eur J Pharm Biopharm. 2004;58(2):317-26. https://doi.org/10.1016/j.ejpb.2004.04.014

17. Sun C, Himmelspach MW. Reduced tabletability of roller compacted granules as a result of granule size enlargement. J Pharm Sci. 2006;95(1):200-6. https://doi.org/10.1002/jps.20531

18. Mosig J, Kleinebudde P. Critical evaluation of root causes of the reduced compactability after roll compaction/dry granulation. J Pharm Sci. 2015;104(3):1108-18. https://doi.org/10.1002/jps.24321

19. Sun C, Kleinebudde P. Mini review: Mechanisms to the loss of tabletability by dry granulation. Eur J Pharm Biopharm. 2016;106:9-14. https://doi.org/10.1016/j.ejpb.2016.04.003

20. Shekunov BY, Chattopadhyay P, Tong HH, Chow AH. Particle size analysis in pharmaceutics: principles, methods and applications. Pharm Res. 2007;24(2):203-27. https://doi.org/10.1007/s11095-006-9146-7

21. Alderliesten M. Mean particle diameters. Part IV: Empirical selection of the proper type of mean particle diameter describing a product or material property. Part Part Syst Char. 2004;21(3):179-96. https://doi.org/10.1002/ppsc.200400917

22. Madarasz L, Nagy ZK, Hoffer I, Szabo B, Csontos I, Pataki H et al. Real-time feedback control of twin-screw wet granulation based on image analysis. Int J Pharm. 2018;547(1-2):360-7. https://doi.org/10.1016/j.ijpharm.2018.06.003

23. Chan LW, Tan LH, Heng PWS. Process Analytical Technology: Application to Particle Sizing in Spray Drying. AAPS PharmSciTech. 2008;9(1):259-66. https://doi.org/10.1208/s12249-007-9011-y

24. Nalluri VR, Schirg P, Gao X, Virdis A, Imanidis G, Kuentz M. Different modes of dynamic image analysis in monitoring of pharmaceutical dry milling process. Int J Pharm. 2010;391(1-2):107-14. https://doi.org/10.1016/j.ijpharm.2010.02.027

25. Greaves D, Boxall J, Mulligan J, Montesi A, Creek J, Sloan ED et al. Measuring the particle size of a known distribution using the focused beam reflectance measurement technique. Chem Eng Sci. 2008;63(22):5410-9. https://doi.org/10.1016/j.ces.2008.07.023

26. Närvänen T, Lipsanen T, Antikainen O, Räikkönen H, Heinämäki J, Yliruusi J. Gaining fluid bed process understanding by in-line particle size analysis. J Pharm Sci. 2009;98(3):1110-7. https://doi.org/10.1002/jps.21486

27. Petrak D. Simultaneous measurement of particle size and particle velocity by the spatial filtering technique. Part Part Syst Char. 2002;19(6):391-400. https://doi.org/10.1002/ppsc.200290002

28. Mangal H, Derksen E, Lura A, Kleinebudde P. In-line particle size measurement in dry granulation: Evaluation of probe position. 10th World Meeting on Pharmaceutics, Biopharmaceutics and Pharmaceutical Technology. 2016.

29. Wilms A, Kleinebudde P. Particle size distribution in the product stream after roll compaction/dry granulation. 3rd European Conference on Pharmaceutics; Bologna2019.

30. Mangal H. Implementierung der Trockengranulierung in eine kontinuierliche Produktionsanlage für feste Arzneiformen; translates to "Implementation of dry granulation in a continuous manufacturing line for solid oral dosage forms". PhD thesis Heinrich Heine University Düsseldorf. 2018.

31. McAuliffe MAP, O'Mahony GE, Blackshields CA, Collins JA, Egan DP, Kiernan L et al. The Use of PAT and Off-line Methods for Monitoring of Roller Compacted Ribbon and Granule Properties with a View to Continuous Processing. Org Process Res Dev. 2015;19(1):158-66. https://doi.org/10.1021/op5000013

32. Wilms A, Knop K, Kleinebudde P. Combination of a rotating tube sample divider and dynamic image analysis for continuous on-line determination of granule size distribution. Int J Pharm X. 2019;1:100029. https://doi.org/10.1016/j.ijpx.2019.100029

33. Wilms A, Meier; R., Kleinebudde, P. Development and Evaluation of an In-line and On-line Monitoring System for Granule Size Distributions in Continuous Roll Compaction/Dry Granulation Based on Laser Diffraction. J Pharm Innov. 2020. https://doi.org/10.1007/s12247-020-09443-3

34. Wiedey R, Šibanc R, Wilms A, Kleinebudde P. How relevant is ribbon homogeneity in roll compaction/dry granulation and can it be influenced? Eur J Pharm Biopharm. 2018;133:232-9. https://doi.org/10.1016/j.ejpb.2018.10.021

35. Freitag F, Reincke K, Runge J, Grellmann W, Kleinebudde P. How do roll compaction/dry granulation affect the tableting behaviour of inorganic materials?: Microhardness of ribbons and mercury porosimetry measurements of tablets. Eur J Pharm Sci. 2004;22(4):325-33. https://doi.org/10.1016/j.ejps.2004.04.001

36. Wiedey R, Kleinebudde P. Infrared thermography — A new approach for in-line density measurement of ribbons produced from roll compaction. Powder Technol. 2017. https://doi.org/10.1016/j.powtec.2017.01.052

37. Wiedey R, Kleinebudde P. Potentials and limitations of thermography as an in-line tool for determining ribbon solid fraction. Powder Technol. 2018. https://doi.org/10.1016/j.powtec.2018.03.047

38. Wilms A, Kleinebudde P. Towards better understanding of the influence of process parameters in roll compaction/dry granulation on throughput, ribbon microhardness and

granule failure load. Int J Pharm X. 2020;100059:100059. https://doi.org/10.1016/j.ijpx.2020.100059.

39. Singh R, Ierapetritou M, Ramachandran R. An engineering study on the enhanced control and operation of continuous manufacturing of pharmaceutical tablets via roller compaction. Int J Pharm. 2012;438(1-2):307-26. https://doi.org/10.1016/j.ijpharm.2012.09.009

40. Mangal H, Kleinebudde P. Is the adjustment of the impeller speed a reliable attempt to influence granule size in continuous dry granulation? Adv Powder Technol. 2018;29(6):1339-47. https://doi.org/10.1016/j.apt.2018.02.029

41. Reimers T, Thies J, Stöckel P, Dietrich S, Pein-Hackelbusch M, Quodbach J. Implementation of real-time and in-line feedback control for a fluid bed granulation process. Int J Pharm. 2019;567:118452. https://doi.org/10.1016/j.ijpharm.2019.118452

42. Reimers T, Thies J, Dietrich S, Quodbach J, Pein-Hackelbusch M. Evaluation of in-line particle measurement with an SFT-probe as monitoring tool for process automation using a new time-based buffer approach. Eur J Pharm Sci. 2019;128:162-70. https://doi.org/10.1016/j.ejps.2018.11.026

43. Agachi PS, Cristea MV. Basic Process Engineering Control. Berlin/Boston: Walter de Gruyter GmbH & Co KG; 2014.

44. Sun CC. Mechanism of moisture induced variations in true density and compaction properties of microcrystalline cellulose. Int J Pharm. 2008;346(1–2):93–101. https://doi.org/10.1016/j.ijpharm.2007.06.017

45. Sun A, CC. Quantifying effects of moisture content on flow properties of microcrystalline cellulose using a ring shear tester. Powder Technol. 2016;289:104–8. https://doi.org/10.1016/j.powtec.2015.11.044

46. Shah A, Mlodozeniec A. Mechanism of surface lubrication: Influence of duration of lubricant-excipient mixing on processing characteristics of powders and properties of compressed tablets. J Pharm Sci. 1977;66(10):1377-82. https://doi.org/10.1002/jps.2600661006

47. Billany M, Richards J. Batch variation of magnesium stearate and its effect on the dissolution rate of salicylic acid from solid dosage forms. Drug Dev Ind Pharm. 1982;8(4):497-511. https://doi.org/10.3109/03639048209022117

48. Mosig J, Kleinebudde P. Evaluation of lubrication methods: How to generate a comparable lubrication for dry granules and powder material for tableting processes. Powder Technol. 2014;266:156-66. https://doi.org/10.1016/j.powtec.2014.06.022

Acknowledgments

This work was supported by the Drug Delivery Innovation Center (DDIC), INVITE GmbH, Leverkusen. The author thanks Malvern Panalytical for supporting this work and DFE Pharma for supplying the excipient SuperTab® 21AN.

Funding Open Access funding provided by Projekt DEAL.

5 Towards better understanding of the influence of process parameters in roll compaction/ dry granulation on throughput, ribbon microhardness and granule failure load

Annika Wilms[a,b], Peter Kleinebudde[a]

[a] Institute of Pharmaceutics and Biopharmaceutics, Heinrich Heine University, Universitaetsstrasse 1, 40225 Duesseldorf, Germany

[b] INVITE GmbH, Drug Delivery Innovation Center (DDIC), CHEMPARK Building W32, 51364 Leverkusen, Germany

5.1 Pretext

The following research paper has been published by the International Journal of Pharmaceutics: X in Volume 2 (2020).

https://doi.org/10.1016/j.ijpx.2020.100059

Evaluation of authorship:

author	idea [%]	study design [%]	experimental [%]	evaluation [%]	manuscript [%]
Annika Wilms	70	80	100	100	70
Peter Kleinebudde	30	20	0	0	30

Evaluation of Copyright permission:

Towards better understanding of the influence of process parameters in roll compaction/ dry granulation on throughput, ribbon microhardness and granule failure load.

Annika Wilms[a,b],Peter Kleinebudde[a]

[a] Institute of Pharmaceutics and Biopharmaceutics, Heinrich Heine University, Universitaetsstrasse 1, 40225 Duesseldorf, Germany

[b] INVITE GmbH, Drug Delivery Innovation Center (DDIC), CHEMPARK Building W32, 51364 Leverkusen, Germany

International Journal of Pharmaceutics: X 2 (2020): 100059.

https://doi.org/10.1016/j.ijpx.2020.100059

Abstract

A key quality attribute for solid oral dosage forms is their hardness and ability to withstand breaking or grinding. If the product is to be manufactured continuously, it can be of interest to monitor the hardness of the material at different stages of manufacturing. Using the controlled process parameters of roll compaction/dry granulation specific compaction force, roll speed and gap width, hardness of the resulting ribbons and granules can be predicted. For the first time, in this study two yield variables (corrected torque of the granulation unit and throughput of material) are used to predict the granules failure load. The increase in granule hardness was monitored in-line when the specific compaction force was increased during the compaction process. This opens the way for in-line control of material hardness, and its use for feedback and feedforward control loops for future continuous manufacturing processes.

Keywords

Continuous manufacturing, roll compaction/dry granulation, microhardness, granule strength / failure load, process monitoring, process analytical technologies

Abbreviations

CM – continuous manufacturing; CQA – critical quality attribute; RCDG – roll compaction/dry granulation; MCC – microcrystalline cellulose; SCF – specific compaction force; DCPA – dibasic calciumphosphate anhydrate

Graphical abstract

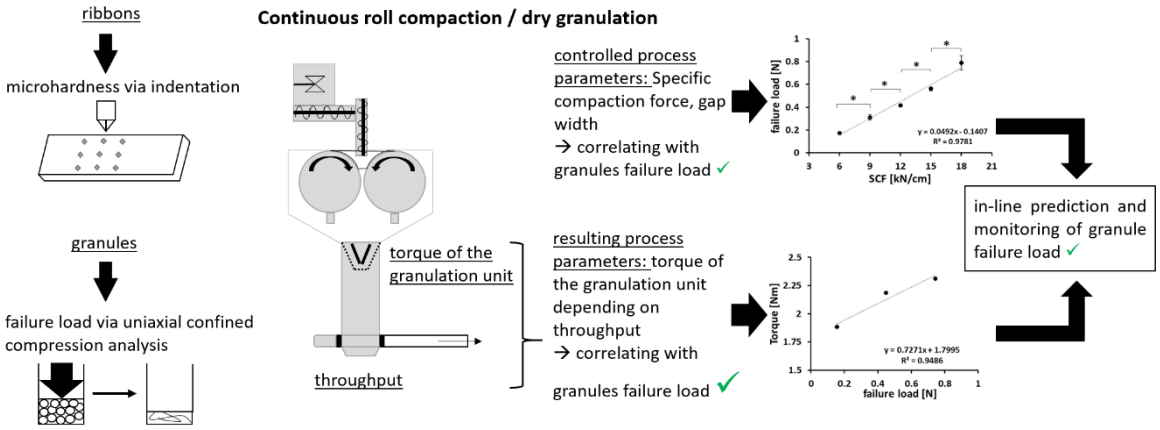

1. Introduction

With recent advancements in implementing continuous manufacturing (CM) in pharmaceutical production of solid oral dosage forms there is a need to continuously monitor and control critical quality attributes (CQA) (Chatterjee, 2012; U.S. Food and Drug Administration, 2017; Lee, 2016; Lee et al., 2015; U.S. Food and Drug Administration, 2019). Detailed process understanding is necessary to identify CQAs and their influencing factors. A promising approach to continuous manufacturing, if direct compression is not feasible, is roll compaction/dry granulation (RCDG). It is a well-established, fast, comparably low-cost and, by nature, continuous granulation method, in which powder is compacted to ribbons between two counter rotating rolls and these ribbons are afterwards milled down to granules (Fonteyne et al., 2015; Kleinebudde, 2004; Shlieout et al., 2000). A major CQA for the intermediate ribbon is the ribbon porosity/solid fraction as it impacts the CQAs of the later produced granules, such as granule size distribution (Jaminet and Hess, 1966; Kleinebudde, 2004). In-line methods to determine ribbon solid fraction have been previously published (McAuliffe et al., 2015; Wiedey and Kleinebudde, 2018). However, Gupta et al. showed that microcrystalline cellulose (MCC) ribbons of similar density can vary in hardness (Gupta et al., 2005).

When looking at tablets as the final dosage form, mechanical strength is an essential CQA as it prohibits breaking and grinding. On the other hand, early studies showed that if the mechanical strength is increased dissolution can be impeded (Chowhan, 1979; Kitazawa et

al., 1975). In 1985, Jetzer et al. correlated tensile strength with indentation hardness of tablets and showed that the correlation is linear as long as fracture or capping at higher pressure ranges is avoided (Jetzer et al., 1985). This is also backed by more recent work by Patel and Sun, who found that an increase in tablet porosity will lead to a decrease in hardness (Patel and Sun, 2016). Therefore, tablet hardness has similar informational value as the more popular tensile strength and cannot be equated with tablet density (Gupta et al., 2005). In a continuous manufacturing process, based on process understanding it is valuable to track the development of hardness through all intermediates with the aim of achieving optimal tablet hardness/tensile strength.

By definition, hardness is the surface property, which quantifies a materials resistance to a permanent shape modification (Broitman, 2017; Walley, 2012). Its relation to further mechanical properties of solid materials (e.g. strength and ductility) is the base for hardness testing as a cheap and fast material quality control method (Broitman, 2017), as mechanical strength is a critical factor for pharmaceutical manufacturing. In RCDG it is valuable information to determine the hardness of ribbons and granules. Reported indentation experiments for pharmaceutical applications are scarce (Hiestand et al., 1971; Jetzer et al., 1985; Leuenberger, 1982; Leuenberger and Rohera, 1986; Rowe, 1976). However, Freitag et al. reported the use of micro-indentation to determine ribbon hardness (Freitag et al., 2004). An increase in the specific compaction force (SCF) during RCDG lead to harder ribbons and, if granules are then tableted, to tablets with decreased tensile strength. Determining granule hardness poses the issue of dealing with agglomerated product of variate particle sizes. Adams et al. first published a confined uniaxial compression test to determine granule strength, and its failure load, which also takes the particle size into consideration (Adams et al., 1994). The method was recently transferred to a modern tablet press (Arndt et al., 2018). Their study proved that increasing SCF leads to granules with increased failure load and tablets with decreased tensile strength.

Studies on correlating the torque of the granulation unit of a roll compactor to ribbon hardness were first published in 2012 (Müller, 2012). A roll compactor including an asymmetrical, oscillating sieve was used to granulate MCC and the clockwise and counter-clockwise torque during granulation was recorded. Hardness of the resulting ribbons was determined using a tablet drill. A correlation between the SCF, the torque values and the drilling forces needed to drill a hole into the ribbon was found. Increasing roll speed

increased the torque of the granulation unit while it did not affect the drilling forces. Various aspects of the milling unit (e.g. size of sieve, erosion of the sieve, milling gap) were found to influence the torque. The ribbon hardness was, in retrospective, determined by recording the torque of the granulation unit and interpolation of the correlation between the torque and the ribbon hardness. The throughput was found to have major impact on the torque of the granulation unit, but for further experiments was regarded as a constant as settings were not changed. In RCDG, the throughput can show relevant fluctuations (Wilms et al., 2020), and this should be taken into consideration for in-line determination of CQAs. No experiments were conducted to determine the impact of hardness on the torque independent from the changing throughput as SCF is varied. Furthermore the relation of the torque and hardness to varying process parameters should be analyzed for brittle material and a pharmaceutical formulation as well. Granule hardness was not investigated. For further processing, especially the granule characteristics are of high importance and a method to predict granule characteristics based on ribbon mechanic properties would be valuable.

The same group later focused on the development of using vibration- and acoustic pressure in-line measurements to determine ribbon hardness in-line, which is promising but also bears limitations as the system reacts sensitively to the attachment of the sensors and the surrounding vibration/acoustic environment (Schorr, 2016).

For continuous manufacturing efforts it is of interest to re-evaluate the impact of controlled process parameters (SCF, gap width, roll speed) on microhardness of ribbons and failure load of granules with regards to the torque of the granulation unit (360° rotating conical sieve) for different types of materials. For the first time, the quality parameter of granule failure load was evaluated in conjunction to the torque of the granulation unit and correlations were established for materials with different behavior upon compaction. A correlation was established to predict hardness parameters based on the yield parameters torque of the granulation unit and the throughput of material and the novel principle was tested using real-time granulation data. The study was performed to establish these correlations in order to progress in advanced process control for RCDG.

2. Materials and methods

2.1. Materials

Dibasic calcium phosphate anhydrate (DCPA, Di-CaFos A150, Chemische Fabrik Budenheim, Germany) was used as brittle model material. Microcrystalline Cellulose (MCC, Vivapur 102, JRS Pharma, Germany) was used as plastic model material.

A formulation was also investigated. It consisted of 25% Diclofenac-sodium (Amoli Organics Pvt. Ltd., India), 10% crosposvidone (Polyplasdone® XL, Ashland Industries Europe GmbH, Switzerland) and 65% MCC (Vivapur® 102, JRS Pharma, Germany).

2.2. Methods

2.2.1. Roll compaction/dry granulation

All materials were processed on a development to small scale manufacturing roll compactor (BRC 25, L.B. Bohle Maschinen + Verfahren GmbH, Germany) that was equipped with a hybrid sealing system and a 360° rotating conical sieve (BTS100, L.B. Bohle Maschinen + Verfahren GmbH, Germany). A 1.5 mm rasp sieve was used for all experiments. Depending on the planned analytics, smooth or knurled rolls were used. The gap width was varied between 1.5 and 2.5, the roll speed between 1 and 6 rpm and the SCF between 2 and 18 kN/cm. The specific process parameters are listed for each experiment in the results section. The throughput of the process was determined using a lab scale balance (CPA5201, Sartorius AG, Germany) that was placed underneath the outlet of the compactor. A collection vessel was placed on the balance and a software (SartoConnect, Sartorius AG, Germany) was used to track the mass every 10 s.

2.2.2. Determination of the torque, the corrected torque and the power of the granulation unit

The torque of the granulation unit was tracked together with the process parameters of the roll compactor in the compactor's software. The parameter is tracked every 10 s in the unit of Nm. It is not the average over 10 s but the as-is value at the tracking time-point. The torque of the granulation unit without material was tracked to determine the idle torque for each impeller speed. Idle torque values are listed in Table 1.

Table 1. Idle torque values at different impeller speeds.

Impeller speed [rpm]	Idle torque [Nm]	Idle power consumption [W]
200	1.57 ± 0.02	32.9 ± 0.4
300	1.87 ± 0.02	58.8 ± 0.6
400	2.13 ± 0.01	89.2 ± 0.4

The idle torque values were deducted from the observed torque values to obtain the corrected torque (corr. torque). For results shown in 3.2 Influence of SCF on torque of the granulation unit and granule failure load, 3.3 Impact of SCF and roll speed on throughput, 3.4 Impact of roll speed on the torque of the granulation unit and granule failure load, 3.5 Prediction of hardness based on resulting process parameters, 3.6 Relevance for pharmaceutical manufacturing – how do formulations behave?, impeller speeds of 200 rpm were chosen. Therefore, the corrected torque is tracked in these experiments and it is not necessary to convert the corrected torque to power consumption values. To compare different impeller speeds, as needed in Section 3.1, the additional power consumption of the granulation unit (apart from the idle power consumption) was calculated as shown in Eq. (1).

$$power\ consumption = corr.torque * impeller\ speed * 2 * \pi\ [W] \quad (1)$$

2.2.3. Determination of ribbon microhardness

Ribbon microhardness was determined using a microhardness system (Fischerscope HM2000, Helmut Fischer, Sindelfingen, Germany). The system was equipped with a vickers pyramid indenter which penetrated into ribbons. Penetration depth and indentation load were recorded. A total of 150 data points were recorded in 15 s (10 Hz) for every measurement. The initial 5 s were the loading phase, in which the force increased until 2000 mN were reached. This maximum load of 2000 mN (F_{max}) was held for 5 s. Afterwards, for 5 s, the system was unloaded. The maximum penetration depth (h_{max}) at maximum indentation load is used to calculate the Martens Hardness (HM) according to Eq. (2) (Jennett, 2007).

$$HM = F_{max}/((26.43\ \times (h_{max})^2)\ [N/mm^2] \quad (2)$$

To allow precise measurements, only ribbons with a smooth surface were used for microhardness determination. A smooth surface allows the indenter to land on an even surface and track penetration depth and indentation load. Ribbons are inhomogeneous concerning their density (Wiedey and Kleinebudde, 2018). Therefore, indentation was only performed in the center of the ribbon (determined with the measurement apparatuses microscope). Measurement spots were 10 mm apart from each other (Fig. 1). Four measurements were performed for each ribbon and averaged.

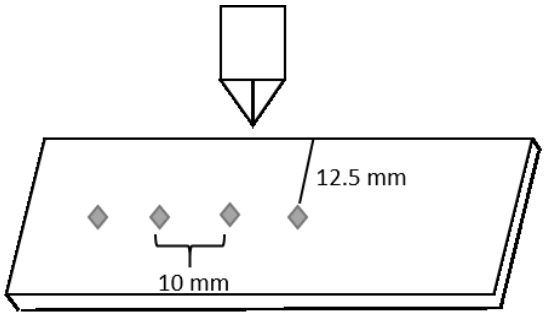

Figure 1. Microindentation experimental procedure.

2.2.4. Determination of granule failure load

Determination of failure load/granule strength was performed based on an uniaxial confined compression analysis. The granules were divided into the following size classes: 125–315 µm, 315–500 µm, 500–800 µm, 800–1250 µm and 1250–1500 µm. Afterwards, they were compressed using a Styl'One Evolution tablet press (Medelpharm S.A.S., France) in a round die of 100 mm^2 base area and 10 mm height. The upper punch speed was set to 3.5 mm/min and the granule bed was compressed to a final height of 5 mm. Depending on data variability, the test was repeated 3 to 6 times.

Analysis was performed according to Arndt et al. (Arndt et al., 2018) and is based on Eqs. (3), (4) (Adams et al., 1994). The compaction pressure P is calculated from the force and the cross-sectional area of the punch. The natural strain ϵ can be obtained using the current and the initial difference in height of the punches. For large values of ϵ, the relationship described in Eq. (3) is linear (Adams et al., 1994). The slope and the y-intercept of the linear equation are used to obtain the friction coefficient (α) and the cohesive strength (τ).

To obtain the individual failure load, the mean value of the cohesive granule strength is multiplied with the particles cross-sectional area. In this case, the cross-sectional area of a

sphere with a diameter of the mean value of the sieve class (da) was used for the calculation of each sieve class (see Eq. (4)).

$$lnP = \ln\left(\frac{\tau}{\alpha}\right) + \alpha\epsilon + \ln\left(1 - e^{-\alpha\epsilon}\right) \quad (3)$$

$$F_{calc} = \frac{\pi d_{\alpha}^{2}}{4}\tau \quad (4)$$

Afterwards, the weighted average failure load for a granule type was calculated by cumulating all size classes' failure loads after multiplying them with their respective relative mass fraction.

2.2.5. Design of experiments

Using MCC as excipient, a 2^3 full factorial experimental design was conducted to determine the effect of the process parameters SCF, gap width and impeller speed on ribbon microhardness and granule failure load as well as the torque of the granulation unit. Factors and their levels are shown in Table 2.11 experiments were executed (the center point was tested in threefold). The randomized plan for execution of experiments was given by the software Modde Pro 11 (Umetrics, MKS Data Analytics Solutions, Sweden) and data analysis was also performed using this software.

Table 2. Experimental overview

Factor level	SCF [kN/cm]	gap width [mm]	impeller speed [rpm]
-1	2	1.5	200
+1	6	2.5	400

3. Results and discussion

3.1. Effect of process parameters on ribbon microhardness, granule failure load, torque of the granulation unit and throughput

Table 3 displays the results of the 2^3 full factorial experiment while Figure 2 shows the resulting coefficient plots and Fig. 3 exemplary contour plots for varying gap width and SCF.

Table 3. Results of the 2^3 full factorial experimental design, mw ± sd.

Factors			yield variables				
SCF [kN/cm]	**Gap width [mm]**	**Impeller speed [rpm]**	**Ribbon microhardness [N/mm²]**	**Granule failure load [N]**	**Corr. torque of the granulation unit [Nm]**	**Additional sieve power consumption [W]**	**Throughput [kg/h]**
			n = 4	**n = 3 - 6**	**n = 18**	**n = 18**	**n = 3**
2	1.5	200	18.1 ± 4.1	0.27 ± 0.03	0.67 ± 0.09	14.0 ± 1.9	2.92
6	1.5	200	60.8 ± 12.0	0.95 ± 0.10	1.11 ± 0.15	23.3 ± 3.1	4.35
2	2.5	200	17.3 ± 5.0	0.12 ± 0.01	0.42 ± 0.07	8.8 ± 1.5	4.73
6	2.5	200	46.0 ± 7.7	0.60 ± 0.02	1.37 ± 0.41	28.7 ± 8.6	6.84
2	1.5	400	18.2 ± 3.6	0.20 ± 0.02	0.31 ± 0.06	13.0 ± 2.5	2.82
6	1.5	400	69.0 ± 11.6	0.80 ± 0.05	0.46 ± 0.14	19.3 ± 5.9	4.05
2	2.5	400	12.7 ± 1.5	0.09 ± 0.01	0.51 ± 0.06	21.4 ± 2.5	4.89
6	2.5	400	52.0 ± 4.7	0.48 ± 0.03	1.12 ± 0.22	46.9 ± 9.2	6.16
4	2	300	36.2 ± 2.5	0.43 ± 0.01	0.62 ± 0.16	19.5 ± 5.0	4.99
4	2	300	30.4 ± 2.8	0.41 ± 0.02	0.69 ± 0.09	21.7 ± 2.8	5.06
4	2	300	26.1 ± 9.7	0.37 ± 0.02	0.62 ± 0.16	19.5 ± 5.0	5.68

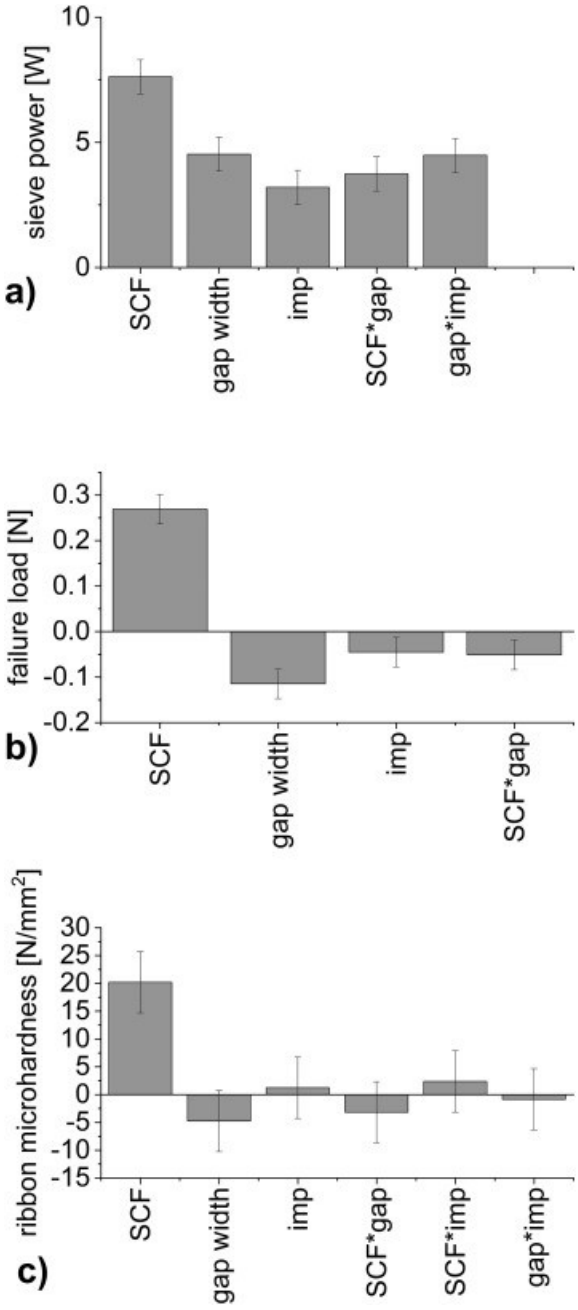

Figure 2. Coefficient plots. Effects on a) sieve power: additional power consumption of the granulation unit, b) failure load and c) ribbon microhardness. Error bars indicating 95% confidence interval (sieve power R2: 0.98, Q2:0.85., failure load R2: 0.99, Q2: 0.95, ribbon microhardness R2: 0.96, Q2:0.74).

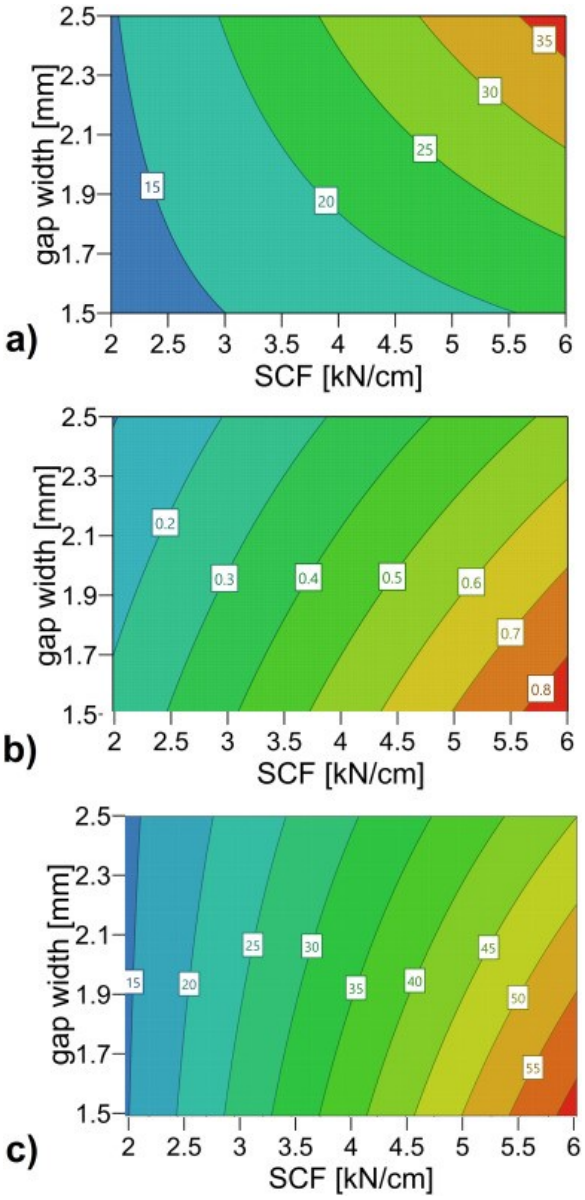

Fig. 3. Contour plots. Effects on a) sieve power, b) failure load and c) ribbon microhardness. (sieve power R2: 0.98, Q2:0.85., failure load R2: 0.99, Q2: 0.95, ribbon microhardness R2: 0.96, Q2:0.74).

Increasing the SCF led to a significant increase in failure load of the granules, the ribbon microhardness as well as the additional power consumption of the granulation unit. For all output parameters the SCF showed the largest impact. As it is the dominant process parameter in RCDG this is not surprising and in-line with published research (Arndt et al., 2018; Freitag et al., 2004; Müller, 2012). The increased ribbon hardness could lead to the significant increase the SCF exerted on the additional power consumption of the granulation unit. However, the impact of increased throughput at increased SCF has to be kept in mind. This can be seen as the impact of the process parameter gap width is taken

into consideration. At constant SCF but increased gap width, the SCF is exerted on more material. Therefore, the material itself shows decreased granule failure load (Fig. 2 b) and 3 b)). However, while the hardness decreases, the additional power consumption of the granulation unit increases significantly (Fig. 2 a) and 3 a)). This can be reasoned in the increased throughput at larger gap widths. To no surprise, the interaction of increased SCF and increased gap width increases the additional power consumption of the granulation unit as well (Fig. 2 a) and 3 a)).

Ribbon microhardness significantly increases at increasing SCF (Fig. 2 c) and 3 c)). The SCF is the only process parameter that has a significant impact on ribbon microhardness (Fig. 2 c)). This can be due to the fact that ribbon microhardness characterizes the surface of the ribbon. The surface is also the part of the ribbon on which the SCF is exerted on. Effects of increasing the gap width on ribbon microhardness are not significant in contrast to results of granule failure load.

By nature, adjusting the impeller speed affects the additional power consumption of the granulation unit (Fig. 2 a), Eq. (1)). At an increased impeller speed, granules show a smaller granule size (Mangal and Kleinebudde, 2018) and a slight decrease in failure load (Fig. 2b)). Since the impeller speed cannot influence the ribbon microhardness, this factor and all its interactions show non-significant effects close to zero on ribbon microhardness (Fig. 2c)).

As expected, the results of the experiments show that hardness of the ribbons and failure load of the granules react similarly to changes of SCF. The torque of the granulation unit reacts to the changes in process parameters as well but not in the same way as the hardness does. Supposedly, this is based on the effect of the throughput and it has to be analyzed in detail, whether a change in hardness itself has an impact on the torque of the granulation unit. As an increase in SCF will increase the failure load of the granules (Arndt et al., 2018) and similarly the ribbon microhardness (Freitag et al., 2004), only the granules failure load was used for a more detailed analysis of impact on the additional power consumption of the granulation unit. Its behavior can be correlated to the behavior we would expect from ribbon microhardness. In the more detailed analysis, the sieve impeller speed will be kept constant at 200 rpm, therefore it is not necessary to calculate the additional power consumption of the granulation unit. The corrected torque of the granulation unit bears all necessary information (see Eq. (1)).

3.2. Influence of SCF on torque of the granulation unit and granule failure load

Fig. 4 shows the impact of SCF on the torque of the granulation unit and the failure load of the resulting granules at otherwise constant controlled process parameters (2 mm gap width, 3 rpm roll speed for DCPA and 1 rpm roll speed for MCC). Similarly to the results in Fig. 2, increasing the SCF lead to an increase in the corrected torque of the granulation unit (Fig. 4 a) and c)) and failure load of the resulting granules (Fig. 4 b) and d)). In both cases a linear correlation describes the applied SCF and the resulting torque of the granulation unit (Fig. 4 a) and c)).

Correlation of SCF and failure load (Fig. 4 b) and d)) works well for DCPA but shows a lower coefficient of determination R^2 of 0.808 for MCC. Obtaining reproducible failure load values for high SCF for MCC was challenging, as reproducible volumetric filling of the die is more difficult, if the granule sizes are large. At 5 and 6 kN/cm, a large quantity of material was in size classes of 850–1200 µm and 1200–1500 µm. The impact of these difficulties was larger, if more material was produced at these sizes as the weighted average was calculated (see 2.2.4. Determination of granule failure load). Based on these difficulties, linear correlation results for MCC are acceptable.

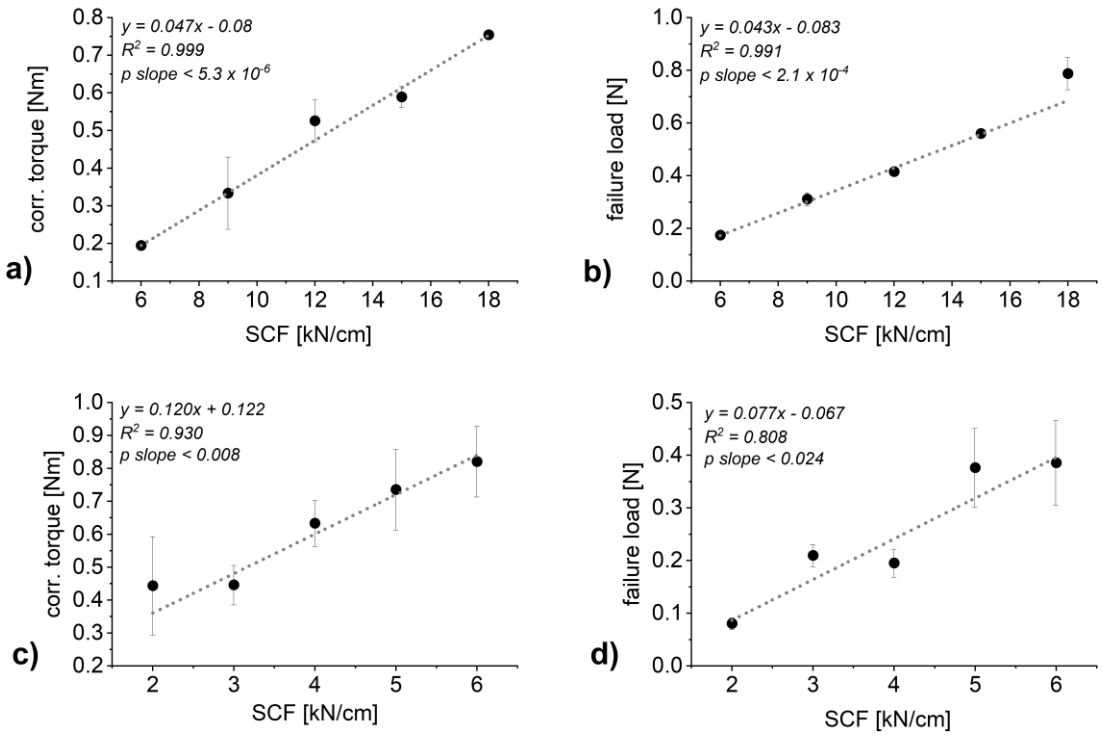

Figure 3. Plot of SCF against a) and c) the torque of the granulation unit (n = 3-7; mean ± sd) and b) and d) the failure load of the resulting granules (n = 5; mean ± sd). a) and b) DCPA c) and d) MCC.

It is therefore possible to predict the failure load of the granules based on linear correlation when looking at the SCF at constant gap width and roll speed. The linear increase of the torque of the granulation unit has to be further investigated, as the increase based on increased hardness and increased throughput have to be differentiated.

3.3. Impact of SCF and roll speed on throughput

Fig. 5 shows the impact of the SCF and roll speed on the throughput of material for DCPA (Fig. 5 a) and b)) and MCC (Fig. 5 c) and d)). As expected, the throughput increased at increasing SCF and, for a constant SCF, increased at increasing roll speed. Compacting MCC at 6 kN/cm and increasing the roll speed (Fig. 5 d), squares) did not lead to increasing throughput at 4 rpm and above. There was a decrease of throughput at 5 rpm compared to 4 rpm. This can be reasoned, as during production, the milling unit filled up with material when compacting at 6 kN/cm and above 3 rpm roll speed. Less material could be milled down than was produced leading to an accumulation of material in the mill and a stagnant throughput. In all other cases all material could be milled down.

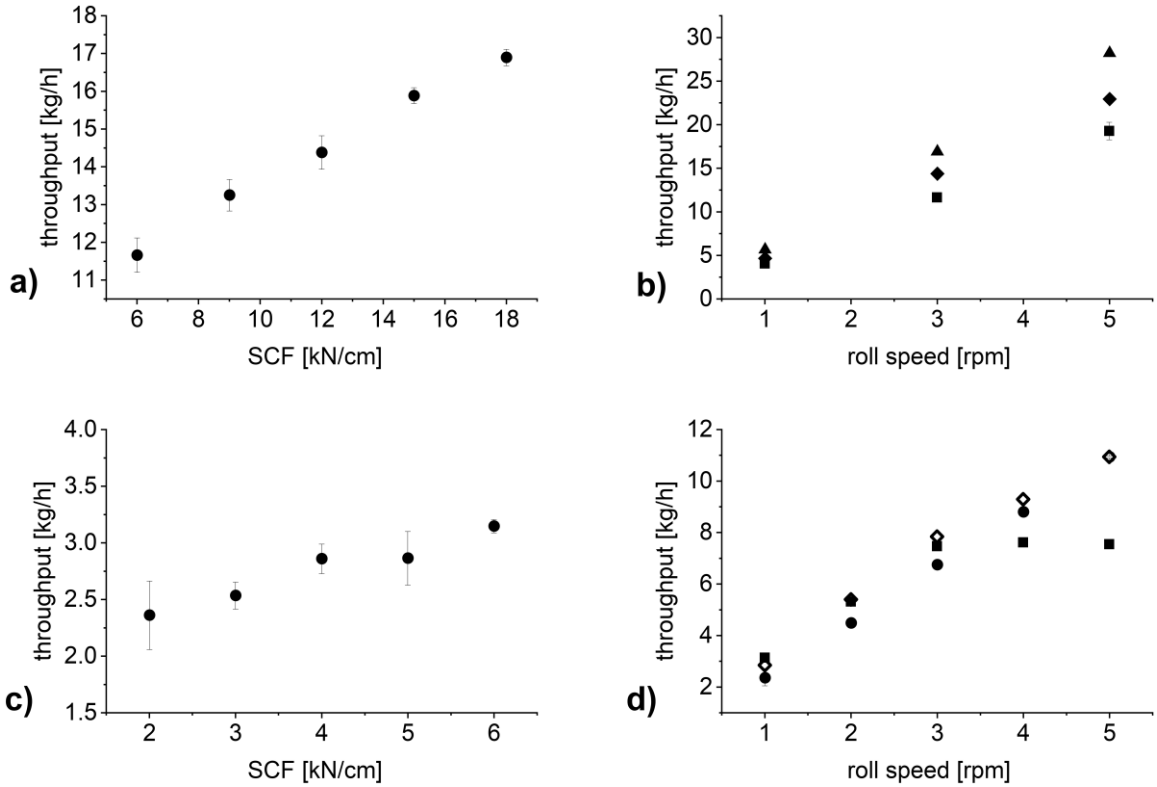

Fig. 5. Plots of a) and c) SCF against throughput, (n = 3–6; mean ± sd) and b) and d) roll speed against throughput for 2 kN/cm (circle), 4 kN/cm (unfilled square), 6 kN/cm (square), 12 kN/cm (diamond) and 18 kN/cm (triangle) (n = 3–6; mean ± sd). a) and b) DCPA, c) and d) MCC. Gap width in all experiments: 2.0 mm.

3.4. Impact of roll speed on the torque of the granulation unit and granule failure load

As mentioned in Section 3.2., the impact of throughput and hardness on the torque of the granulation unit have to be differentiated.

At three SCFs, the speed of the compaction rolls was varied (1, 3 and 5 rpm for DCPA and 1, 2, 3, 4 and 5 rpm for MCC) to vary the throughput of material (Fig. 6 a) and c)). In all cases, an increase in throughput lead to an increase in torque of the granulation unit. The plot is an interaction plot of throughput on the torque of the granulation unit at varying SCF. For both materials, an increase in SCF resulted in an increased slope of the throughput – torque correlation. Therefore, the impact of the throughput is dependent on the applied SCF. More specifically, at higher SCF the impact of throughput on the resulting torque of the granulation unit will increase. This can be reasoned in the increasing hardness at increasing SCF (Fig. 4 b) and d)).

Increasing roll speed reduces the dwell time in the compaction zone. Therefore, it had to be tested, whether increasing the roll speed might decrease the hardness of the resulting granules. For both materials, the failure load of granules produced at two SCFs (6 and 18 kN/cm for DCPA and 2 and 6 kN/cm for MCC, Fig. 6 b) and d)) were tested at varying throughputs. Concerning DCPA, the probability of the slope being zero is above 79% at 18 kN/cm and above 29% at 6 kN/cm. The low percentage at 6 kN/cm is based on the low standard deviations obtained in failure load measurements. No relevant trend in granule hardness can be found for both of the SCF. Detailed values are included in the supplementary material (see Table S1 for raw data DCPA and Table S2 for raw data MCC). For MCC, obtaining reproducible failure load values at 6 kN/cm was challenging and thus, relevant standard deviations were obtained. This can be reasoned in the previously discussed lacking impact on throughput of increasing the roll speed above 4 rpm (see Section 3.3.) resulting in a cluster of values located slightly below 8 kg/h. Furthermore, as discussed in Section 3.2., it was difficult to obtain reproducible results of failure load due to die filling issues. However, there is no visible trend to decreasing hardness at increased roll speeds for both SCF. The probability of the slope equaling zero is above 87% and above 95% for 6 kN/cm and 2 kN/cm respectively. Therefore, the hardness values plotted in Fig. 4 b) and d) are the experimentally determined values for a certain SCF regardless of the roll speed (see Tables S1 and S2).

Fig. 6 a) and c) show the throughput – corr. torque of the granulation unit plots including their linear correlation and correlation coefficients R. To evaluate the sole effect of SCF on the torque of the granulation unit, the linear correlations were used to calculate torque values at specific throughputs. The resulting plot (Fig. 7) is the interaction plot of SCF on the corrected torque of the granulation unit depending on different throughputs. In all cases, increasing the SCF at constant throughputs resulted in higher corrected torque values of the granulation unit. While for MCC linear correlations show R-values of above 0.98 (Fig. 7 b)), this is not the case for DCPA (Fig. 7 a)). The data points seem as if, for the brittle material, at increasing SCF the torque values could flatten while hardness still increases linearly (Fig. 4 b)). This non-linearity is based on data shown in Fig. 6 a). The torque values of the material produced at 12 kN/cm is not located centered between 6 and 18 kN/cm.

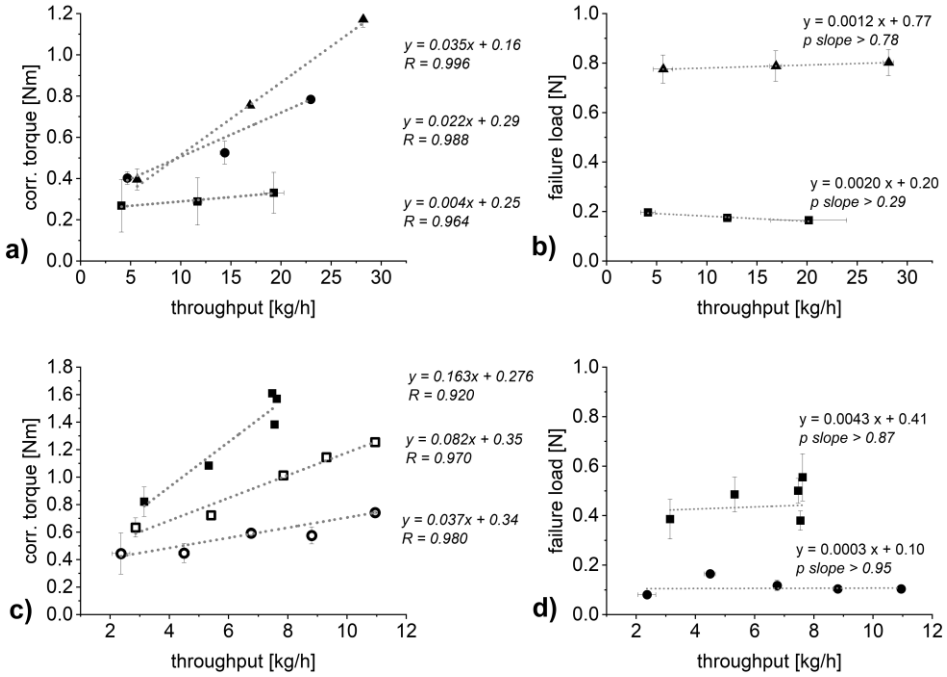

Fig. 6. Plot of throughput against a) and c) the torque of the granulation unit (n = 1–6; mean ± sd) b) and d) the failure load of the resulting granules (n = 3–5; mean ± sd). 2 kN/cm (unfilled circle), 4 kN/cm (unfilled square), 6 kN/cm (square), 12 kN/cm (circle) and 18 kN/cm (triangle). a) and b) DCPA and c) and d) MCC. Gap width in all experiments: 2.0 mm.

For both materials, the slope increases at increasing throughput proving that the impact of SCF is more profound at higher throughputs and vice versa. This plot confirms that independent from throughput, the SCF, and thus increasing hardness of the material, has impact on the torque of the granulation unit.

It can be concluded that increasing the throughput by increasing compaction roll speed will not affect the hardness of the resulting granules. Therefore, material of similar hardness

will generate different torque values based on the current throughput. These torque values increase steeper for harder materials. The effect of the hardness itself on the torque of the granulation unit was proven. If the throughput of material is known, the hardness should therefore be predictable by using the corrected torque of the granulation unit.

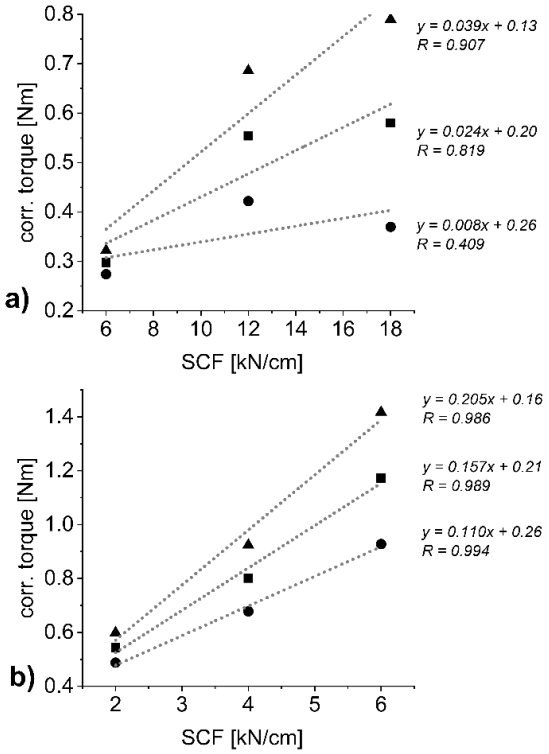

Figure 7. Interaction plot of SCF against the torque of the granulation unit at varying throughputs for a) DCPA; 6 kg/h (circle); 12 kg/h (square); 18 kg/h (triangle) and b) MCC; 4.0 kg/h (circle); 5.5 kg/h (square); 7.0 kg/h (triangle).

3.5. Prediction of hardness based on resulting process parameters

The prediction of granule hardness was tested by using data obtained by compacting DCPA at 15 kN/cm and MCC at 5 kN/cm (see Table 4, Fig. 4 and Tables S1 and S2 in the supplementary material). Based on the results discussed in 3.2 Influence of SCF on torque of the granulation unit and granule failure load, 3.4 Impact of roll speed on the torque of the granulation unit and granule failure load, two predictions can be made.

Firstly, based on the linear correlation of SCF and failure load (Fig. 4 b) and d)) the failure load at a certain SCF can be calculated. This is shown in Table 4 as “failure load [N] – calc”. Only the applied SCF is necessary for this calculation since it was determined that roll speed does not influence the resulting granules failure load (Fig. 6 b) and d)).

Secondly, a prediction of granule failure load based on current throughput and corrected torque can be made. The correlations shown in Fig. 6 a) and c) can be used to determine the torque values expected for the current throughput at three different SCF. Since these SCF linearly translate to granule failure load values (Fig. 4 b) and d)), a granule failure load – corrected torque of the granulation unit plot can be derived (Fig. 8). Using the average corrected torque that was registered during granulation, a predicted failure load value of the resulting granules can then be calculated using the linear correlations shown in Fig. 8. The result is listed as "failure load [N] – pred." In Table 4.

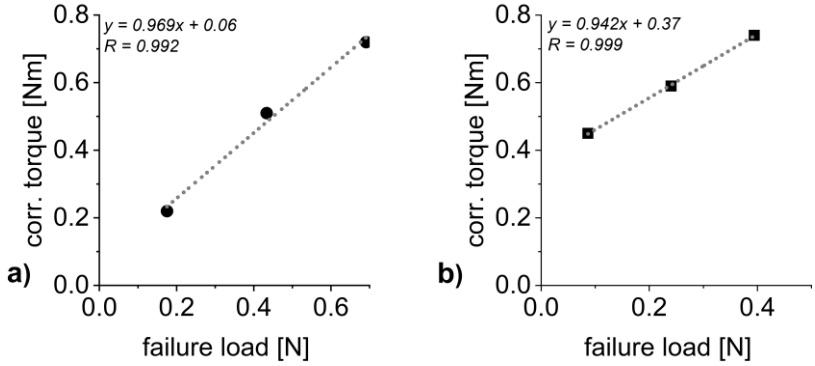

Figure 8. Plots of failure load against the torque of the granulation unit for throughputs of a) 15.89 kg/h and b) 2.87 kg/h with a) DCPA and b) MCC.

These values can then be compared to the failure load measured (Table 4, "failure load [N] – meas.", data points plotted in Figure 4 b) and d)).

Table 4. SCF, torque of the granulation unit and throughput values for specific data points

DCPA					
SCF [kN/cm]	Torque of the granulation unit [Nm]	Throughput [kg/h]	Failure load [N] – pred.	Failure load [N] – calc.	Failure load [N] – meas.
15	2.163	15.89	0.55	0.56	0.56
MCC					
5	2.310	2.87	0.39	0.32	0.38

The variation between the measured and the calculated failure load can also be seen in Fig. 4 b) and d). They are described by the coefficient of variation R^2 (0.991 for DCPA and 0.808 for MCC). The value for DCPA (0.56 N), lies almost perfectly on the linear

correlation plot whereas, in an overall less convincing correlation for MCC based on strong fluctuations, the calculated failure load for 5 kN/cm deviates stronger from the measured value (Fig. 4 d)). Therefore, the calculated and measured failure load for DCPA compacted at 15 kN/cm are both 0.56 N while they differ (0.32 N to 0.38 N) for MCC.

The predicted failure load values deviate from the measured and calculated ones. For DCPA, the predicted failure load is slightly below the measured failure load (0.55 N to 0.56 N), however this difference cannot be regarded as relevant. In conclusion, both methods to determine the granule failure load in-line (based on SCF only and based on corrected torque and throughput) can be regarded as equally suitable. For MCC, the prediction of granule hardness based on the corrected torque and the throughput outshine the prediction based on SCF alone. With only a slight deviation to the measured value (0.39 N to 0.38 N), there is no relevant discrepancy in granule failure load using the real-time prediction based on resulting process parameters. Therefore, the method has proven usable for real-time hardness prediction.

Fig. 9 displays results of an experiment compacting DCPA. The process parameters SCF and gap width are plotted against time. Furthermore, the predicted failure load is plotted in black. It was predicted using real-time throughput and corrected torque data. The throughput was determined every minute and a linear correlation between failure load and torque was determined for every throughput. The current corrected torque values were then used to determine the predicted failure load. The moving average over 2 min was plotted. Gray areas highlight process parameters that were not in equilibrium, as a change in SCF lead to a necessary adjustment in feeding screw speed and an instability in gap width. As shown in Fig. 2 c), both of these process parameters have significant effects on the granules failure load. Therefore, for each SCF the failure load values predicted in process equilibrium should be evaluated. It can be seen that the failure load, despite being calculated by using only the current throughput and torque values, reacted to changes in process parameters. An increase in SCF lead to an increase in the granules failure load.

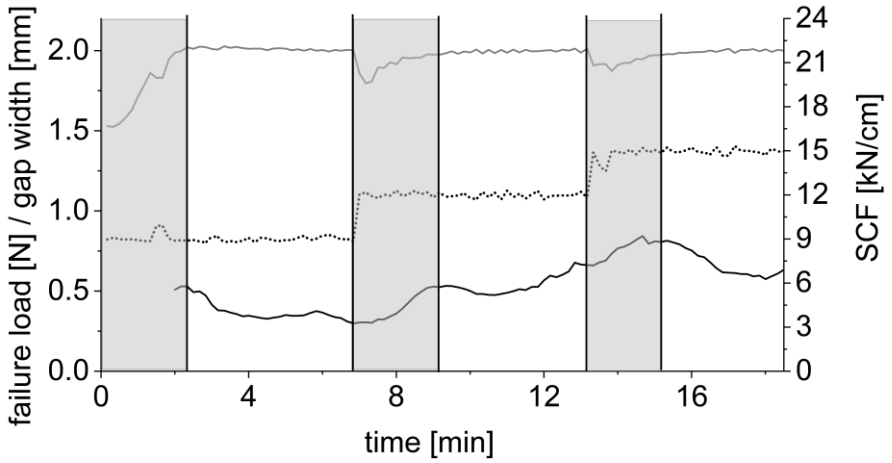

Fig. 9 Plot of failure load (solid black), gap width (solid gray) and SCF (dotted black) against time. Gray coloring highlights time periods of instable process conditions. DCPA as excipient. Failure load moving average over 2 minutes. Gap width and SCF values every 10 seconds. Real-time data, n =1

3.6. Relevance for pharmaceutical manufacturing – how do formulations behave?

To test whether the dependencies of torque, throughput and SCF are also valid for a mixture of API and excipients, a formulation was prepared and granulated. Raw data is listed in Table S3 in the supplementary material.

Fig. 10 shows plots for the formulation comparable to those previously shown for pure excipients. It can be seen that the formulation behaves similarly to the pure excipients as trends that were reported previously are found for the formulation as well.

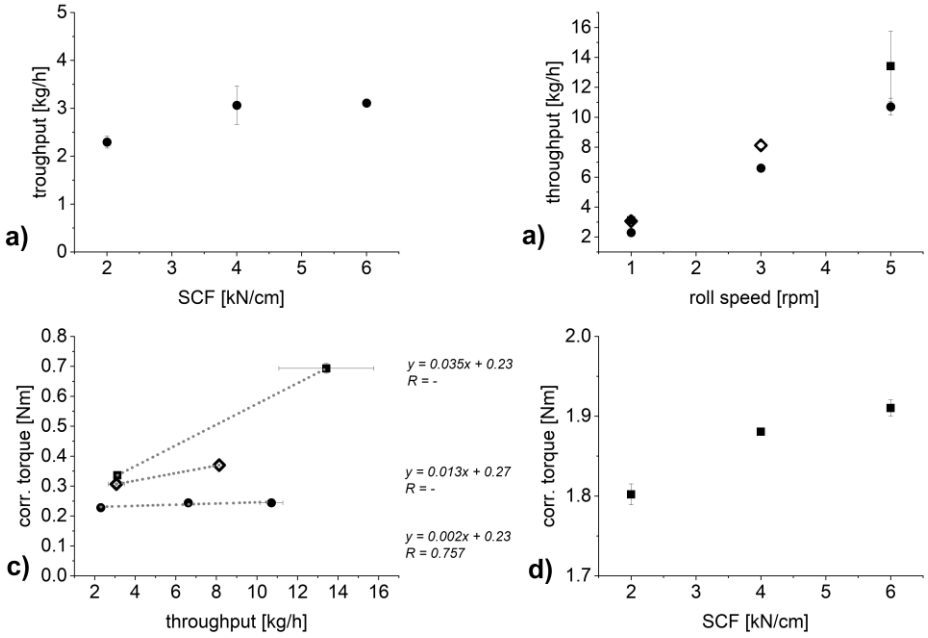

Fig 10. Plots of a) SCF against throughput b) roll speed against throughput at 2 kN/cm (circle), 4 kN/cm (horizontal line), 6 kN/cm (square) c) throughput against corrected torque of the granulation unit d) SCF against corrected torque of the granulation unit. n = 1–3; mean ± sd.

Analogous to Fig. 7 it is possible to plot the correlation of SCF and the torque of the granulation unit independent from throughput (Fig. 11). Good linear correlations are obtained for the two throughputs furthest apart that could be compared using interpolation.

It can be concluded that the behavior of the torque of the granulation unit while processing a formulation is similar to pure excipients.

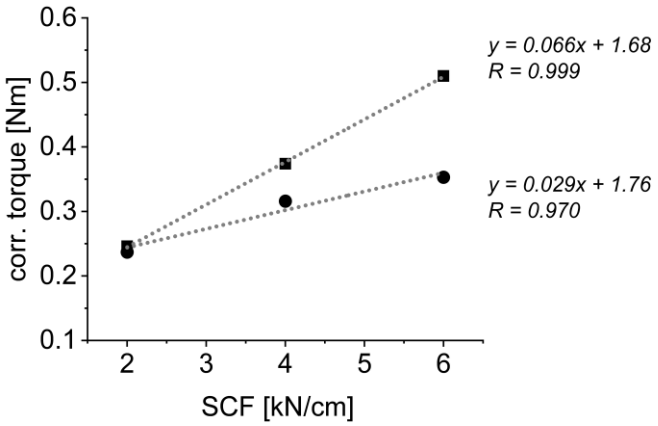

Fig 11. Plot of SCF against the interpolated torque of the granulation unit at 3.5 kg/h (circle) and 8 kg/h (square).

4. Conclusion

Linear correlations of SCF and failure load were established for two materials. It was proven that failure load is independent from the chosen roll speed. Based on the torque of the granulation unit that were measured for different SCF at varying throughputs, a correlation was established that allows to evaluate the impact of the material hardness on the torque of the granulation unit for a specific throughput at constant impeller speed. This correlation was used to predict the granule hardness completely based on process parameters. Therefore, the expected failure load of granules produced with controlled process parameters e.g. SCF and gap width can be compared to the in-line predicted failure load based on resulting process parameters (throughput and the corrected torque of the granulation unit). This opens the possibility of a feedback control loop based on granule failure load controlling the SCF.

Furthermore, if the current granule failure load can be predicted, the optimal compression pressure to obtain tablets of a certain tensile strength could be calculated. This could lead to an in-line determination of compression pressure that can be incorporated into a feedforward control loop. This would allow varying the process parameter of compression pressure in real-time in order to obtain in-specification tablets during the whole production

run. More work and validation of the shown correlations is required in order to implement these control loops.

5. Funding

This research did not receive any specific grant from funding agencies in the public, commercial, or not-for-profit sectors. This work was supported by the Drug Delivery Innovation Center (DDIC), INVITE GmbH, Leverkusen.

6. Declaration of competing interest

The authors declare that they have no known competing financial interests or personal relationships that could have appeared to influence the work reported in this paper.

7. Acknowledgements

This work was supported by the Drug Delivery Innovation Center (DDIC), INVITE GmbH, Leverkusen. The authors thank L.B. Bohle Maschinen + Verfahren GmbH for implementing the tracking of the torque of the granulation unit. The authors furthermore thank JRS Pharma, Chemische Fabriken Budenheim and Ashland Industries Europe GmbH for providing excipients for this study.

8. References

Adams, M.J., Mullier, M.A., Seville, J.P.K., 1994. Agglomerate strength measurement using a uniaxial confined compression test. Powder Technol 78, 5-13.

Arndt, O.-R., Baggio, R., Adam, A.K., Harting, J., Franceschinis, E., Kleinebudde, P., 2018. Impact of different dry and wet granulation techniques on granule and tablet properties: a comparative study. J Pharm Sci 107, 3143-3152.

Broitman, E., 2017. Indentation hardness measurements at macro-, micro-, and nanoscale: a critical overview. Ribol Lett 65, article number 23.

Chatterjee, S., 2012. FDA perspective on Continuous Manufacturing, IFPAC Annual Meeting, Baltimore.

Chowhan, Z., 1979. Moisture, hardness, disintegration and dissolution interrelationships in compressed tablets prepared by the wet granulation process. Drug Dev. Ind. Pharm. 5, 41-62.

Fonteyne, M., Vercruysse, J., De Leersnyder, F., Van Snick, B., Vervaet, C., Remon, J.P., De Beer, T., 2015. Process analytical technology for continuous manufacturing of solid-dosage forms. Trac-Trend Anal Chem 67, 159-166.

U.S. Food and Drug Administration, 2017. Advancement of emerging technology applications for pharmaceutical innovation and modernization: guidance for industry.

Freitag, F., Reincke, K., Runge, J., Grellmann, W., Kleinebudde, P., 2004. How do roll compaction/dry granulation affect the tableting behaviour of inorganic materials?: Microhardness of ribbons and mercury porosimetry measurements of tablets. Eur J Pharm Sci 22, 325-333.

Gupta, A., Peck, G.E., Miller, R.W., Morris, K.R., 2005. Influence of ambient moisture on the compaction behavior of microcrystalline cellulose powder undergoing uni-axial compression and roller-compaction: a comparative study using near-infrared spectroscopy. J Pharm Sci 94, 2301-2313.

Hiestand, E.N., Bane, J.M., Jr., Strzelinski, E.P., 1971. Impact test for hardness of compressed powder compacts. J Pharm Sci 60, 758-763.

Jaminet, F., Hess, H., 1966. Studies on compacting and dry granulation. Pharm Acta Helv 41, 39-58.

Jennett, N., 2007. An introduction to instrumented indention testing. NPL Measurement Good Practice Guide No.92.

Jetzer, W., Johnson, W., Hiestand, E., 1985. Comparison of two different experimental procedures for determining compaction parameters. Int J Pharm 26, 329-337.

Kitazawa, S., Johno, I., Ito, Y., Teramura, S., Okado, J., 1975. Effects of hardness on the disintegration time and the dissolution rate of uncoated caffeine tablets. J Pharm Pharmacol 27, 765-770.

Kleinebudde, P., 2004. Roll compaction/dry granulation: pharmaceutical applications. Eur J Pharm Biopharm 58, 317-326.

Lee, S.L., 2016. Current FDA perspective for continuous manufacturing [conference presentation], MIT-CMAC 2nd International Symposium on Continuous Manufacturing of Pharmaceuticals, September 26-27, 2016, Cambridge, MA, USA.

Lee, S.L., O'Connor, T.F., Yang, X.C., Cruz, C.N., Chatterjee, S., Madurawe, R.D., Moore, C.M.V., Yu, L.X., Woodcock, J., 2015. Modernizing pharmaceutical manufacturing: from batch to continuous production. J Pharm Innov 10, 191-199.

Leuenberger, H., 1982. The compressibility and compactibility of powder systems. Int J Pharm 12, 41-55.

Leuenberger, H., Rohera, B.D., 1986. Fundamentals of powder compression. I. The compactibility and compressibility of pharmaceutical powders. Pharm. Res. 3, 12-22.

Mangal, H., Kleinebudde, P., 2018. Is the adjustment of the impeller speed a reliable attempt to influence granule size in continuous dry granulation? Adv Powder Technol 29, 1339-1347.

McAuliffe, M.A.P., O'Mahony, G.E., Blackshields, C.A., Collins, J.A., Egan, D.P., Kiernan, L., O'Neill, E., Lenihan, S., Walker, G.M., Crean, A.M., 2015. The Use of PAT and Off-line Methods for Monitoring of Roller Compacted Ribbon and Granule Properties with a View to Continuous Processing. Org Process Res Dev 19, 158-166.

Müller, N., 2012. Untersuchungen zur Prozessüberwachung und - regulierung bei der Walzenkompaktierung mittels Drehmomenterfassung an der Granuliereinheit. PhD thesis in german, title translates to "Investigations on process monitoring and control during roll compaction using the torque of the granulation unit.", Universitäts - und Landesbibliothek Bonn.

Patel, S., Sun, C.C., 2016. Macroindentation hardness measurement—modernization and applications. Int J Pharm 506, 262-267.

Rowe, R., 1976. Microindentation-a method for measuring the elastic properties and hardness of films on conventionally coated tablets. Journal of Pharmacy and Pharmacology 28, 310-311.

Schorr, F., 2016. Walzenkompaktierung: Untersuchungen zur in-line Überwachung der Schülpenfestigkeit mittels Vibrations - und Schalldruckanalyse im Bereich der Zerkleinerungseinheit. PhD thesis in german, title translates to "Roll compaction: Investigations for an in-line control tool of ribbon hardness using vibration and acoustics analysis in the granulation unit.", Rheinische Friedrich-Wilhelms-Universität Bonn.

Shlieout, G., Lammens, R.F., Kleinebudde, P., 2000. Dry granulation with a roller compactor Part I: The functional units and operation modes. Pharm Technol Eur 12, 24-35.

U.S. Food and Drug Administration, 2019. Quality considerations for continuous manufacturing guidance for industry.

Walley, S.M., 2012. Historical origins of indentation hardness testing. J Mater Sci Technol 28, 1028-1044.

Wiedey, R., Kleinebudde, P., 2018. Infrared thermography — a new approach for in-line density measurement of ribbons produced from roll compaction. Powder Technol 337, 17-24.

Wilms, A., Meier; R., Kleinebudde, P., 2020. Development and Evaluation of an In-line and On-line Monitoring System for Granule Size Distributions in Continuous Roll Compaction/Dry Granulation Based on Laser Diffraction. J Pharm Innov.

Supplementary material

Table S1. raw data DCPA

SCF	rpm	throughput [kg/h]	corr. torque [Nm]	failure load [N]
		n = 3 - 6	n = 3 - 6	n = 5
6	1	4.1 ± 0.7	0.13 ± 0.02	0.20 ± 0.01
6	3	11. ± 0.5	0.29 ± 0.12	0.17 ± 0.01
6	5	19.3 ± 1.0	0.34 ± 0.10	0.17 ± 0.01
12	1	4.7 ± 0.2	0.41 ± 0.03	-
12	3	14.4 ± 0.4	0.53 ± 0.06	-
12	5	23.0 ± 0.1	0.79 ± 0.01	-
18	1	5.7 ± 1.0	0.40 ± 0.05	0.78 ± 0.06
18	3	16.9 ± 0.6	0.76 ± 0.01	0.79 ± 0.06
18	5	28.2 ± 0.5	1.18 ± 0.04	0.80 ± 0.05
9	3	13.3 ± 0.4	0.34 ± 0.10	0.31 ± 0.03
15	3	15.9 ± 0.5	0.59 ± 0.08	0.56 ± 0.02

Table S2. raw data MCC

SCF	rpm	throughput [kg/h]	corr. torque [Nm]	failure load [N]
		n = 1-3	n = 1- 3	n = 3 - 5
2	1	2.4 ± 0.3	0.45 ± 0.15	0.08 ± 0.01
2	2	4.5 ± 0.2	0.45 ± 0.07	0.17 ± 0.02
2	3	6.8 ± 0.1	0.60 ± 0.01	0.12 ± 0.02
2	4	8.8 ± 0.2	0.58 ± 0.06	0.10 ± 0.01
2	5	11.0 ± 0.0	0.75 ± 0.00	0.10 ± 0.01
4	1	2.9 ± 0.1	0.64 ± 0.07	
4	2	5.4 ± 0.10	0.73	
4	3	7.9	1.02	
4	4	9.3	1.15	
4	5	11.0	1.25	
6	1	3.2 ± 0.1	0.83 ± 0.11	0.39 ± 0.08
6	2	5.3	1.09	0.49 ± 0.07
6	3	7.5	1.61	0.50 ± 0.05
6	4	7.6	1.57	0.56 ± 0.10
6	5	7.6	1.39	0.38 ± 0.04
3	1	2.5 ± 0.1	0.45 ± 0.06	0.21 ± 0.02
5	1	2.9 ± 0.2	0.74 ± 0.12	0.38 ± 0.08

Table S3. raw data formulation

SCF	rpm	throughput [kg/h]	corr. torque [Nm]
		n = 2-4	n = 3- 4
2	1	2.3 ± 0.1	0.23 ± 0.01
2	3	6.6 ± 0.18	0.25 ± 0.01
2	5	10.7 ± 0.6	0.25 ± 0.01
4	1	3.1 ± 0.4	0.31 ± 0.00
4	3	8.1 ± 0.2	0.37 ± 0.02
6	1	3.1 ± 0.1	0.34 ± 0.01
6	5	13.4 ± 2.3	0.70 ± 0.02

6 Optimization of residence time distribution in RCDG and an assessment of its applicability in continuous manufacturing

Annika Wilms[a,b], Peter Kleinebudde[a]

[a] Institute of Pharmaceutics and Biopharmaceutics, Heinrich Heine University, Universitaetsstrasse 1, 40225 Duesseldorf, Germany

[b] INVITE GmbH, Drug Delivery Innovation Center (DDIC), CHEMPARK Building W32, 51364 Leverkusen, Germany

6.1 Pretext

The following research paper has been published by Particuology (2020, article in press).

https://doi.org/10.1016/j.partic.2020.09.009

Evaluation of authorship:

author	idea [%]	study design [%]	experimental [%]	evaluation [%]	manuscript [%]
Annika Wilms	50	70	100	100	80
Peter Kleinebudde	50	30	0	0	20

Therefore, the manuscript is not part of this document.

7 Summary and Outlook

Studies on monitoring granule size distribution and granule hardness, controlling granule size distribution, determination of residence time distribution and representative sampling in continuous roll compaction/dry granulation are presented.

The granule size was determined using two different techniques, which are well-established in size determination: dynamic image analysis and laser diffraction. In order to use real-time dynamic image analysis in a dry granulation process, it was necessary to implement a representative sampling method. Only a rotating tube sample divider could provide representative samples. This sampling approach was so far not described in literature and representative sampling of pharmaceutical granules was first proven in the scope of this thesis. For future development of process analyzers, this sampling method can therefore be implemented, if sampling is necessary.

Subsequently, dynamic laser diffraction was linked to the rotating tube sample dividing approach. Thereby, granule size measurements were conducted and the shape of the particles was assessed. For a first evaluation, this was done off-line using material that was previously granulated. Differently sized granules were poured into the sample divider at defined rates and analyzed. Back mixing in the sample divider was inhibited by the adding procedure. The dynamic image analyzer itself included a vibration chute, which can result in a time delay and potential for back mixing based on the time the material is transferred on the vibration chute. This can be seen in the results as two to three minutes are needed between addition of a new material type and a response particle size distribution in equilibrium. The method was then transferred to a dry granulation process, in which the principle was confirmed. Further research should aim at evaluating the sensitivity of the method.

As a second technique, laser diffraction was used to determine the granule size distribution. For implementing laser diffraction, a sufficient dispersion through the laser beam was necessary. Pneumatic conveyance was used to transfer material from the granulator to a collection vessel. The dispersion by the pneumatic conveyance was found to be sufficient for laser diffraction. Therefore, in-line granule size determination was executed. The granule size distribution was monitored at varying SCFs. Residence time between the compaction gap and the measurement was short and can be attributed to mainly the time the ribbons spend in the milling unit. Increasing the throughput to up to 16.6 kg/h led to a

drop in transmission below 50 %. Low transmission can indicate insufficient dispersion. Therefore, on-line laser diffraction was established to be able to measure granules at throughputs up to 27.5 kg/h. The complete product stream was sampled by a tube that was inserted in the main product stream and a venturi nozzle for additional dispersion. The granule size distribution was also monitored at varying SCFs. Representative sampling using the bypass was successful for small granule sizes but failed for larger particles. Therefore, representative sampling in pneumatic conveyance must be improved further. The in-line monitoring was tested by compacting a formulation and then replacing it by a similar formulation which was over-lubricated with magnesium stearate. The monitoring system was able to measure the drop in granule size triggered by the over-lubricated formulation. The fast response time and the sensitivity to changes in process parameters underlined the system's ability to be used as a control tool in continuous dry granulation.

Therefore, laser diffraction was implemented in a feedback control loop. A PI-controller was programmed to react to changes in particle size in adjusting one of the critical process parameters SCF, gap width and sieve speed. Sieve speed was evaluated to be most suitable, as it does not affect the ribbon properties itself. Changing the ribbon properties will also lead to a change in hardness. Adjusting the sieve speed impacted the granule sizes of the resulting granules. However, the impact is limited, and only small deviations can be counteracted. Changing the gap width to imitate a fluctuating gap during a process could be successfully counteracted by adjusting the sieve speed using a PI-controller. In an experiment similar to the one to test the monitoring strategy, an over-lubricated and a non over-lubricated formulation were granulated. The drop in granule size was evident but could not be counteracted by adjusting the sieve speed. Adjusting the SCF was successful in adjusting the granule size distribution but was not sufficient to reach the level of the properly lubricated formulation. The total value of the mean particle size at constant material and process parameters fluctuated strongly throughout a two week period, in which experiments were conducted. To develop a robust control strategy, influencing factors of the granule size should be carefully evaluated and strategies to keep the absolute values constant for certain process parameter settings should be developed.

Another critical quality attribute that was evaluated in the scope of this thesis was granule hardness, characterized by granule failure load. In a statistical design of experiments the impact of SCF, gap width and sieve speed on ribbon microhardness and granule strength was evaluated. It was proven that ribbon microhardness and granule failure load react

similarly to changes in SCF and gap width and can therefore be used interchangeably if needed. The sieve speed could not impact ribbon hardness while it decreased the granule failure load. This effect can be mainly attributed to a change in particle size at varying sieve speeds. Subsequently, a material with brittle and a material with plastic deformation behavior were dry granulated and the torque of the granulation unit and the throughput were tracked. The impact of SCF and roll speed were evaluated at various levels. In conjunction with granule failure load values, linear regression models were established. Using these, it was feasible to estimate the resulting granule failure load by tracking the torque of the granulation unit and the throughput in real-time. Based on those, the expected granule failure load increased as the SCF was increased in an experiment. For future research, more intricate models could be derived. The sensitivity and accuracy of the model could then be improved and validated.

Finally, the knowledge about residence time distribution in continuous dry granulation was broadened by characterizing the impact of the impeller in the powder inlet unit of the roll compactor. Material was colored using wet granulation. This allowed a high intensity of color that could be tracked readily using a camera and analytical software. At the same time, the amount of colored tracer needed was low (0.21 m/m% in the final material) and thereby the impact of tracer on material properties was kept low. This meant that a comparably easy technique could be used to determine residence time in a dry granulation line and the low amount of tracer also made this technique cost-efficient. The method also proved to be robust as determinations carried out under varying lightning conditions resulted in similar absolute intensity values. The exponential function of the calibration curve between intensity of color and content of colored material was therefore characterized by a small coefficient of variation. Absolute residence times, e.g. the time needed to replace 95 % of the non-colored material with colored material, was significantly decreased by increasing the roll speed and decreasing the impeller speed in the milling unit. Therefore, the roll speed should be large and the impeller speed should be low for short and narrow residence time between the powder inlet unit and the ribbon. In continuous manufacturing, it is questionable whether this knowledge can be implemented as a high roll speed also results in large throughputs which might not be desirable in many cases.

Based on the work presented in this thesis, monitoring of granule size and hardness can be realized during continuous dry granulation. A control strategy approach for granule size was presented and could be implemented in the installation of a continuous manufacturing

line with a dry granulation unit. Characterization of the residence time in dry granulation deepened the process understanding and can be used in the development of control strategies as well. In conclusion, the understanding of continuous dry granulation was advanced by the present investigations and the realization of a fully controlled manufacturing line is coming closer.

8 Acknowledgements / Danksagung

Meinem Doktorvater, Herrn Prof. Dr. Dr. h.c. Peter Kleinebudde, möchte ich zuallererst für die Möglichkeit danken in seinem Arbeitskreis diese Promotionsarbeit anzufertigen. Ich möchte ihm dafür danken, dass er bei Nachfragen und Problemen stets zeitnah erreichbar war. Seine ehrliche und konstruktive Kritik haben diese Arbeit bereichert (und mich das ein oder andere Mal ermutigt „signifikant“ durch „relevant“ zu ersetzen). Zudem möchte ich mich herzlich für die Weinverkostung bedanken. Ebenfalls in bester Erinnerung bleiben die Geburtstagsfeiern inklusive Partybahn, Biergarten und gemütlichen Altstadtabenden.

Ich danke meinem Mentor Prof. Dr. Jörg Breitkreutz für die Übernahme des Koreferats und der vielen hilfreichen Vorschläge, die er mir während der vielen Fokus-Gruppen und Vorträgen gemacht hat.

Der Invite GmbH möchte ich mich für die Anstellung danken, welche mir die Promotion ermöglicht hat. Herrn Werner Hoheisel danke ich herzlich für seine Arbeit als mein direkter Vorgesetzter. Mit viel Herz war er stets bei der Sache und ansprechbar für alles was angefallen ist. Ich wünsche dem Drug Delivery Innovation Center für die Zukunft alles Gute.

Dr. Klaus Knop danke ich für die vielen fachlichen Ratschläge während meiner gesamten Promotion. Ohne seine Erfahrung wären viele Experimente bereits am Anfang gescheitert und der Start meiner Promotion deutlich schwieriger gewesen. Vielen Dank auch für die offene und herzliche Art mit der wir über viele Problemstellungen und Ideen diskutieren konnten.

Dr. Raphael Wiedey danke ich für den fachlichen Rat während meiner gesamten Promotion und geduldige Hilfe mit Excel und Python. Die gemeinsame Arbeit zum Start meiner Promotion hat mich auf die eigenen Versuche bestens vorbereitet. Ich wünsche dir viel Erfolg in der weiteren Forschung.

Ich danke Dr. Julian Quodbach ebenfalls für hilfreiche Diskussionen und fachliche Ratschläge in Fokusgruppen und Fortschrittsberichten.

Dr. Robin Meier danke ich für seine Unterstützung bei der Durchführung zahlreicher Experimente. Ohne die Kooperation mit L.B. Bohle und Dr. Meiers fachlichem Rat wären viele essentielle Versuche nicht möglich gewesen. Ich möchte mich außerdem bedanken,

dass er jedes meiner Manuskripte gelesen und mir wertvolle Verbesserungsvorschläge unterbreitet hat. Ein Manuskript welches durch die Hände von Herrn Prof. Kleinebudde und Dr. Meier gegangen ist wurde wahrlich auf Herz und Nieren getestet. Bedanken möchte ich mich auch für viele spaßige Unterhaltungen in Ennigerloh und die besten Motivationsgespräche meiner Promotion.

Ebenfalls möchte ich mich bei Andreas Altmeyer, Andreas Teske, Damian Mika, Daniel Emmanuele, Philipp Harbaum, Daniel Bexte, Sven Kämmering und Andreas Tillkorn von der Firma L.B. Bohle bedanken. Alle Mitarbeiter waren vor Ort stets hilfsbereit und haben die vielen Arbeitstage für mich vor Ort sehr angenehm gestaltet.

Oliver Schmitt und Dieter Makowlew der Firma Malvern Panalytical danke ich für das aufrichtige Interesse an meiner Arbeit und die Möglichkeit über lange Zeiträume das Insitec auszuleihen.

Thomas Möller der Firma Haver & Böcker danke ich für das aufrichtige Interesse an meiner Arbeit und die Möglichkeit mit dem CPA diverse Experimente durchzuführen.

Den WPP-Gruppen Sara Al-Subaidi, Nastasiya Breyn, Lina Strohmeyer und Fabienne Walter danke ich für den Einsatz den sie im Rahmen ihres WPPs gezeigt haben.

Meinen Bürokollegen Dr. Isabell Speer, Dr. Raphael Wiedey, Jhinuk Rahman und Anja Göbel danke ich für eine tolle Zeit, viele fachliche und private Gespräche sowie den Spaß, den wir zusammen hatten.

Bei Dr. Julia Harting möchte ich mich für die wunderbare Freundschaft (auf den ersten Blick) inkl. Shopping, Fechtunterricht, Abendessen, Konferenzbesuche und legendäre 90er Partys bedanken. Du hast mir den Anfang in Düsseldorf sehr leicht gemacht.

Sebastian Pohl danke ich für die schönsten gemeinsamen Tage in Ennigerloh und der Promotion. Mit niemanden sitze ich lieber stundenlang nachts (in meiner Zeitrechnung, *früher Nachmittag* für dich) auf der Couch und vermesse Schneckenelemente als mit dir. Vielleicht schaffen wir es noch gemeinsam zum Mettwurstmarkt und zu diesem ominösen Badesee. Ich hätte mir niemand besseren wünschen können, um gemeinsam in die Promotion zu starten.

Sabrina Berkenkemper danke ich für zahllose gemeinsame Stunden bei Coffein und/oder Ethanol haltigen Warm- oder Kaltgetränken. Danke auch dafür, dass du immer mit anpackst, wenn Hilfe gebraucht wird und man sich zu 100 % auf dich verlassen kann.

Dina Kottke verdient ewige Dankbarkeit für diverse Rettungen vor heimtückischen Käfern. Ebenso sind Singstar Einlagen auf dem Weg zur Arbeit, Taxidienste, Pancakes und wundervolle Nachbarschaft in bester Erinnerung. (P.S. Du parkst fantastisch.)

Jhinuk Rahman danke ich für witzige Gespräche (man hört besser mit Brille!) und ihre geduldige Art mir zuzuhören, wenn es mal nicht so lief. Danke außerdem, dass du immer ein Friends-Zitat und guten Rat parat hast. Nicht umsonst gab es Institutsangehörige die uns angeblich ausschließlich mit Rücken zum Schreibtisch gedreht kennen.

Den Büros Chamberlain/Hansen/Windolf sowie Bollmann/Pohl/Ponsar danke ich für die stetige Versorgung mit Kaffeemilch und Nervennahrung. Hanna Ponsar danke ich für kreative Stunden und leckeres Essen. Rebecca Chamberlain, Laura Falkenstein, Hanna-Lou Keizer, Olga Kiefer und Hellen Windolf danke ich außerdem für ihre Freundschaft und das gemeinsame Durchstehen von Höhen und Tiefen. Jerome Hansen danke ich für einen feuchtfröhlichen Konferenzbesuch und seinen überragenden Musikgeschmack. Hellen Windolf danke ich zudem für das Maßschneidern von Ersatzteilen, den dazugehörigen 3D-Druck, das gemeinsame beenden von Veranstaltungen und nötige Abkühlungen im Hochsommer.

Lieber Dr. Vincent Lenhart, danke, dass du seit Beginn meiner Promotion jedes Gerät, welches nicht funktionieren wollte repariert hast. In < 1 % der Fälle sitzt das Problem halt nicht vor dem Gerät. Die Tage der Promotion waren schöner, wenn wir sie mit einem frühmorgendlichen Gespräch begonnen haben und Konferenzen waren schöner, wenn wir dort gemeinsam angestoßen haben.

Allen nicht namentlich genannten Mitgliedern des Instituts danke ich ebenfalls für die gemeinsame Zeit.

Meiner Familie danke ich für grenzenlose Unterstützung und Liebe.

9 Eidesstattliche Erklärung

Ich versichere an Eides Statt, dass die Dissertation von mir selbständig und ohne unzulässige fremde Hilfe unter Beachtung der „Grundsätze zur Sicherung guter wissenschaftlicher Praxis an der Heinrich-Heine-Universität Düsseldorf“ erstellt worden ist.

_____

Annika Wilms